The Dissertation Committee for Trevor John Williamson Certifies that this is the approved version of the following dissertation:

The Relationship Between Composition, Structure, and Solubility in Sodium Aluminosilicate Hydrates

Committee:

Maria Juenger, Supervisor

Lynn Katz

Kevin Folliard

Philip Bennett

Gaurav Sant

The Relationship Between Composition, Structure, and Solubility in Sodium Aluminosilicate Hydrates

by

Trevor John Williamson

Dissertation

Presented to the Faculty of the Graduate School of

The University of Texas at Austin

in Partial Fulfillment

of the Requirements

for the Degree of

Doctor of Philosophy

The University of Texas at Austin

December 2017

Dedication

For Mom, who taught me how to treat others with love and care, and Dad, who taught me that family comes first.

Acknowledgements

I would like to thank The Federal Highway Administration's Exploratory Advanced Research Program for funding Project DTFH61-13-H-00011, which provided financial support for the work presented in this dissertation. Thank you Jack Youtcheff, for being a great host during our visit to the FHWA headquarters.

I would especially like to thank my advisor, Dr. Maria Juenger. You have been an amazing advisor and mentor over the last 6 years, and I'm grateful for the friendship we've developed through working together. You made me into a better writer, a harder worker, and a better person.

I would also like to thank my unofficial co-advisor, Dr. Lynn Katz. You are one of the kindest, warm-hearted people I know, and I truly enjoyed all of our time together. I walked into your aqueous chemistry class 4 years ago hardly knowing the difference between an acid and a base, and walked out with the foundation I needed for this work and inspired to learn more. I'll always consider you a mentor and a friend.

Thank you to Kevin Folliard, Phil Bennett, and Gaurav Sant, my committee members. Kevin, you were always willing to help, and it was your class that first inspired me to pursue materials research. It was nice to have someone with whom to share the Patriots' ups and downs over the last few years, too. Phil, I never could have overcome some of the practical considerations for setting up my experiments without your generous help. And Gaurav, you continue to be an inspiration by setting an amazing example of working hard and bringing talented people together to tackle the world's biggest challenges.

Katy Aughenbaugh and Lisa Burris, thank you both for making me feel welcome and showing me around the lab when I first showed up at 18B. Katy, you opened the door and paved the way for geopolymer research. Lisa, you were a great office mate for your last year at UT, and I really enjoyed our conversations, whether about science or life.

Mike Rung, you were always willing to lend a hand in the lab or when I had questions about how to cook a brisket. I told myself when I moved to Texas that first priority was learning how to barbecue, and second was learning a little something about engineering. You made the first possible, and contributed in many ways to the second. Thank you for both!

Sherian Williams, you provided amazing logistical support for my research, but more importantly, I loved being able to stop in to chat when research felt a little overwhelming. I could always count on your for a smile and a chocolate when they were needed.

Thank you Amit Bhasin for graciously letting us use your oven for the last couple of years to run our experiments. It was a pleasure getting to know you and you were always willing to help.

Thank you Phil Tomlin, Michael Williams, and Lamont Prosser. All of you were very supportive and happy to help in the ECJ shop when I worked on my experimental setups.

Saif Al-shmaisani and Victoria Ibarra, this work would not have been possible without your support in the lab. Saif, you've become a great friend and I love the positive energy you always carry with you. And Victoria, it was a real pleasure working with you. You always brought an amazing work ethic and smile to the lab, and both made all that time working in the glovebox much easier. Good luck to both of you in graduate school!

Fred Aguayo, Thano Drimalas, and Racheal Lute, I'll always consider the three of you some of my closest friends. Whether it was a favor in the lab, a coffee break, or a visit to ABW at the end of the day, you guys were always there for me.

Thank you to all of the other graduate students that helped and inspired me along the way: Chris Clement, Anthony Bentivegna, Mitchel Dornak, Rachel Cano, Aasiyah Baig, Jose Garcia, Nick Tiburzi, Bruno Fong-Martinez, Anthony Garcia, and all of the others. Your friendship and support in the lab meant so much.

Hugo Celio, Charlie Perego, Shouliang Zhang, and Steve Swinnea, thank you all very much for your technical support with the TGA, ICP, SEM, and XRD. This work would not have been possible without you.

Ryan Varner, Arlo Bush, and Max Kerwick, the three of you kept me sane outside the lab. Thank you for being amazing friends and for reminding me when it was time to take a break from the lab to jump in Barton Springs or grab a cold beer.

And last, but certainly not the least, thank you to the best girl I could ask for, Alex. You've been amazingly patient with me as my two year masters degree turned into a 5 year PhD, and my 5 year PhD turned into a 6 year PhD. You've been my partner the whole way, inspiring me to keep at it and encouraging me when the end seemed out of sight. Your love and support has meant the world. I love you.

The Relationship Between Composition, Structure, and Solubility in Sodium Aluminosilicate Hydrates

Trevor John Williamson, PhD

The University of Texas at Austin, 2017

Supervisor: Maria Juenger

This work seeks to identify the fundamental precursor-to-product composition relationships by which inorganic polymer binders (IPBs) derive their chemical structure and to link that chemical structure to their engineering properties. IPBs, also known as geopolymers, are a new class of construction materials that will potentially serve as a low-energy, low-CO_2 alternative to ordinary portland cement (OPC). These binders are synthesized by the activation of an aluminosilicate solid, such as coal fly ash, by a highly alkaline aqueous solution generally consisting of an alkali hydroxide with added sodium silicate to control the system's silica content. The IPB products are similar in composition to zeolites, but are amorphous to semi-crystalline. An extensive body of research has demonstrated comparable mechanical properties (compressive strength, stiffness) as well as superior dimensional stability and durability (resistance to corrosion, alkali-silica reaction, acid attack) of IPB concrete compared to OPC concrete. Much of the existing research, however, has focused on the characterization and evaluation of a variety of aluminosilicate sources with significant levels of variation from one source to the next and inhomogeneity within a given source; the basic mechanisms that govern product formation, microstructure development and ultimately engineering properties are still poorly understood.

The research presented here aimed to reduce the large number of variables present when using natural precursors to better understand the effects of manipulating each variable on the composition and structure of reaction products. This was accomplished by synthesizing and examining sodium aluminosilicate hydrate, the primary binding phase in IPBs, from reagent grade materials across a range of compositions, allowing complete stoichiometric control of the constituents by eliminating variability in the composition of solid precursors. The impact of temperature and bulk composition on the structure and composition of the solids was investigated. Additionally, temperature dependent solubility products (K_{sp}) of the IPB products were determined by monitoring the ionic concentration of the solutions over time. Solubility products are a necessary prerequisite for the future development of thermodynamic models that can help predict IPB mechanical properties and durability.

Table of Contents

List of Tables

List of Figures

Chapter 1: Introduction

Inorganic polymer binders (IPBs) are a novel type of concrete binder synthesized by activating an aluminosilicate powder, often coal fly ash, with a highly alkaline aqueous solution, such as sodium hydroxide [1]. Previous research has demonstrated comparable mechanical properties (compressive strength, stiffness) [2–4] as well as superior dimensional stability [5] and durability (resistance to corrosion, alkali-silica reaction, acid attack) [6–8] of IPC compared to portland cement concrete. Much of the previous work on these materials, however, has taken a trial-and error approach to dealing with the significant variation in solid precursor composition and morphology between sources; widespread use of these materials requires a better understanding of the basic chemistry that governs product formation, microstructure development and ultimately engineering properties of IPBs.

The research presented here examines the precursor-to-product relationships of IPB development, specifically aiming to quantify the effects of solution composition and speciation as well as reaction temperature on composition, structure, and solubility of sodium aluminosilicate hydrate (N-A-S-H), the primary binding phase in low-calcium IPBs. N-A-S-H phases are synthesized by mixing dilute solutions of sodium aluminate and sodium silicate across a range of compositions and allowing the solids to form and equilibrate at temperatures ranging from 4 to 70 °C. By working with dilute systems, the complicating effects of kinetics (i.e., simultaneous dissolution of precursors and formation of products) are essentially eliminated. This approach allows complete stoichiometric control of the solution to elucidate directly the effect of a given solution composition on the development of N-A-S-H composition, structure, and solubility. Solubility products for N-A-S-H are calculated, and are a necessary prerequisite for the

development of thermodynamic models that can help predict the binder phase assemblages, and ultimately, engineering properties, for IPBs.

The body of this dissertation is split into three chapters. Chapter 2 presents a rigorous method for measuring N-A-S-H solubility that was developed and refined as part of this research. The chapter starts with a discussion of why there is a need for measuring the solubility of N-A-S-H and for developing thermodynamic models to predict its performance. Next, a review of previous studies on thermodynamic models and solubility of other concrete binders is presented, followed by a brief discussion of some important considerations for the method development. Finally, Chapter 2 presents the method in detail, with the hope that other researchers will build on the method in the future.

Chapter 3 presents the composition-structure-solubility relationships of sodium aluminosilicate hydrate reacted at 50 °C with bulk molar Si/Al ratios from 1 to 2. The relationship between bulk composition and N-A-S-H composition is discussed, and is important in understanding the relationship between pore solution chemistry and solid binder phases in IPBs. The effect of varying activator Si/Na ratio is also investigated, as the speciation of silicate species is highly dependent on this ratio and is known to have a significant impact on binder chemistry and performance.

Finally, Chapter 4 investigates the relationship between temperature and N-A-S-H composition, structure, and solubility. It is well understood that temperature significantly impacts the mechanical performance and durability of these materials, perhaps even more so than with portland cement concrete. Because of the wide range of curing temperatures used to fabricate these materials (generally in a precast setting), as well as the range of service temperatures that concrete is subjected to, understanding the impact of temperature on the binder properties is an important step in enabling the wide use of these materials. The hope is that this work will serve as the start to a database for N-A-S-

H thermodynamic properties and provide the starting point for other researchers to build on that database, ultimately transforming our ability to use these novel concrete binders.

Throughout this dissertation, the term *phase* is used to describe solids or liquids that are uniform in chemical composition and physical properties. Callister [9] defines a phase as "a homogeneous portion of a system that has uniform physical and chemical characteristics."

The author of this dissertation, Trevor Williamson, designed and performed all of the experiments and analyzed all of the data presented, with the exception of the Nuclear Magnetic Resonance data presented in Section 3.3.1. Hoard Dobbs, a graduate student at The University of California Santa Barbara designed and performed those experiments, and wrote the corresponding analysis presented in that section.

Chapter 2: A Rigorous Method for Measuring N-A-S-H Solubility

2.1 INTRODUCTION

Inorganic polymer binders (IPBs) are a promising new alternative to portland cement that are made by activating an aluminosilicate powder, often coal fly ash, with a highly alkaline activating solution, most commonly sodium hydroxide. Potassium hydroxide is a viable alternative to sodium hydroxide, and regardless of which alkali cation is used, the OH^- plays the role of a dissolution catalyst, while the Na^+ or K^+ become charge-balancing element in aluminum tetrahedra [1]. Sodium hydroxide generally provides greater release of silicates and aluminates from the aluminosilicate source, while potassium hydroxide tends to form larger silicate oligomers in solution at a given alkali to silicon ratio [1]. In the case of sodium hydroxide, which is the activator of focus in this study, the primary binding phase is sodium aluminosilicate hydrate (N-A-S-H). IPBs have comparable mechanical properties, and, according to some studies, superior durability than portland cement binders, all with lower energy expenditure and reduced CO_2 emissions. Perhaps the greatest technical challenge that must be overcome to promote the widespread use of these materials is the fact that the primary aluminosilicate source material, fly ash, varies significantly from source to source. The successful implementation of these materials is dependent on our ability to quickly identify promising fly ash sources, and then to predict and optimize mechanical properties and chemical stability for a given fly ash under a specific set of processing conditions.

The mechanical properties and durability of IPBs, like other, cementitious materials are highly dependent on the final phase assemblages, and especially the relative portion of voids compared to solid phases [10]. The occurrence and extent of many durability issues are dependent on the chemical stability of the solid phases as well as the

pore solution chemistry [11–14]. Thermodynamic modeling of calcium silicate hydrate (C-S-H) has successfully enabled the prediction of phase assemblages and porosity for portland cement-based materials [15]. More recently, Myers et al. [16–19] expanded the data on C-S-H to include calcium aluminosilicate hydrate (C-A-S-H), as well. Experimental measurement of the solubility of a cementitious binding phase is a prerequisite for developing a thermodynamic model. To date, there are little, if any, reliable solubility data for N-A-S-H. While the results presented in Chapters 3 and 4 of this dissertation are a step towards the necessary solubility data, more work needs to be done. The goal of this chapter is to present, in detail, a method for measuring N-A-S-H solubility data. The hope is that other researchers will build on the thermodynamic database for N-A-S-H, ultimately enabling the development of reliable thermodynamic models that can help promote the widespread use of IPB concrete.

Measuring solubility and tabulating solubility products are common practices for geochemists and environmental engineers, but detailed methods for these experiments are not always readily available in the field of cement chemistry. The objective of this chapter is to provide the concrete community with the resources necessary to conduct experiments using methods that are familiar to many geochemists and environmental engineers and to modify those experiments so they are more applicable to concrete phases. To achieve this end, first, the need for thermodynamic models to predict phase balances and engineering properties is discussed. Then, a review of previous solubility measurements and thermodynamic models for other cementitious materials is presented. Next, some general considerations are discussed, so that if the method presented here is modified, future researchers will better understand the impacts. Finally, a rigorous method for measuring the solubility of N-A-S-H is presented in detail. Many aspects of

this method can be extended to solubility measurements of other cementitious phases, as well.

In the method for measuring N-A-S-H solubility presented here, N-A-S-H is synthesized by mixing sodium silicate and sodium aluminate stock solutions with varying proportions to achieve desired Si/Al molar ratios. The N-A-S-H is allowed to react until supernatant Si^{4+} and Al^{3+} concentrations stabilize, indicating that the N-A-S-H has equilibrated. Equilibrium supernatant Na^{+}, Si^{4+}, and Al^{3+} concentrations are measured using inductively coupled plasma optical emission spectometry (ICP-OES, hereafter referred to as ICP). The composition of N-A-S-H is determined by mass balance, hydrofluoric acid digestion with ICP, and thermogravimetric analysis (TGA). The solubility products are then determined by calculating the ion activity product (IAP) at equilibrium conditions.

2.2 THE NEED FOR N-A-S-H THERMODYNAMIC MODELS

The alkali-activation of aluminosilicates involves a complex series of reactions, further complicated by the fact that at any given time, multiple reaction steps occur simultaneously. When solid aluminosilicate particles come in contact with an alkaline solution, dissolution by alkali hydrolysis proceeds rapidly, consuming water and releasing silicate and aluminate monomers:

$$SiO_2 + H_2O + OH^- \rightarrow H_3SiO_4^- \quad (2.1)$$

$$SiO_2 + 2OH^- \rightarrow H_2SiO_4^{2-} \quad (2.2)$$

$$Al_2O_3 + 3H_2O + 2OH^- \rightarrow 2Al(OH)_4^- \quad (2.3)$$

These monomers combine through a series of condensation reactions, forming a complex combination of soluble aluminate, silicate, and aluminosilicate oligomers, depending on the transient Si/Al ratio in the solution, for example:

$$\text{-Si-OH + HO-Si-} \rightarrow \text{-Si-O-Si-} + H_2O \quad (2.4)$$

Aluminum plays an important role in the polymerization process. Even though dissolved silicon tends to form soluble oligomers, sodium silicate solutions are stable at even relatively high concentrations [1]. In fact, it is the inherent low solubility of alkali-aluminosilicates that makes them a viable candidate for a primary binder in a cementitious system, and adding aluminum to the solution is what allows the solid phases to form. It is well known that the total amount of aluminum available for reaction and the rate of release of aluminum can greatly affect the final phase balances, microstructure, and engineering properties (compressive strength, stiffness, tensile strength, durability) of IPBs [20].

In solutions with low Si/Al (<1), condensation of silicate and aluminate monomers to form poly(sialate)-based gel is favored, while a higher Si/Al favors condensation of silicate monomers with other silicate monomers to form silicate oligomers, which then condense with aluminate monomers. As dissolution proceeds, the solution quickly becomes supersaturated with respect to alkali-aluminosilicates that precipitate by forming large networks by further condensation. The resulting structure is referred to as a gel because of its bi-phasic nature, with the precipitated aluminosilicate and water released during condensation reactions forming the two phases.

The engineering properties of the precipitated gel are heavily dependent on its composition, microstructure, and atomic structure, all of which are greatly affected by,

but not easily correlated with: precursor properties, mixture proportions, and processing conditions (i.e. curing duration, temperature, relative humidity). For example, higher Si/Al ratios in solution lead to more Si-O-Si bonds, which are known to be stronger than Si-O-Al bonds. Compressive strength reaches a maximum at intermediate Si/Al, indicating that other factors outside of composition control the strength. Duxson et al. [4] found that increasing Si/Al to 1.4 leads to a less porous microstructure, but increasing Si/Al beyond 1.65 decreases the lability of silicate species within the gel, ultimately reducing strength.

Correlating precursor properties to engineering properties is complicated by the fact that bulk Si/Al is often not an accurate predictor of solution Si/Al, which ultimately governs the structure and composition of precipitating gel. This is especially true for fly ash systems due to the highly variable reactivity of aluminosilicate phases in fly ash. Dissolution of source material and precipitation of the binding phase happen simultaneously [1], and hardening is generally completed prior to complete dissolution of soluble phases from the source powder, meaning that reactive aluminosilicate particles will remain in the final material. When correlating composition to strength, a further complicating factor is that these remaining source particles alter the final microstructure and therefore affect the compressive strength of the binder [4].

Solution Si/Al evolves over time and is dependent on the kinetics and extent of silicate and aluminate dissolution at a given temperature, pH, and the initial silica content in solution, which not only affects Si/Al directly, but also indirectly by significantly enhancing aluminosilicate dissolution rates at concentrations above ~200mM [21]. For activating solutions with little or no added silica, Si/Al at the time of mixing is low because aluminate dissolution is generally faster than silicate dissolution. Initial Si/Al will thus be less than 1. For solutions with low Si/Al, most aluminum in solution is

present as $Al(OH)_4^-$ [22]. Since the Si/Al of precipitated gel is >1 because Al-O-Al bonds are unfavorable according to Loewenstein's principal, the Si/Al in solution will decrease further as gel precipitates, and high concentrations of $Al(OH)_4^-$(aq) are expected in solution even after setting. This was, in fact, observed in metakaolin precursor IPBs studied by Duxson et al. [23].

For high silicate activating solution, Si/Al is high at initial mixing and decreases as aluminum is released preferentially. The Si/Al is dependent on (1) the initial amount of aluminum that is released prior to stoichiometric release and (2) the initial silicate concentration in the activator. For solutions where Si/Al remains high, no $Al(OH)_4^-$(aq) is expected to remain in solution after setting, and this was also observed by Duxson et al. [23]. Alternatively, Si/Al sometimes starts high (no $Al(OH)_4^-$(aq)) and then decreases as solids with Si/Al > 1 precipitate. If Si/Al falls bellow about 2, the remaining aluminosilicate species in solution will depolymerize, resulting in the presence of $Al(OH)_4^-$(aq) in solution after setting [23].

Further complicating the task of linking composition to engineering properties is the fact that initial speciation of the silicates in sodium silicate activating solution is highly complex and greatly impacts gel formation and structure. It is well known that properties of sodium silicate solutions, including viscosity and speciation of silicates, are highly dependent on the Si/Na ratio of the solution [24,25]. As Si/Na increases, the number of Q^0 and Q^1 Si sites (monomeric and dimeric silicates) decreases rapidly [25]. This can cause a large change in gel microstructure[1], as aluminate anions react preferentially with silicate anions of lower connectivity [26]. In fact, Duxson et al. [1] state that silicate speciation in the activating solution is probably more important than the absolute silicate concentration in determining the gel's microstructure.

Much attention as been paid to factors impacting dissolution of various silicate and aluminate-bearing phases from fly ash and to the effect of bulk Si/Al ratio of the system on engineering properties. The development of the "solid" gel from the liquid phase has been explored only briefly, however, and is critical in developing a full understanding of the factors influencing engineering properties [4]. Linking bulk Si/Al ratio directly to engineering properties is often futile because of the difficulties in deconvoluting the effects of the many variables discussed hitherto. The current study addresses that challenge by mixing solutions containing fully dissolved reagent grade silicates and aluminates, eliminating the complex variables that lead to a given aqueous phase composition. This approach allows complete stoichiometric control over the solution composition to elucidate directly the development of N-A-S-H structure and composition as it relates to a given solution composition.

Clearly, there are a lot of factors that come in to play when it comes to linking the properties of solid precursors to the engineering properties of IPBs for a given set of processing conditions. Thermodynamic models, which require reliable solubility data to develop, can help predict final phases assemblages and pore solution chemistry based on solid precursor properties and processing conditions. This could allow for the rapid selection of promising precursor materials and streamline the process of optimizing process conditions for a given solid precursor.

The work presented here focuses on understanding the composition and solubility relations of N-A-S-H and thus emphasizes the relationship between the product phases and the solution resulting from alkaline hydrolysis of the aluminosilicate solid. It is important to note that to successfully model the reaction from the precursor aluminosilicate powder and activating solution to the balance of product phases, an understanding is needed of how the oversaturated solution develops over time as a result

of the dissolution of soluble phases from the source material. Many factors can affect the rate and extent of dissolution of the source material aluminosilicate phases. The extent of dissolution, for example, decreases with increasing Si/Na ratio (at constant NaOH concentration) due to the resulting drop in pH and increase in viscosity [1,23].

2.3 Previous Thermodynamic Models and Solubility Measurements for Cementitious Phases

Thermodynamic models for C-S-H, the primary binding phase in portland cement, have been presented previously [10,15,27]. C-S-H solubility has been studied experimentally as well [28–30], and is important in predicting both mechanical properties and durability of portland cement concrete. More recently, several studies have been published related to the solubility and thermodynamics of C-A-S-H [16–19,31]. C-A-S-H is one of the primary binding phases existing in both portland cement-based systems with aluminum-bearing supplementary cementitious materials, and, in high-calcium inorganic polymer binders.

Lothenbach et al. [15] developed a thermodynamic model to predict the effect of temperature on the temporal development of phase composition and porosity for hydrated portland cements, and successfully linked the modeled porosity to compressive strength. Sugiyama and Fujita [32] developed a model that could predict both the dissolution and precipitation of C-S-H with changing Ca/Si ratio. Berner [33], using solubility data for C-S-H from the literature, successfully modeled the degradation of portland cement exposed to groundwater with and without radioactive waste.

To measure the solubility of C-S-H experimentally, several approaches have been taken. Macphee et al. [29] prepared C-S-H in two different ways: by dissolving lime and silicic acid in sodium hydroxide or potassium hydroxide solutions, and by hydrating tricalcium silicate (C_3S, one of the key phases in anhydrous portland cement, in sodium

hydroxide solutions. Ramachandram and Grutzeck [34] measured the effect of pH on C-S-H solubility by suspending C_3S in solutions of sodium hydroxide. Atkinson et al. [30] directly reacted colloidal SiO_2 with $Ca(OH)_2$ to form C-S-H, and once again, measured the composition of the resulting solid phases and supernatant solution.

C-A-S-H solubility has been measured experimentally by L'Hopital et al. [31] and Myers et al. [16,18]. Both took a similar approach, dissolving amorphous SiO_2, CaO (obtained by calcining $CaCO_3$), and $CaO{\bullet}Al_2O_3$ in Milli-Q water and measuring the composition of the precipitated C-A-S-H phases as well as supernatant ion concentrations. Myers et al. [19] then used these data to develop a model describing the formation of various phases in the C-A-S-H systems.

García-Lodeiro et al. [35,36] created synthetic N-A-S-H phases by combining sodium aluminate, sodium silicate, and sodium hydroxide, with the aim of studying the effects of adding calcium, specifically on the stability of C-A-S-H versus N-A-S-H in alkaline aluminosilicate systems containing both sodium and calcium. While they didn't specifically study the solubility of the synthesized phases, their work represents an important contribution towards the understanding of IPBs containing moderate to high levels of calcium.

2.4 General Considerations for Method Development

There are some general considerations that were taken into account when developing the method presented in this study. Those considerations are discussed briefly in this section with the hope that it will help researchers understand the implications of modifying the method for measuring solubility presented here, or, help them create a new method altogether.

One of the most important considerations is ensuring that all work with solutions at high pH is conducted in a CO_2-free environment, preferably an N_2-filled glovebox. It is well known that aqueous solutions with high pH readily absorb CO_2, forming carbonic acid, which can quickly reduce the pH of the solution [37]. Additionally, carbonate-bearing phases, such as sodium carbonate, can form if CO_2 is introduced to the system. While having some carbonates in the system may be more realistic, their effect is hard to control and quantify. A better approach is to measure solubility in a CO_2-free system, and then study the effects of adding CO_2 by introducing it in a controlled manner by maintaining a constant CO_2 concentration and monitoring the CO_2 levels. In fact, this will be a necessary step toward modeling real-world IPBs.

A second important consideration in any experiment where dissolved Na^+, Si^{4+}, or Al^{3+} are measured, especially at high pH, is that silicate glasses dissolve readily at high pH [24,38]. As such, glass labware should be avoided at all costs when measuring N-A-S-H solubility, or the solubility of any cementitious phases. Better choices include polypropylene and polyethylene, but labware made from other polymers is available as well. As with any lab work, it is important to understand the stability of the materials used when coming in contact with the chemicals needed for the given experiment.

Finally, the final measured ion concentrations that are used to calculate solubility are only as accurate as the dilution factors, so it is highly preferable to measure dilution factors gravimetrically. This is especially important when measuring solubility at temperatures that vary significantly from 25 °C, as volumetric pipettes are designed to operate at standard laboratory temperatures. Significant errors can result from pipetting at temperatures that vary substantially from 25 °C. Volumetric pipettes are a great instrument for transferring an approximate desired amount of solution, but measuring the amount transferred by mass is far more accurate, especially at extreme temperatures.

2.5 RIGOROUS METHOD FOR MEASURING N-A-S-H SOLUBILITY

2.5.1 N-A-S-H synthesis

N-A-S-H samples were prepared by mixing appropriate proportions of de-aired Milli-Q water (Merk Millipore) with 0.2 M H_4SiO_4 (0.2 M Si^{4+}) and 0.1 M $Na_2Al_2O_4$ (0.2 M Al^{3+}) solutions in an N_2-filled glove box to achieve a nominal pH of 14 (1 M NaOH) and bulk molar Si/Al ratios between 1 and 2. Various studies in the literature have aimed at optimizing inorganic polymer composition have reported optimum molar Si/Al ratios in the range of 1 to 2 [2,23,39,40]. In the most of the experiments whose results are presented in Chapters 3 and 4, the sodium silicate activating solution had a Si/Na molar ratio of 0.1 (2 M NaOH and 0.2 M H_4SiO_4). This ratio was intentionally selected to be low enough so that the dissolved silicate species in this solution would be monomeric [25]. A separate set of samples was prepared with the silicate stock solution Si/Na molar ratio varying from 0.1 to 1.0 and bulk Si/Al varying from 0.89 to 9.58 to investigate the effect of silicate activating solution on N-A-S-H composition. In these experiments, Si/Na was manipulated by increasing the silicate solution Si^{4+} concentration so that the final sodium hydroxide concentration in all samples remained constant (and the same as in the experiments with constant silicate solution Si/Na ratio) at 1 M. The same sodium aluminate stock solution (0.1M sodium aluminate) was used in these experiments as in the previous experiments.

Generally, there are two choices for manipulating the bulk molar ratios in the synthesis of N-A-S-H. The first option is to change the relative volumes of stock solutions that are mixed. This is the preferred method if the effects of bulk compositions, rather than the chemistry of the individual stock solutions, are of interest. The second option is to change relative concentrations of the stock solutions; for example, the Si^{4+} concentration of the sodium silicate solution could be increased, resulting in a higher

sodium silicate Si/Na ratio and a higher bulk Si/Al ratio if the same relative volumes of each stock solution are mixed. This approach is preferred if is desired to study the effects of changing the chemistry of the individual stock solutions.

The synthesis conditions were based loosely on those employed by Myers et al. [18] and L'Hôpital et al. [31] in the synthesis of calcium aluminosilicates. The total volume of solution added to all reactors was 40 mL, 20 mL of which was the sodium silicate stock solution used to achieve a bulk NaOH concentration of 1 M. The volume of sodium aluminate solution was adjusted to control the bulk Si/Al ratio, and the difference in volume was made up with de-aired Milli-Q water.

2.5.1.1 Stock Solution Preparation

Sodium silicate and sodium aluminate stock solutions were prepared in polypropylene (PP) volumetric flasks inside an N_2-filled glovebox. All water was Milli-Q water de-aired by boiling in a glass 2 L Erlenmeyer flask set on a hotplate for ten minutes. The de-air water was then stored for up to 3 months with as little head space as possible in 1 L Pyrex round media storage bottles with tightly fastened screw-on caps.

The sodium silicate stock solution was prepared by dissolving silicic acid (Sigma Aldrich, 20 um, 99.9%, purified by refining) in 5 M sodium hydroxide (Dilut-It, J.T. Baker) and diluting with de-aired Milli-Q water to final concentrations of 2 M sodium hydroxide and 0.2 M silicic acid. The appropriate amount of silicic acid was weighed outside the glovebox, and transferred into the glovebox in a sealed container along with the 5 M sodium hydroxide and de-aired water. Once in the glovebox, 200 mL of 5 M sodium hydroxide was added to a 1 L polymethylpentene volumetric flask, followed by the pre-weighed silicic acid. The flask was then capped and inverted 25 times, after which a stir bar was added, and the flask was filled to approximately 900 mL with de-

aired water. The flask was then placed on a stir plate (still inside the glovebox) and stirred for 24 hours. Then, the stir bar was removed, and the flask filled with de-aired to the 1 L mark, accounting for the water that had been displaced by the stir bar. Finally, the flask was capped and again inverted 25 times, and the solution was transferred to 500 mL high-density polyethylene (HDPE) bottles with screw-on caps for storage inside the glove box until ready for use (up to 3 months).

Silicic acid is hygroscopic, so measuring the silicic acid by weight to achieve exactly 0.2 M SiO_2 was not possible since the amount of water absorbed by the powder was not known. As such, a solution with 2 M NaOH and slightly higher than 0.2 M Si^{4+} was prepared, and its concentration was measured using ICP. When the actual concentration of SiO_2 was known, it could then be diluted to 0.2 M Si^{4+} using 2 M NaOH (diluting the solution that already contained 2 M NaOH with more 2 M NaOH, ensured that the final NaOH concentration was 2 M). The final Si^{4+} concentration was then once again measured and recorded, along with the final Na^+ concentration.

Sodium aluminate solution was prepared at a concentration of 0.1 M by dissolving sodium aluminate (Sigma Aldrich, technical grade, anhydrous; Al: 50-56% as Al_2O_3, Na: 40-45% as Na_2O) in de-aired Milli-Q water. Approximately 500 mL of de-aired water was added to a polymethylpentene 1 L volumetric flask. Sodium aluminate powder that was pre-weighed outside of the glovebox and transferred to the glovebox in a sealed container was then added to the flask. The flask was filled to approximately 900 mL, capped, and inverted 25 times. A stir bar was then added and the solution was stirred for 24 hours at which point the stir bar was removed and the flask was filled to the 1 L mark with de-aired Milli-Q water. The flask was again capped, and once more inverted 25 times. As with the silicic acid, the Al^{3+} concentration of the sodium aluminate concentration was measured, and the solution was diluted to 0.1 M $Na_2Al_2O_4$. The final

Al^{3+} and Na^{+} concentrations were then measured and recorded, and the solution was stored in 500 mL HDPE bottles with screw-on caps for storage inside the glove box until use (up to 3 months).

For both the silicic acid and sodium silicate stock solutions, the 24 hour stir period was deemed to be enough because the concentrations of Si^{4+} and Al^{3+} in aliquots from the respective solutions passed through a 0.2 μm syringe filter did not change between 24 and 48 hours, indicating that there were no particles larger than 0.2 μm remaining in the solution after 24 hours.

2.5.1.2 Combining stock solutions to begin N-A-S-H synthesis

The sodium silicate and sodium aluminate stock solutions were combined in 40 mL Oak Ridge high-speed polpypropylene copolymer centrifuge tubes with screw-on tops to achieve bulk Si/Al molar ratios between 1 and 2. The volume of sodium silicate solution was 20 mL in all reactors, and the volume of sodium aluminate required to reach the desired bulk Si/Al was calculated using the measured values of Si^{4+} and Al^{3+} concentrations. Milli-Q water was then added to reach a total volume of 40 mL. The sodium silicate stock solution, then, made up half the volume of solution in each reactor. Concentrations of NaOH and Si^{4+} in the sodium silicate stock solution were 2 M and 0.2 M, respectively, so the bulk concentrations in each reactor were 1 M NaOH and 0.1 M Si^{4+}. The stock solutions were added to each reactor by volume, using a volumetric pipette, but the mass of each addition was recorded to more accurately determine bulk concentrations.

To prepare each reactor, the mass of the empty vessel was first recorded to the nearest mg. Then, inside the N_2-filled glovebox, 20 mL of the sodium silicate stock solution was added to the reactor vessel. At the same time, the appropriate volume of the

sodium aluminate stock solution was added to a separate vessel, either a 15 mL or 50 mL PP centrifuge tube (the sodium aluminate vessel was not weighed empty until after mixing of the stock solutions, discussed later in this section). The appropriate amount of de-aired Milli-Q water was added by volume to a third vessel, a 15 mL PP centrifuge tube (there was no need to weigh this vessel). All three vessels were then sealed tightly and removed from the glovebox, and the mass of the sodium silicate and sodium and aluminate vessels were recorded to the nearest mg. The three vessels were then placed in an oven or temperature-controlled room at 4, 25, 50, or 70 °C (matching the reaction temperature for the given experiment) for two hours, long enough for the temperature of the solutions to equilibrate.

Once the temperature of solutions in all three vessels reached the reaction temperature, they were placed in a cooler and transported back to the glovebox. Inside the glove box, the sodium aluminate solution and de-aired Milli-Q water were carefully poured in the reaction vessel, which already contained the sodium silicate solution. Care was taken to make sure that all of the sodium aluminate solution and Milli-Q water made it into the reaction vessel. The reaction vessel was sealed tightly and removed from the glove box along with the now empty sodium aluminate vessel, and both were once again weighed to the nearest mg. The seam of the reaction vessel was sealed with paraffin film as an added protective measure against CO_2 contamination, and the vessel was returned to the temperature-controlled environment at the reaction temperature and placed on a rotisserie, rotating continuously at 8 rpm. At any given temperature and composition, multiple reactors were prepared in this way simultaneously so that a fresh sample could be analyzed at each time point of the experiment. Since N-A-S-H equilibration times can be very long, especially at lower temperatures, extra samples were prepared beyond the samples that were expected to be analyzed at the multiple time points.

At this point, the mass of the following was recorded: (1) empty reaction vessel, (2) reaction vessel with sodium silicate solution, (3) empty sodium aluminate vessel (measured after emptying the solution into the reaction vessel), (4) sodium aluminate vessel with the sodium aluminate solution, and (5) the reaction vessel with sodium silicate, sodium aluminate, and de-aired Milli-Q water. The mass of sodium silicate solution was determined by subtracting (1) from (2); the mass of sodium aluminate solution was determined by subtracting (3) from (4), and the total solution mass was determined by subtracting (1) from (5). Knowing the mass of sodium silicate solution, sodium aluminate solution, and the overall mass of the sample, along with the Si^{4+} and Na^{+} concentrations in the sodium silicate solution as well as the Al^{3+} and Na^{+} concentrations in the sodium aluminate solution, the initial concentrations of Si^{4+}, Al^{3+}, and Na^{+} in each reactor could be accurately determined.

2.5.1.3 Determining equilibration times

The reactors were rotated continuously at 8 rpm and supernatant Si^{4+} and Al^{3+} concentrations were monitored over time using ICP-OES to determine how long it would take the precipitated N-A-S-H to equilibrate. Since there was little information available about equilibration times for N-A-S-H, the selection of initial time points for each temperature were based on the equilibration times for C-A-S-H at various temperatures reported by Myers et al. [18]. Those C-A-S-H equilibration times were 1 year at 7 °C, 182 days at 20 °C, and 56 days at 50 °C and 80 °C and were chosen based on changes (<25%) in dissolved Si^{4+}, Al^{3+}, and Ca^{2+} concentrations. In the study on N-A-S-H presented here, several time points were chosen between 0 days and the anticipated equilibration time to better understand the path to equilibrium and because it was not known whether equilibration times for N-A-S-H would match equilibration times for C-

A-S-H. The time points when the supernatants were analyzed for Si^{4+} and Al^{3+} concentrations in the study presented here were 83, 211, and 407 days at 4 °C, 28, 57, 84, 112, 137, and 183 days at 25 °C; 3, 7, 10, 14, 29, and 56 days at 50 °C; and 7, 14, and 28 days at 70 °C. At all concentrations and temperatures, there was less than a 10% change in Si^{4+} and Al^{3+} concentrations before the last two time points, and the final time point was taken as the equilibrium time for each temperature. Since the focus of this study was on the equilibrium conditions, after the initial path and time to equilibrium was understood, replicate samples were generally only analyzed at the equilibrium time.

2.5.2 Measuring Na^{+}, Si^{4+}, and Al^{3+} concentrations with ICP

2.5.2.1 ICP sample preparation

At each of the time points described in section 5.1.3, aliquots of supernatant were prepared for ICP to measure Si^{4+}, Al^{3+}, and Na^{+}. The aliquots were filtered, diluted and acidified with 3% nitric acid, all inside the N_2-filled glovebox. Care was taken to maintain the reactors at the reaction temperature during the process, and dilution factors were determined by mass since errors in pipetting are higher when solution temperatures are further from room temperature. This section describes the sample preparation methodology in detail.

All labware used for the dilution and storage of samples for ICP was acid washed. This was accomplished by rinsing seven times with deionized (DI) water, then submerging the labware completely in a 20% (v/v) nitric acid bath for at least 8 hours. The labware was then once again rinsed seven times using DI water, then 2 additional times with Milli-Q water, and finally, air-dried. The 3% (v/v) nitric acid used for dilution was prepared in advance using Milli-Q water (not de-aired since carbonation is not a concern at low pH) and trace metal grade nitric acid. The 3% nitric acid was prepared and

stored for up to 6 months in a 10 L HDPE carboy, the inside of which was initially allowed to soak with 20% (v/v) nitric acid for 8 hours.

While the dilutions were performed volumetrically, dilution factors were measured gravimetrically for improved accuracy. Since supernatant dissolved Na^+ concentrations were on the order of 1 M compared to dissolved Si^{4+} and Al^{3+} concentrations, which were general less than 0.1 M, different dilution factors had to be used to bring the concentrations in a measurable range. Aliquots were diluted approximately 1000x for measurement of Na^+ concentrations, and approximately 100x for measurement of Si^{4+} and Al^{3+} concentrations. For both, 100 μL of filtered sample was diluted into the appropriate amount of 3% nitric acid to achieve the desired dilution factor. As such, 1000x dilutions for Na^+ concentration measurements were carried out in 125 mL HDPE narrow-mouth bottles, while 100x dilutions for Si^{4+} and Al^{3+} concentration measurements were carried out in 15 mL PP centrifuge tubes. Prior to the dilution, the empty dilution vessels were weighed, with the cap on, to the nearest 0.1 mg[1]. Then, 99 grams of 3% nitric acid were added to the 125 mL vessel, and 9.9 mL of 3% nitric acid were added to the 15 mL vessel. At the same time, 9.9 mL was added to an extra 15 mL PP centrifuge tube to use as a blank. Again, both dilution vessels were weighed, with the caps on, to the nearest 0.1 mg.

The reactors were then quickly transported from the rotisserie in the temperature controlled environment to the N_2-filled glovebox in a cooler to keep them as near to the reaction temperature as possible. The dilution vessels were transferred inside the glovebox at the same time as the reactors. Once inside the glovebox, the reactors were immediately placed in a dry bath incubator that was already equilibrated to the reaction

[1]As a practical note, it was found that wearing cotton gloves instead of standard laboratory gloves while weighing PP or HDPE vessels significantly reduced the effects of static electricity-induced drift.

temperature of the current experiments. The dry bath incubator ensured that the samples remained at the reaction temperature until the dilutions were performed.

Once the reactors were in the dry bath incubator, the cap of one of the reactors was removed, and a 6 mL syringe was used to draw up about 1 mL of supernatant from the top of the reactor. Then, a 0.2 μm polyvinylidene fluoride syringe filter was placed on the syringe, and the supernatant was transferred into a separate acid-washed 15 mL PP centrifuge tube. From there, 100 μL of filtered supernatant was pipetted into the 125 mL dilution vessel (which already contained 99 g 3% nitric acid), and another 100 μL of filtered supernatant was pipetted into the 15 mL dilution vessel (which already contained 9.9 mL 3% nitric acid). Both dilution vessels were immediately inverted 25 times, and the diluted samples were removed from the glove box and once again weighed to the nearest 0.1 mg, then stored up to 3 months prior to ICP analysis.

2.5.2.2 ICP standard preparation

Two sets of standards were used for the measurement of dissolved Si^{4+}, Al^{3+}, and Na^{+} in the filtered, diluted, and acidified supernatants. The most important consideration when preparing ICP standards is that the matrix of the standard set closely matches the matrix of the sample being analyzed. For the samples prepared to measure Na^{+} concentrations, which had been diluted 1000x, Na^{+} concentrations were on the order of 1 mM, and Si^{4+} and Al^{3+} concentrations were less than 0.1 mM. Since the background ion (Si^{4+} and Al^{3+}) concentrations were so low in the Na^{+} samples, it was assumed that they did not need to be included in the standard matrix. This assumption was tested, and found to be valid, using the method of standard additions [41], a method commonly used to asses the extent of matrix effects. For the samples prepared to measure Si^{4+} and Al^{3+}, on the other hand, Na^{+} concentrations were approximately 10 mM, so Na^{+} had to be added to

the standard (in the form of NaOH). For these samples, a combined standard was prepared to measure Si^{4+} and Al^{3+}. Again, the method of standard additions was used to make sure the matrix effects were accounted for properly and to ensure that the Si^{4+} and Al^{3+} were not interfering with each other. Both sets of standards were prepared with a 3% nitric acid matrix to match the diluted, acidified samples.

All standards were prepared gravimetrically in 125 mL HDPE narrow-mouth bottles by adding predetermined amounts of concentrated nitric acid, 2 M sodium hydroxide (Si^{4+} and Al^{3+} combined standards only), and reference standards to Milli-Q water. The reference standards were 1000 µL/mL Na^{+} in a 0.1% (v/v) nitric acid matrix (Inorganic Ventures), 1000 µL/mL Si^{4+} in a 0.2% (w/v) sodium hydroxide matrix (Inorganic Ventures), and 1000 µL/mL Al^{3+} in a 0.1% (v/v) nitric acid matrix (Inorganic Ventures).

The total mass of each standard solution was 99 g. From the total solution weight, the weight of reference standard to achieve the desired standard concentration could be calculated. Since the reference standards included their own matrix (nitric acid for Na^{+} and Al^{3+} reference standards, sodium hydroxide for Si^{4+} reference standard), the amounts of matrix compounds from the added reference standards were determined and subtracted from the amount of additional nitric acid or sodium hydroxide that would be added. As a result, the total final matrix concentrations matched between standards, even though different amounts of reference standards were added for each sample. Once the amounts of concentrated nitric acid or sodium hydroxide added to each standard were determined, the total mass of nitric acid, sodium hydroxide, and reference standard were subtracted from the total target solution mass (99 g), to determine the amount of Milli-Q water needed to reach 99 g solution.

While the calculations were performed gravimetrically, reference standards and matrix components were added by volume using a volumetric pipette. Water was added by mass because the amount of water was generally greater than 90 g, so pipetting the water was impractical. For all standards, water was added first, followed by the nitric acid. This ensured that even after adding the reference standards and matrix sodium hydroxide, the pH remained low enough to dismiss any concerns about carbonation. Finally, the sodium hydroxide and reference standards were added. After each addition, the weight was recorded (to the nearest 0.1 mg), and the bottle was inverted 25 times. Sodium hydroxide and the Si^{4+} standard (with sodium hydroxide matrix) were added inside the glovebox to avoid carbonation. The final concentrations were determined based on the mass of reference standard added and based on the final solution mass (determined by subtracting the mass of the empty bottle from the final total mass).

The target standard concentrations for Na^{+} standards and combination Si^{4+} and Al3+ standards are shown in Tables 2.1 and 2.2, respectively. These concentrations were chosen based on several considerations. First, the upper and lower detection limits for the ICP instrument were considered (this was an important factor in determining the sample dilution factors, as well). Second, the concentration of diluted samples were considered and were anticipated to fall between 10 and 40 μg/g for Na^{+}, 0.75 and 30 μg/g for Si^{4+}, and 0.2 and 10 μg/g for Al^{3+}. It was desired that at least 4 standards, in addition to the blanks (Na-0 and C-0), were used to analyze each sample. Because of the wide range of Si^{4+} and Al^{3+} concentrations, nine standards were prepared in addition to the blank. When Si^{4+} concentrations fell below 6 μg/g, standards C-1 to C-5 were used for Si^{4+} concentration calculations, and when Si^{4+} concentrations fell above 6 μg/g, standards C-5 to C-9 were used for Si^{4+} concentrations. Likewise, when Al^{3+} concentrations fell below 1.75 μg/g, standards C-1 to C-5 were used for Al^{3+} concentration calculations, and when

Al^{3+} concentrations fell above 1.75 µg/g, standards C-5 to C-9 were used for Al^{3+} concentrations.

Table 2.1: ICP standard target concentrations for determining supernatant dissolved sodium concentrations

Std ID	$[Na^{+}]$, µg/g
Na-0	0
Na-1	10
Na-2	20
Na-3	30
Na-4	40

Table 2.2: ICP standard target concentrations for determining supernatant dissolved silicon and aluminum concentrations

Std ID	$[Si^{4+}]$, µg/g	$[Al^{3+}]$, µg/g
Std C-0	0	0
Std C-1	0.75	0.2
Std C-2	1.5	0.5
Std C-3	3	0.75
Std C-4	4.5	1.25
Std C-5	6	1.75
Std C-6	7.5	2.5
Std C-7	15	5
Std C-8	22.5	7.5
Std C-9	30	10

2.5.2.3 ICP data collection and analysis

Supernatant Na^{+}, Si^{4+}, and Al^{3+} concentrations were determined using a Varian 10-ES ICP-OES with a SPS 3 autosampler and *ICP Expert II* software (v 1.1). For both standards and samples, for Na^{+}, intensities of two wavelengths were measured (568.821 and 589.592 nm), while for Si^{4+} and Al^{3+}, the intensities of three wavelengths were measured for each (185.005, 250.690, 251.611 nm for Si^{4+}; 237.312, 394.401, 396.152 nm for Al^{3+}). At each wavelength, intensities were taken in triplicate, and the average of

the three intensities was used to determine the ion concentrations. A separate calibration curve was prepared for each wavelength, where the average measured intensities of the calibration curves were plotted against their calculated concentrations. Microsoft Excel's LINEST function was used to determine the slope and intercept of each calibration curve, which were in turn used to calculate the ion concentrations in the diluted samples from the measured sample intensities. The average of the ion concentrations for all wavelengths for a given element in a particular sample was taken as the diluted sample concentration, and multiplying by the measured dilution factor gave the original supernatant ion concentration.

2.5.3 Solid composition measurements

In addition to supernatant Na^{+}, Si^{4+}, and Al^{3+} concentrations, the relative elemental compositions of the precipitated N-A-S-H phases were required in order to calculate solubility products. To determine the N-A-S-H Si/Al compositions, a mass balance approach was taken. Changes in the supernatant Si^{4+} and Al^{3+} concentrations between the initial concentrations and the equilibrium concentrations were determined by subtraction. The difference in concentrations was the relative amount of that element that was determined to have precipitated out of solution. For example, if the bulk Si/Al concentration was 2 with initial supernatant Si^{4+} concentration of 200 mM and initial Al^{3+} concentration of 100 mM, and equilibrium supernatant concentrations were measured as 50 mM and 20 mM for Si^{4+} and Al^{3+}, respectively, then 150 mmol of Si^{4+} would have fallen out of solution per liter of solution while 80 mM of Al^{3+} would have fallen out. The elemental molar ratio in the solid for this example would then be calculated as 150 divided by 80, or 1.88.

To validate the mass balance approach for determining the relative Si and Al concentrations in the N-A-S-H phases, some of the solids were centrifuged, freeze-dried, and digested using a mixture of hydrofluoric and hydrochloric acids and analyzed by ICP to determine the solid composition. The solids were triple-rinsed with Milli-Q water by dispersing them in the water, centrifuging at 3000 g for 10 minutes, and decanting. They were then frozen with liquid N_2 for 5 minutes, freeze dried at -50 °C and 5 Pa for 48 hours using a Labconco Freezone Bulk Tray Dryer and stored at -20 °C under N_2 until further analysis.

The solids were digested following a detailed protocol developed by Inorganic Ventures specifically for the compositional analysis of zeolites. The protocol uses two premixed, proprietary solutions: (1) Inorganic Ventures UA-1, comprised of proprietary proportions hydrofluoric and hydrochloric acids to digest the solids, and (2) Inorganic Ventures UNS-1, comprised of proprietary proportions of triethanolamine and triethylenetetramine to buffer the acids used for digestion. To perform the digestion, 80 to 100 mg of freeze-dried solids were weighed to the nearest 0.1 mg and added to a polyethylene bottle. Ten drops of deionized water were then added to the solids, and the bottle was swirled to hydrate the surface of the solids. Next, 10 mL of UA-1 and 0.5 mL of concentrated nitric acid (trace metal grade, Fisher) were added and the vessel was capped and shaken for 3 minutes (at this point, the solid appeared completely dissolved to the naked eye). The resulting solution was neutralized by adding 50 mL of UNS-1, and the final solution weight was adjusted to 500 g using deionized water. Finally, the solution was analyzed using ICP in the same way that supernatant concentrations were measured (described previously).

Unfortunately, relative Na concentrations in the solids could not be determined by mass balance or by hydrofluoric acid digestion with ICP. They could not be determined

by mass balance because the relative changes in supernatant Na^+ concentrations were too small compared to the initial Na^+ concentrations, since initial Na^+ concentrations were on the order of 1 M. The N-A-S-H relative Na concentrations could not be determined by ICP analysis, either, because there were matrix issues with the hydrofluoric acid and buffers that prevented linear calibration curves from being established, despite substantial effort. Instead, the molar fractions of Na_2O were assumed to be equal to the molar fractions of Al_2O_3 for each sample (i.e. $Na_2O/Al_2O_3 = 1$) based on the assumption that sodium is present as a charge balancing cation to alumina tetrahedra, which carry a -1 charge [1].

The water contents of N-A-S-H phases were determined by TGA. The solids were vacuum-filtered using nylon filter membranes with a pore size of 0.45 μm and a diameter of 47 mm. While on the filter, with the vacuum running, the soils were triple washed with DI water, and then allowed to sit, with the vacuum running, for 5 minutes to remove excess water. They were then stored, for a maximum of 7 days, under N_2 at 4 °C until undergoing TGA. Thermogravimetric data were collected using a Mettler Thermogravimetric Analyzer, Model TGA/DSC 1 with a sensitivity of 2 μg. The vacuum-filtered samples were equilibrated at 40 °C for one hour and then heated from 40 °C to 600 °C under N_2 at a flow rate of 20 ml/minute with a heating rate of 20 °C/minute in pure aluminum oxide crucibles. The 40 °C equilibration period was to allow for the evaporation of excess water so that the water content contained in the solid phases could be accurately quantified.

2.5.4 Solubility product calculations

To determine solubility products for N-A-S-H synthesized at bulk Si/Al molar ratios between 1 and 2 reacted at 4, 25, 50, and 70 °C, an ion activity product (IAP) was calculated for each of the equilibrated N-A-S-H phases.

The dissolution reaction assumed to calculate solubility products is shown in Equation (2.5):

$$NaAlSi_xO_{(2x+2)} \cdot (H_2O)_{y(S)} + (2x - y - 2)H_2O_{(l)} + 4H^+_{(aq)} \leftrightarrow \mathrm{Na}^+_{(aq)} + Al^{3+*}_{(aq)} + xH_4SiO^o_{4(aq)} \quad (2.5)$$

where x is the Si/Al molar ratio of the solids and y is the stoichiometric coefficient of H_2O in the solids. Here, $\mathrm{Al}^{3+*}_{(aq)}$ refers to the specific species, where previously, $\mathrm{Al}^{3+}_{(aq)}$ referred to the total dissolved aluminum. Following the reaction in Equation (2.5), equilibrium solubility products were calculated with Equation (2.6):

$$K_{sp} = \left\{\mathrm{Na}^+_{(aq)}\right\} \cdot \left\{\mathrm{Al}^{3+*}_{aq}\right\} \cdot \left\{\mathrm{H_4SiO^o_{4(aq)}}\right\}^x \cdot \left\{\mathrm{H}^+_{(aq)}\right\}^{-4} \cdot \left\{\mathrm{H_2O}_{(l)}\right\}^{(y-2x+2)} \quad (2.6)$$

Activities of $\mathrm{Na}^+_{(aq)}$, $\mathrm{Al}^{3+*}_{(aq)}$, $\mathrm{H_4SiO^o_{4(aq)}}$, $\mathrm{H}^+_{(aq)}$, and $\mathrm{H_2O}_{(l)}$ were determined with PHREEQC using the measured supernatant concentrations of $\mathrm{Na}^+_{(aq)}$, $\mathrm{Si}^{4+}_{(aq)}$, $\mathrm{Al}^{3+}_{(aq)}$ with the pH calculated from charge balance. It should be noted that in Equations (2.5) and (2.6), $\mathrm{Al}^{3+}_{(aq)}$ refers to the specific species, where previously it referred to the total dissolved aluminum. An attempt was made to measure pH experimentally, but between the combination of very high pH (close to 14), very high sodium concentrations (on the order of 1 M), and the high variation in temperatures (4 to 70 °C), reliable pH values could not be measured. In fact, the variation in pH values measured for a given sample was greater than the difference in pH between samples.

The Truesdell-Jones version of the extended Debye-Hückel equation was used within PHREEQC with the LLNL database to determine activity coefficients of each species, shown in Equation (2.7):

$$log\gamma_i = \frac{-Az_i^2\sqrt{I}}{1+B\alpha_i\sqrt{I}} + bI \tag{2.7}$$

where γ_i is the activity coefficient of ion "*i*", *A* and *B* are Debye-Hückel parameters based on the dielectric constant of water and the temperature, z_i is the ion valance, α_i is a parameter accounting from the ionic radius, *b* is an empirical parameter, and *I* is the ionic strength of the solution. Robinson and Stokes [42] found that the Truesdell-Jones extension of the Debye-Hückel equation predicts activity coefficients consistent with experimental data for ionic strengths up to at least 1 M. In the study presented here, ionic strengths were very near 1 M for all samples (see Appendix A) and fall at the upper limit of Truesdell-Jones applicability. The Pitzer model is often used to determine activity coefficients of solutions with high ionic strength, and would have been a suitable choice here except for the fact that it lacks a mechanism to account for changes in temperature [43].

2.6 CONCLUSIONS AND FUTURE WORK

A rigorous method for measuring the solubility of N-A-S-H phases experimentally has been presented in detail. Following this method, N-A-S-H was synthesized by mixing solutions of sodium silicate, sodium aluminate, and sodium hydroxide. The solubility data obtained following this method are presented in Chapters 3 and 4, and are limited to pH of approximately 14 and bulk Si/Al ranging from 1 to 2. To

build on this new database of N-A-S-H solubility data, future research should be conducted, expanding to a wider range of pH and compositions.

In addition to presenting the detailed method for measuring N-A-S-H solubility, the need for solubility data and thermodynamic models for N-A-S-H was discussed. Previous literature relating to the solubility and thermodynamic models of C-S-H and C-A-S-H was also reviewed, and some general considerations for developing the method were discussed.

There is some room for improvement in the method itself, and the hope is that future research will use this method as a starting point, expanding and improving upon it continually. Specifically, the method for determination of solid N-A-S-H composition can be improved upon, especially with regards to sodium concentration. Ideally, the relative sodium composition in N-A-S-H phases could be determined by hydrofluoric acid digestion with ICP analysis. A substantial effort was placed on achieving reliable sodium contents in this way in the study presented here, but the complex matrix that resulted from the digestion itself proved to be difficult to account for.

Chapter 3: The Relationship Between Aqueous Chemistry and Composition, Structure, and Solubility of N-A-S-H

3.1 INTRODUCTION

Inorganic polymer binders (IPBs), also known as geopolymers, are a new class of construction materials that have received substantial attention in the scientific literature recently owing to their potential to serve as a low-energy, low-CO_2 alternative to ordinary portland cement (OPC) [1,44,45]. These binders are synthesized by the activation of an aluminosilicate powder by a highly alkaline aqueous solution, most commonly sodium or potassium hydroxide. Bulk Si/Al, Na/Al, and H_2O/Na ratios, as well as activator Si/Na ratios, are considered the most important compositional parameters, and activating solutions with pre-dissolved silica are often used to achieve target compositions [2,20,46]. Fly ash, which has been used extensively as a partial replacement for OPC in concrete for years, is one of the most promising aluminosilicate source for IPBs since it is available on a large-scale at relatively low cost with the added motivator of diverting fly ash from landfills. Fly ash-based IPBs (often referred to in the literature as alkali-activated fly ash, AAFA) are the primary focus of the research presented here, although much of the discussion is relevant to IPBs based on other aluminosilicate sources (ex. metakaolin).

An extensive body of research has demonstrated comparable mechanical properties (compressive strength, stiffness) [2–4,40] as well as superior dimensional stability [5,47] and durability (resistance to corrosion, alkali-silica reaction, acid attack) [6–8,13,48] of IPB concrete compared to OPC concrete. Much of the existing research, however, has focused on the characterization and evaluation of a variety of aluminosilicate sources with significant levels of variation (in both composition and solubility) from one source to the next and inhomogeneity within a given source; our

understanding of basic mechanisms that govern product formation, microstructure development and, ultimately, engineering properties has advanced significantly, but substantial progress in our understanding of the chemistry is still required [49].

The general process of alkali-activation of aluminosilicate solids is shown schematically in Figure 3.1. The process begins with rapid dissolution of the initial solid particles (Figure 3.1A) through alkaline hydrolysis leading to a highly concentrated aqueous solution containing sodium, $Al(OH)_4^-$, and various silicate species depending on the solution pH and Si/Na ratio (Figure 3.11B). As the solution becomes saturated with respect to binding phases, the hydrolyzed silicate and aluminate species polymerize, condense, and precipitate (Figure 3.1C). Previous literature has paid much attention to factors impacting dissolution of various silicate and aluminate-bearing phases from fly ash and to the effect of bulk Si/Al ratio of the system on engineering properties [50–52]. The development of the solid binding phase from the liquid phase has been explored only briefly, however, and is critical in developing a full understanding of the factors influencing engineering properties [4]. Linking bulk Si/Al ratio directly to engineering properties is often futile because of the difficulties in deconvoluting the effects of the many variables discussed hitherto. The current study addresses that challenge by mixing solutions containing fully dissolved reagent grade silicates and aluminates, eliminating the complex variables that lead to a given aqueous phase composition. This approach allows complete stoichiometric control over the solution composition to elucidate directly the development of N-A-S-H structure and composition as it relates to a given solution composition.

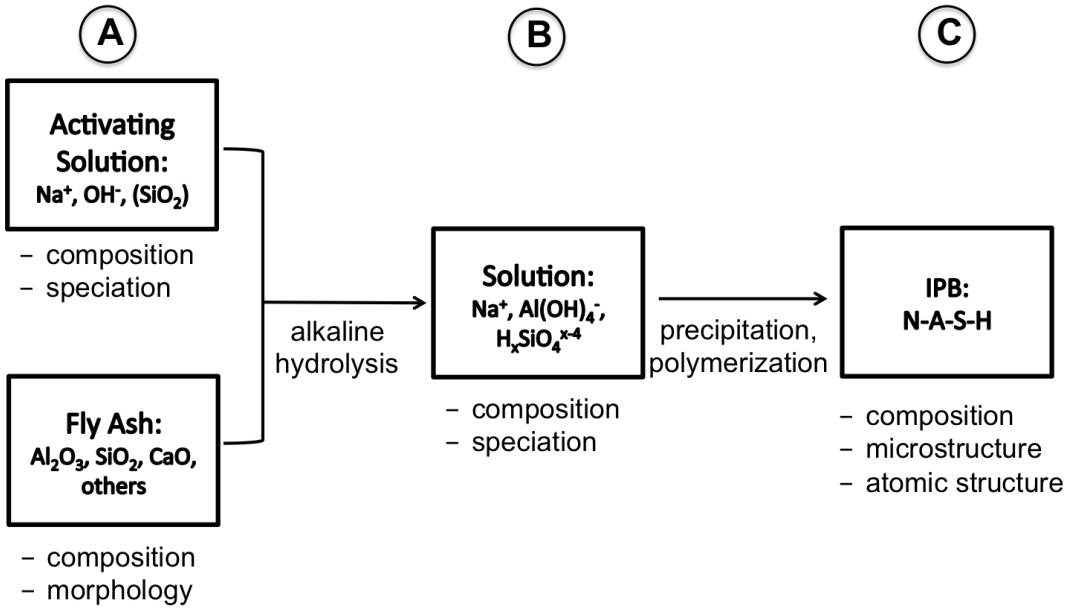

Figure 3.1: Schematic illustration of the IPB precursor to product reaction pathway

The research presented here sought to transform our ability to use OPC-free IPBs by investigating the relationship between pore solution composition on the composition, structure, and solubility of N-A-S-H. To this end, N-A-S-H was synthesized from reagent grade materials across a range of compositions, allowing complete stoichiometric control of the constituents by eliminating variability in the composition and solubility of solid precursors. N-A-S-H composition was determined by mass balance and thermogravimetric analysis (TGA). Nuclear magnetic resonance (NMR) spectroscopy and x-ray diffraction (XRD) were applied to probe the atomic structure of N-A-S-H as a function of solution composition. Additionally, temperature-dependent solubility products (K_{sp}) of N-A-S-H were determined by monitoring the ionic concentration of the supernatant solution over time using inductively coupled plasma optical emission spectroscopy (ICP-OES). The resulting understanding of product composition and structure will be useful in predicting performance of IPBs made from commercial fly

ashes across a range of compositions, while solubility data are critical for the development of thermodynamic models describing IPB product development.

3.2 MATERIALS AND METHODS

3.2.1 N-A-S-H synthesis

N-A-S-H samples were prepared by mixing appropriate proportions of de-aired (by boiling for 10 minutes) Milli-Q water (Merk Millipore) with sodium silicate and sodium aluminate solutions in an N_2-filled glove box to achieve bulk molar Si/Al ratios of 1, 1.5, and 2. Various studies in the literature have aimed at optimizing inorganic polymer composition have reported optimum molar Si/Al ratios in the range of 1 to 2 [2,23,39,40]. The sodium silicate activating solution had a Si/Na molar ratio of 0.1. This ratio was intentionally selected to be low enough so that the dissolved silicate species in this solution would be monomeric [25].

The synthesis conditions were based loosely on those employed by Myers et al. [18] and L'Hôpital et al. [31] in the synthesis of calcium aluminosilicates. Sodium silicate solution was prepared by dissolving silicic acid (20 μm, Sigma-Aldrich) in 5 M sodium hydroxide (Dilut-It, J.T. Baker) and diluting with de-aired Milli-Q water to final concentrations of 2 M sodium hydroxide and 0.2 M silicic acid. Sodium aluminate solution was prepared at a concentration of 0.1 M by dissolving sodium aluminate (Sigma-Aldrich) in de-aired Milli-Q water. The final solution volume in all reactors was 40 mL, and all contained 20 mL of the sodium silicate activator so that the final sodium hydroxide concentration in all samples was approximately 1 M. All stock solutions were allowed to equilibrate for at least 24 hours prior to mixing them at the start of each experiment.

A separate set of samples was prepared with the silicate stock solution Si/Na molar ratio varying from 0.1 to 1.0 and bulk Si/Al varying from 0.89 to 9.58 to investigate the effect of silicate activating solution on N-A-S-H composition. In these experiments, Si/Na was manipulated by increasing the silicate solution Si^{4+} concentration so that the final sodium hydroxide concentration in all samples remained constant (and the same as in the experiments with constant silicate solution Si/Na ratio) at 1 M. The same sodium aluminate stock solution (0.1M sodium aluminate) was used in these experiments as in the previous experiments.

All samples were equilibrated for 56 days at 50 °C in 40 mL polyethylene tubes, rotated continuously at 8 rpm. Supernatant Si^{4+} and Al^{3+} concentrations were monitored over time and only small changes (<10%) in concentrations were observed after 56 days. For the bulk molar Si/Al = 1 and Si/Al = 2 N-A-S-H samples, aliquots were analyzed for Si^{4+} and Al^{3+} concentrations at 3, 7, 10, 14, 29, and 56 days. For the bulk molar Si/Al = 1.5 N-A-S-H samples, aliquots were analyzed for Si^{4+} and Al^{3+} concentrations at 7, 14, 29, 42, and 56 days. For each concentration, multiple samples were prepared so that a fresh sample (with no aliquot removed previously) could be analyzed at the equilibrium time of 56 days.

3.2.2 Aqueous and solid-state characterization

Aliquots from supernatants of equilibrated samples were filtered using a 0.2 mm polyvinylidene fluoride syringe filter and diluted with 3% (v/v) nitric acid. Supernatant Na^{+}, Si^{4+}, and Al^{3+} concentrations were determined using a Varian 10-ES ICP-OES with a SPS 3 autosampler and *ICP Expert II* software (v 1.1). All ICP measurements were taken in triplicate, and each concentration value reported represents the average of three measurements. The solution concentrations along with solid compositions (calculated by

mass balance using solution concentrations combined with TGA data) were used to calculate temperature-dependent solubility products using PHREEQC software (version OS X).

Solids were either centrifuged and freeze dried for XRD, solid-state NRM, and ICP-OES analysis, or vacuum-filtered for TGA. The centrifuged solids were triple-rinsed with Milli-Q water by dispersing them in the water, centrifuging at 3000 g for 10 minutes, and decanting. They were then frozen with liquid N_2 for 5 minutes, freeze dried at -50 °C and 5 Pa for 48 hours using a Labconco Freezone Bulk Tray Dryer and stored at -20 °C under N_2 until further analysis. The vacuum-filtered solids were filtered using nylon filter membranes with a pore size of 0.45 μm and a diameter of 47 mm. The solids were washed and then stored under N_2 at 4 °C until undergoing TGA.

Powder XRD was performed on a Rigaku MiniFlex operated at 40 KV and 15 mA using Cu-Kα radiation. The powder samples were scanned from 5° to 60° 2θ at a rate of 2° 2θ/minute and a step size of 0.02° 2θ. Solid-state NMR was performed on a Bruker AVANCE-II NMR spectrometer, with an 11.7 T wide-bore superconducting magnet, operating at frequencies of 500.24 MHz for ^{1}H, 99.38 MHz for ^{29}Si, and 130.35 MHz for ^{27}Al. Thermogravimetric data were collected using a Mettler Thermogravimetric Analyzer, Model TGA/DSC 1 with a sensitivity of 2 μg. The vacuum-filtered samples were equilibrated at 40 °C for one hour and then heated from 40 °C to 600 °C under N_2 at a flow rate of 20 ml/minute with a heating rate of 20 °C/minute in pure aluminum oxide crucibles. The 40 °C equilibration period was to allow for the evaporation of excess water so that the water content contained in the solid phases could be accurately quantified.

Some of the freeze-dried solids were digested using a mixture of hydrofluoric and hydrochloric acids and analyzed by ICP-OES to determine the solid composition. The solids were digested following a detailed protocol developed by Inorganic Ventures

specifically for the compositional analysis of zeolites. The protocol uses two premixed, proprietary solutions: (1) Inorganic Ventures UA-1, comprised of proprietary proportions hydrofluoric and hydrochloric acids to digest the solids, and (2) Inorganic Ventures UNS-1, comprised of proprietary proportions of triethanolamine and triethylenetetramine to buffer the acids used for digestion. To perform the digestion, 80 to 100 mg of freeze-dried solids were weighed to the nearest 0.1 mg and added to a polyethylene bottle. Ten drops of deionized water were then added to the solids, and the bottle was swirled to hydrate the surface of the solids. Next, 10 mL of UA-1 and 0.5 mL of concentrated nitric acid (trace metal grade, Fisher) were added and the vessel was capped and shaken for 3 minutes (at this point, the solid appeared completely dissolved to the naked eye). The resulting solution was neutralized by adding 50 mL of UNS-1, and the final solution weight was adjusted to 500 g using deionized water. Finally, the solution was analyzed ICP-OES in the same way that supernatant concentrations were measured (described previously).

3.3 RESULTS AND DISCUSSION

3.3.1 Evolution of aqueous chemistry and solid structure

Changes in solution Si^{4+} and Al^{3+} concentrations over time were monitored in order to establish the time required for N-A-S-H solids to reach equilibrium. Changes in Si^{4+} and Al^{3+} were chosen over changes in Na^{+} concentrations, because the relatively high concentrations in Na^{+} (>1 M) in all systems meant that the relative change in Na^{+} was small compared to the total Na^{+}. As a result, the absolute error would have been higher compared to the measured values.

Figures 3.2, 3.3, and 3.4 show changes in Si^{4+} and Al^{3+} concentrations over time for N-A-S-H equilibrated at 50 °C with bulk Si/Al = 1.0, 1.5, and 2.0, respectively.

Initially, both Si^{4+} and Al^{3+} concentrations decreased rapidly at all three compositions, corresponding to rapid precipitation of N-A-S-H solids. Indeed, precipitated solids were observed visually in all experiments within seconds of combining the sodium aluminate and sodium silicate stock solutions.

Concentrations of Si^{4+} and Al^{3+} became relatively stable in N-A-S-H with bulk Si/Al = 1.0 (Figure 3.2) after about 14 days (there was only a 5.4% decrease in Si^{4+} and 5.8% decrease in Al^{3+} between 14 and 29 days) while at Si/Al = 2.0 (Figure 3.4), significant changes in concentrations were observed between 14 and 29 days (17% decrease in Si^{4+} and 82% decrease in Al^{3+}). At Si/Al = 1.5 (Figure 3.3), there were 30% and 84 % drops in Si^{4+} and Al^{3+}, respectively, between 14 and 29 day measurements, after which Si^{4+} and Al^{3+} concentrations remained relatively stable until the 56-day measurements. In all three systems, measurable changes in concentrations were observed until the 56-day measurements, at which point the equilibrated solids and solutions were analyzed to determine solid composition and structure, solution composition, and solubility products.

Interestingly, the presence of an early "plateau" in Si^{4+} and Al^{3+} concentrations can be observed in all three experiments, where concentrations leveled off as if approaching equilibrium, but then rapidly decreased again. For the Si/Al = 2.0 experiment, this plateau started at about 3 days and continues until the 14-day measurements. A much shorter plateau was observable at Si/Al = 1.0, occurring between the 3 and 7 day measurements. At Si/Al = 1.5, the plateau is visible between the 7 and 14 day measurements.

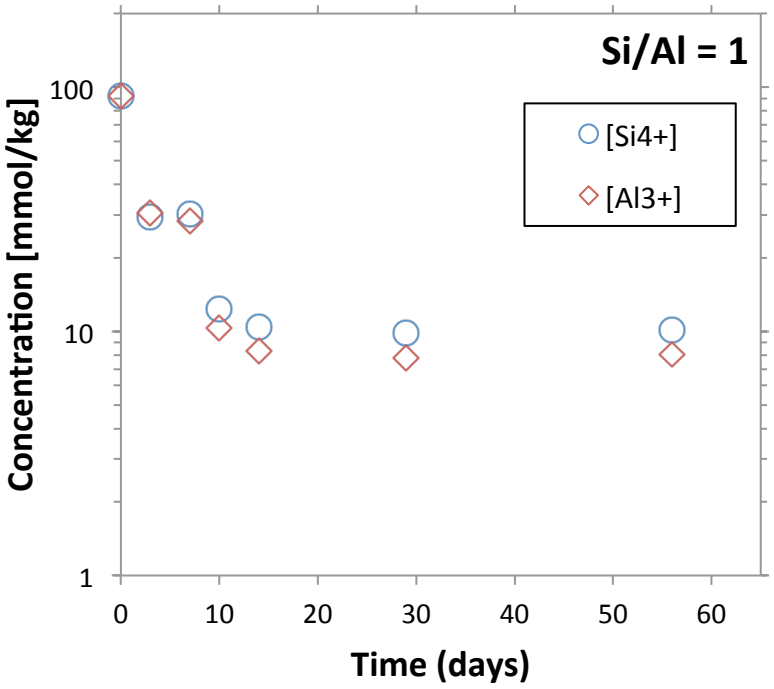

Figure 3.2: Changes in supernatant Si^{4+} and Al^{3+} concentrations over time for N-A-S-H equilibrated at 50°C with bulk Si/Al = 1.0

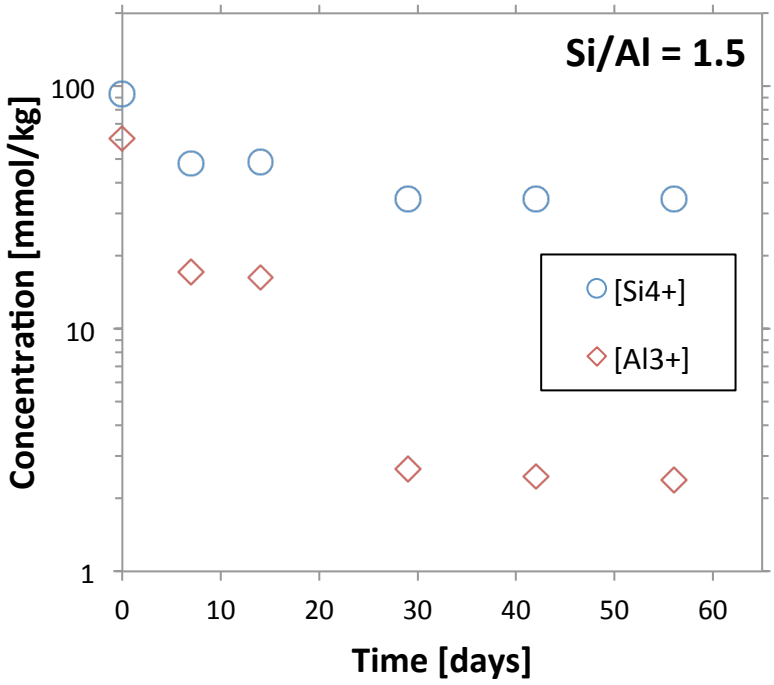

Figure 3.3: Changes in supernatant Si^{4+} and Al^{3+} concentrations over time for N-A-S-H equilibrated at 50°C with bulk Si/Al = 1.5

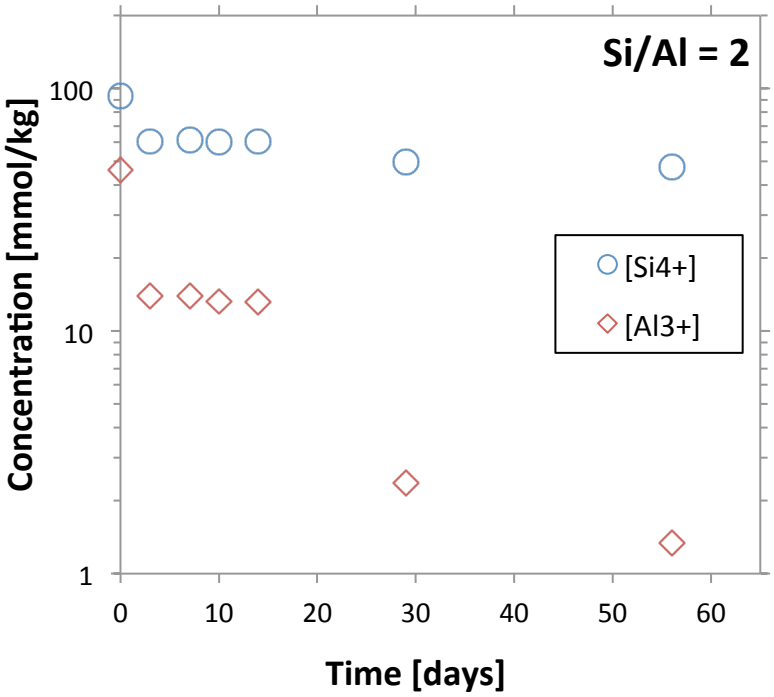

Figure 3.4: Changes in supernatant Si^{4+} and Al^{3+} concentrations over time for N-A-S-H equilibrated at 50°C with bulk Si/Al = 2.0

The solids precipitated from the Si/Al = 1 and Si/Al = 2 systems with supernatant concentrations shown in Figure 3.2 and 3.4 were triple-washed and freeze-dried, and then analyzed by XRD to determine whether the rapid drops in Si^{4+} and Al^{3+} concentrations were accompanied by a structural change in the solids. Diffractograms for solids aged 3, 7, 10, 14, 28, and 56 days (the same time points for which concentrations are shown in Figures 3.2 and 3.4) with Si/Al = 1.0 and 2.0 are shown in Figures 3.5 and 3.6. Both samples are x-ray amorphous at early ages and developed clearly defined peaks as they aged. All peaks observed in both samples are attributed to Na-faujasite (pdf #00-038-0237).

In the Si/Al = 1.0 system, the formation of crystalline faujasite began between 3 and 7 days, and fully defined peaks formed between 7 and 10 days (and remained through

56 days). This timing correlates closely with the rapid drop in Si^{4+} and Al^{4+} concentrations shown for the Si/Al = 1.0 samples in Figure 3.2, which occurred between 7 and 10 days. Similarly, the development of faujasite XRD peaks visible in Figure 3.6 for the Si/Al = 2.0 sample corresponds closely in time with the drop in concentration of Si^{4+} and Al^{3+} concentrations shown in Figure 3.4 for the same system. In the Si/Al = 2.0 system, this transition occurred between 14 and 28 days. The rapid drop in concentrations observed in Si^{4+} and Al^{3+} concentrations is thus attributed to the formation of faujasite, which has a lower solubility than the pseudo-equilibrium x-ray amorphous phase that caused the plateau in concentrations.

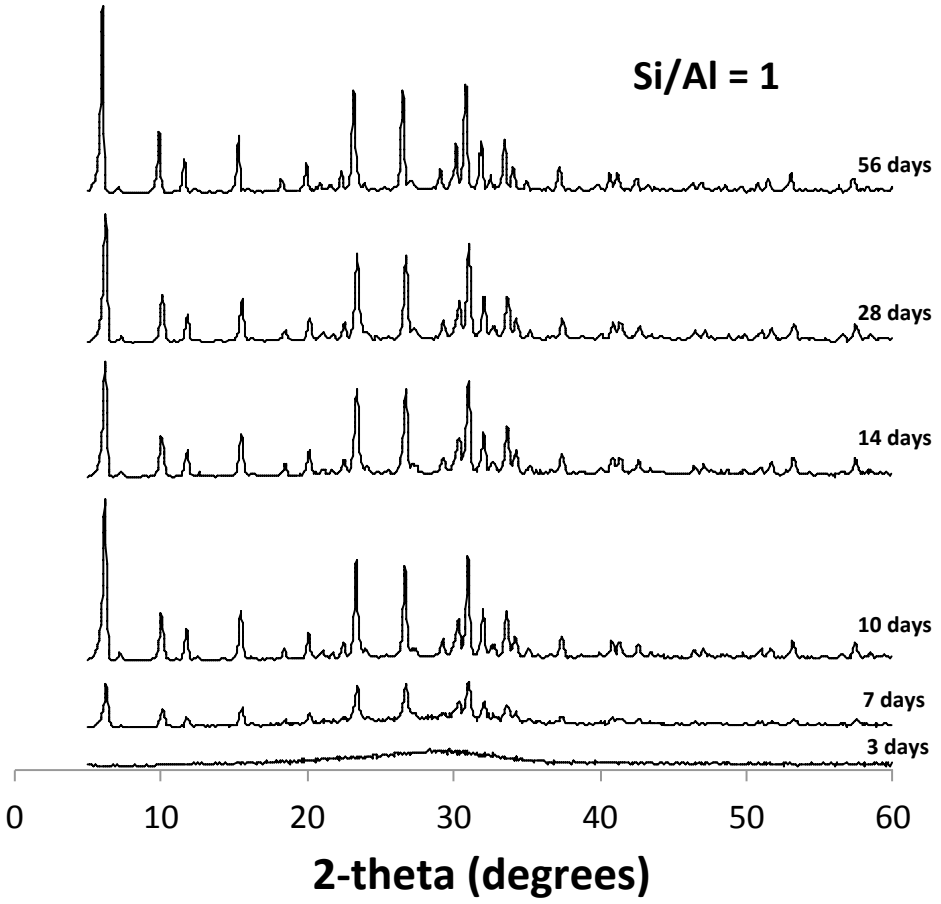

Figure 3.5: Temporal evolution of powder XRD data for N-A-S-H equilibrated at 50°C with bulk Si/Al = 1. All peaks are attributed to faujasite (pdf #00-038-00237)

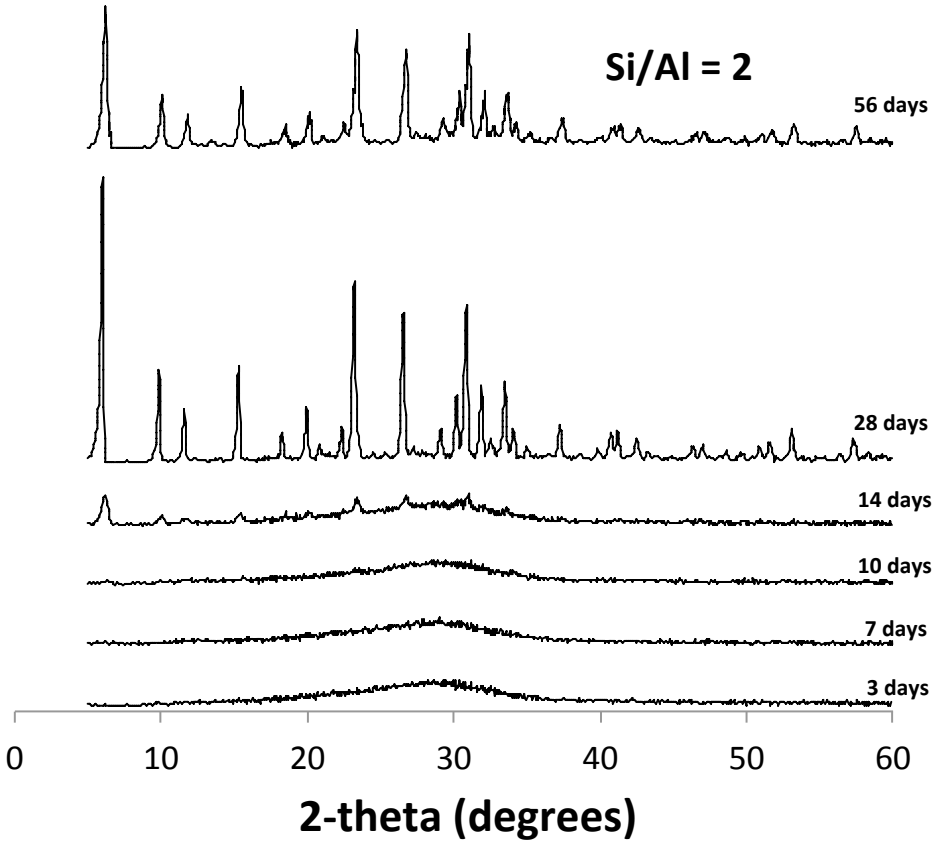

Figure 3.6: Temporal evolution of powder XRD data for N-A-S-H equilibrated at 50°C with bulk Si/Al = 2. All peaks are attributed to faujasite (pdf #00-038-00237)

The discovery of the amorphous phase formation that appears to be at pseudo-equilibrium with the surrounding supernatant solution has significant implications with regards to developing thermokinetic models for N-A-S-H development. Specifically, this discovery emphasizes the importance of taking a stepwise approach to modeling these systems. Since the N-A-S-H composition and structure as well as the supernatant concentrations change over time, a stepwise approach to thermodynamic modeling can account for the simultaneous increase in dissolved silicon and aluminum availability due to precursor dissolution and decrease in silicon and aluminum availability due to incorporation into the N-A-S-H solids. Since the amorphous N-A-S-H develops as a

precursor to the crystalline N-A-S-H, the pathway to amorphous N-A-S-H could be modeled first, and then the conditions reassessed to determine whether the conditions favor a transition to crystalline N-A-S-H.

Evolution of the local molecular environments over time was monitored using ^{29}Si and ^{27}Al solid-state NMR to provide further insight into the initial N-A-S-H network formation and evolution as the samples reached equilibrium concentrations. In contrast to the XRD results, which are sensitive to long-range ordering, solid-state NMR is sensitive to short-range bonding and electronic environments, which enables the characterization of local molecular environments in both crystalline and amorphous materials. Figures 3.7 and 3.8 show the ^{29}Si solid-state single pulse NMR data from the same Si/Al = 1 and Si/Al = 2 specimens that were characterized by XRD at the respective time points.

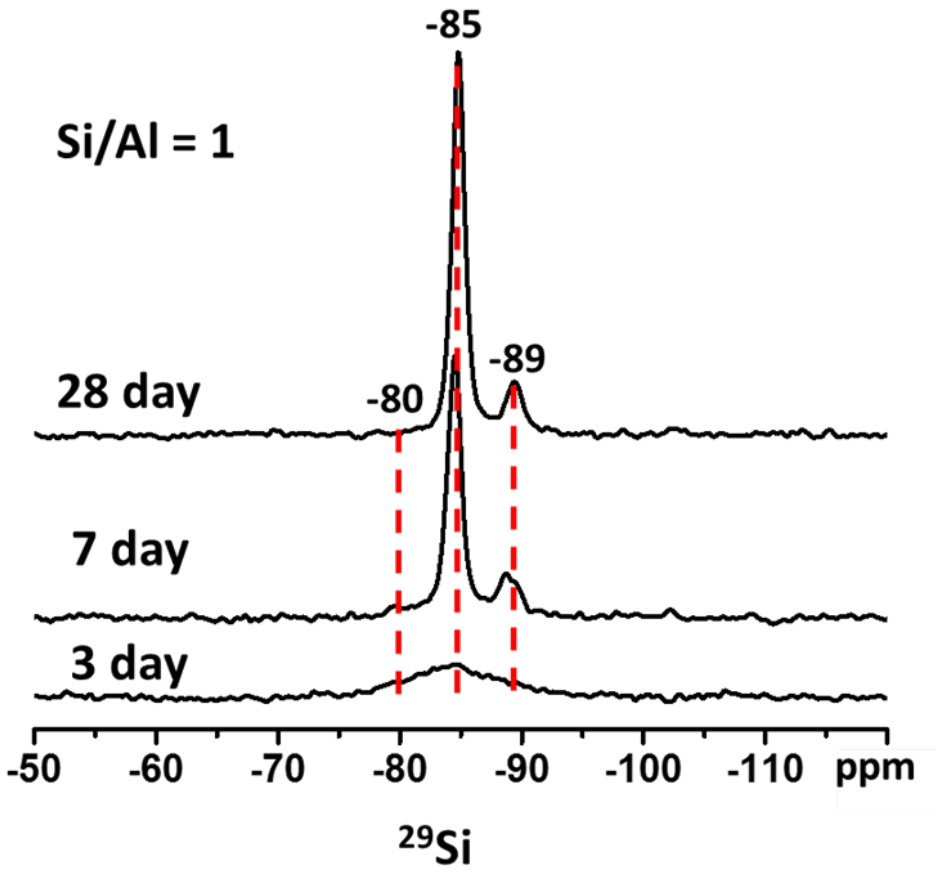

Figure 3.7: 1D ^{29}Si solid-state single-pulse MAS NMR of synthetic aluminosilicate samples prepared from sodium silicate and aluminate solutions at 50°C with a starting molar ratio of Si/Al = 1 for samples allowed to react for three different time points as indicated on the spectra

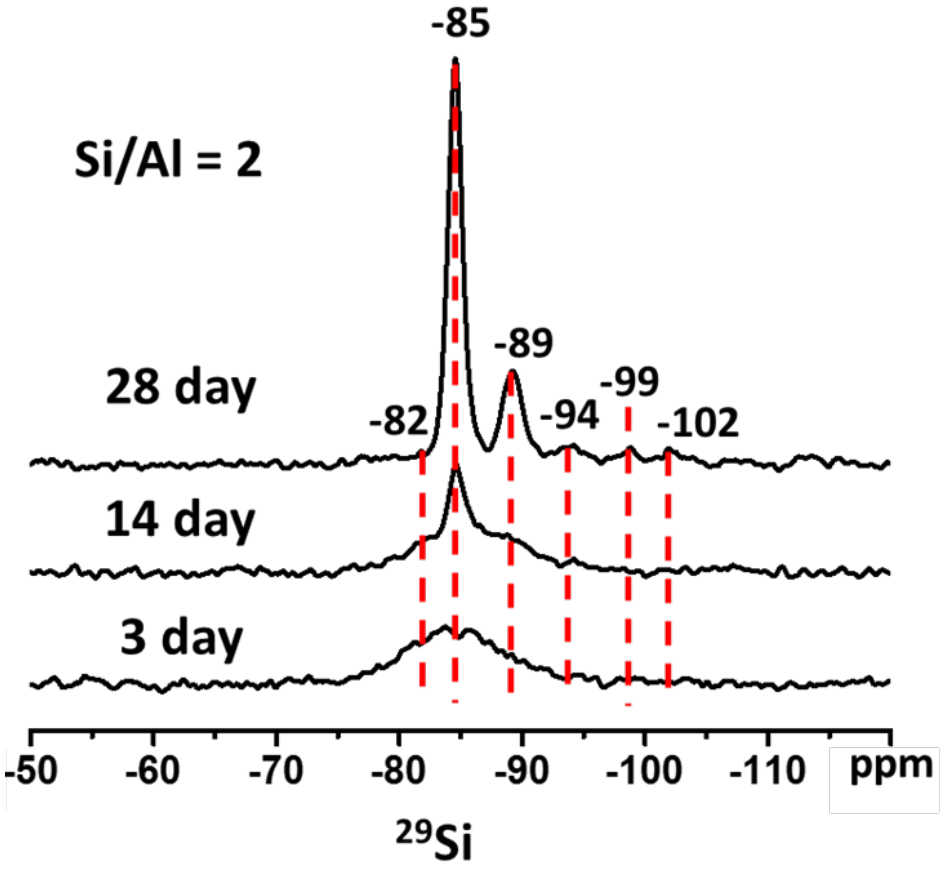

Figure 3.8: 1D ^{29}Si solid-state single-pulse MAS NMR of synthetic aluminosilicate samples prepared from sodium silicate and aluminate solutions at 50°C with a starting molar ratio of Si/Al = 2 for samples allowed to react for three different time points as indicated on the spectra

After 3 days, the ^{29}Si spectra for both Si/Al = 1 and Si/Al = 2 show a broad distribution of ^{29}Si signal intensity centered around -80 and -85 ppm. These two signals are assigned to partially-crosslinked Q^2(1Al) species and an overlapping distribution of partially-crosslinked Q^2(0Al) and Q^3(2Al), respectively [53]. Here, Q^n(mAl) refers to a tetrahedral silicon atom that is covalently bonded through a bridging oxygen atom to n silicon or aluminum atoms, of which m are aluminum. At longer times, i.e., at 7 and 14

days in the Si/Al = 1 and 2 materials, respectively, signals are observed at -80, -85, and -89 ppm. The new signal at -89 ppm is assigned to an overlapping distribution of Q^3(1Al) and Q^4(3Al) species, while the narrow signal at -85 ppm is believed to be fully-crosslinked Q^4(4Al), though further NMR experiments are required to verify the ^{27}Al-^{29}Si connectivity [54]. Longer times also resulted in narrower peak widths for the signals at -85 and -89 ppm, which is consistent with a narrower distribution of ^{29}Si sites in the N-A-S-H solids, such as would be present in a crystalline material. The narrowing of the ^{29}Si signals is accompanied by the observation of reflections in the XRD measurements, further corroborating the development of a more highly-ordered network. At 28 days for each sample, there was a further decrease of the NMR peak widths, again indicating a narrower distribution of the ^{29}Si sites consistent with a long-range ordered, crystalline material. In the case of the Si/Al = 2 solid, new signals arose at -94, -99, and -102 ppm. These three signals are assigned to Q^4(2Al), Q^4(1Al), and Q^3(0Al) species, respectively. The observation of these signals is consistent with the formation of a more highly-coordinated ^{29}Si network in the N-A-S-H solids, again corroborated by the XRD reflections indicating a faujasite-like crystal structure.

Figure 3.9 shows the ^{27}Al solid-state single pulse NMR characterization for the Si/Al = 2 sample at the same time points as presented in Figure 3.8. The ^{27}Al spectra shown were similar, under these field conditions, so only one set of spectra is shown as a representative of the ^{27}Al environment in the N-A-S-H solids.

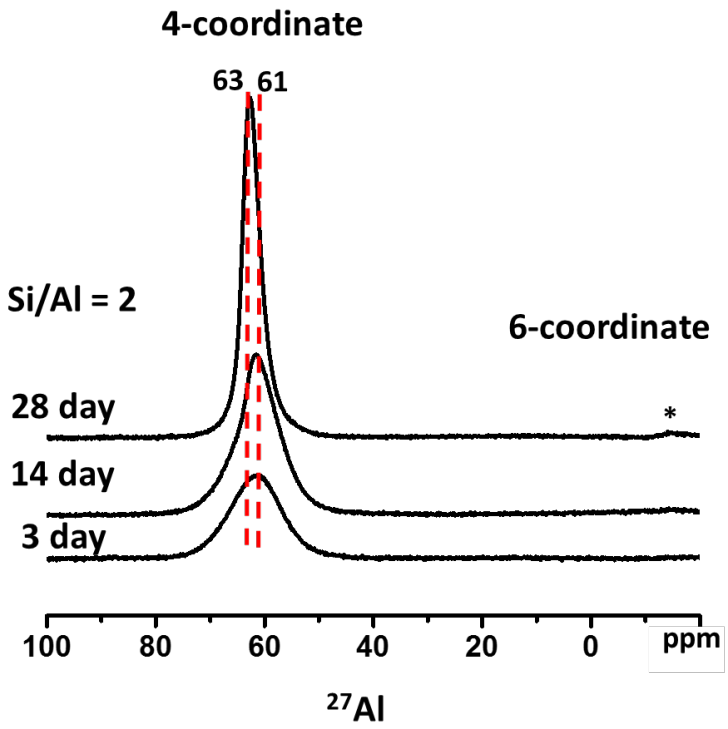

Figure 3.9: 1D 27Al solid-state single-pulse MAS NMR of synthetic aluminosilicate samples prepared from sodium silicate and aluminate solutions at 50°C with a bulk molar ratio of Si/Al = 2 for samples allowed to react for 3, 14, and 28 days as indicated on the spectra

In the 3-day sample, the ^{27}Al shows a broad distribution of signal intensity centered around 61 ppm. The signal at 61 ppm can be attributed to 4-coordinate ^{27}Al sites, which are ^{27}Al species that are incorporated into tetrahedral bonding networks [55]. As time elapsed, a narrowing of the signal peak width is observed, indicating a narrower distribution of ^{27}Al sites, consistent with the long-range order observed by XRD, and a small shift in the position by ca. 2 ppm to higher frequency is observed. Measurements at higher magnetic fields are required to discern more subtle changes in the ^{27}Al 4-coordinate species observed in the solids.

The ^{29}Si and ^{27}Al solid-state NMR data from the N-A-S-H solids at different times provide detailed information regarding the evolution of local molecular structure that the XRD data are not sensitive to. The ^{29}Si and ^{27}Al NMR spectra show signals that are consistent with the formation of an initial, partially-crosslinked, aluminosilica network that condenses as time increases into a more highly-coordinated network that appears to have a structure consistent with that of faujasite. It is apparent from the ^{29}Si NMR results that, even though the XRD measurements show a crystalline faujasite phase, the ^{29}Si 1D NMR shows significant changes in the local molecular structure as equilibration time continues to increase, indicating that the network is still forming and changing over time.

3.3.2 Equilibrium N-A-S-H aqueous chemistry and solid composition

Given the insubstantial changes in solution composition and N-A-S-H structure between 28 and 56 days, it is assumed that the N-A-S-H has reached equilibrium with the supernatant solution at 56 days, and the equilibrium solution and solid-state compositions were evaluated further for 56-day samples. Equilibrium supernatant concentrations for samples equilibrated at 50° C with bulk Si/Al (molar) ranging from 1.0 to 2.0 are shown in Figure 3.10. Error bars show the range of measured concentrations from independent batch reactors prepared with independent stock solutions. For Si/Al = 1 and 2, three replicate reactors were analyzed, and for Si/Al = 1.5, two replicate reactors were analyzed. As bulk molar Si/Al increased from 1 to 2, supernatant Si^{4+} concentrations increased somewhat linearly from 10.4 to 48.0 mmol/kg, and Al^{3+} concentrations decreased from 7.56 to 1.63 mmol/kg. It should be noted that bulk Si/Al ratios were manipulated by adjusting the bulk Al^{3+} in each sample, so at lower Si/Al ratios, bulk Al^{3+} concentrations were highest.

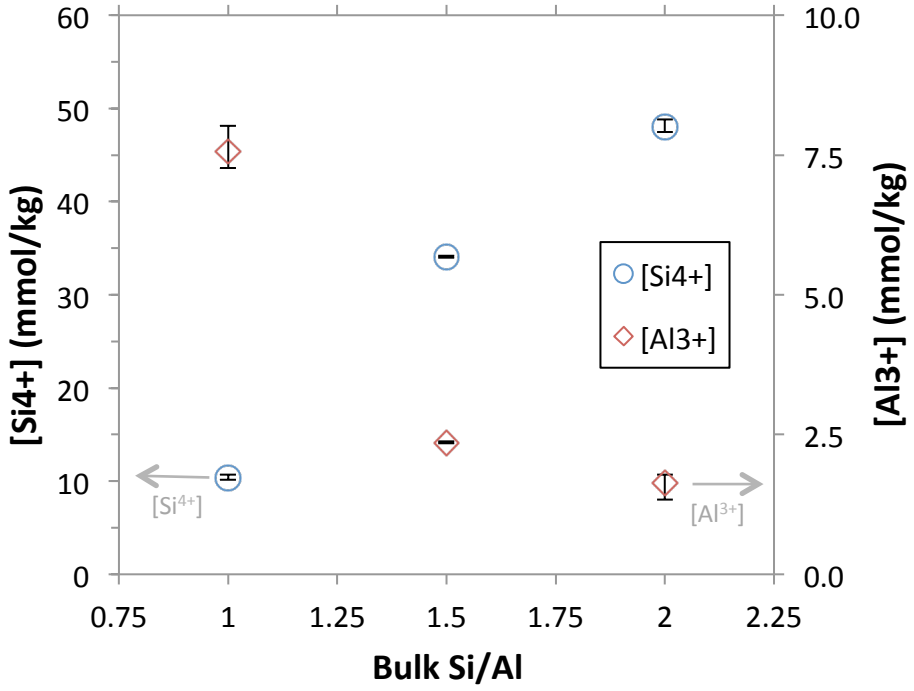

Figure 3.10: N-A-S-H equilibrium Si^{4+} and Al^{3+} concentrations versus bulk Si/Al molar ratios for N-A-S-H equilibrated at 50°C

Thermogravimetric data for N-A-S-H solids synthesized with bulk Si/Al = 1, 1.5 and 2 equilibrated at 50°C to 56 days are shown in Figure 3.11. All of the samples showed continuous mass loss with peaks centered at 150°C to 200°C. The mass losses correspond to a loss in evaporable and non-evaporable water, and total mass loss increased with increasing age for all samples. There was no systematic variation in the temperature at which peak mass-loss occurred (i.e. the temperature at which the derivative of mass loss curve was the most negative) across bulk compositions and no substantial difference in total water loss across bulk compositions. All of the mass losses for all samples occurred between 40°C and approximately 400°C. Peak mass loss is generally observed between 175°C and 400°C for faujasite [56], so the TGA data are

consistent with the XRD data in Figures 3.5 and 3.6. Furthermore, Musyoka et al. [57] found that peak mass loss for zeolite-X, a type of faujasite, to be between 150 and 200 °C. As discussed later in this section, the faujasite precipitated in the study presented here is believed to be zeolite-X, so the peak mass loss between 150 and 200 °C found in this study is consistent with the literature.

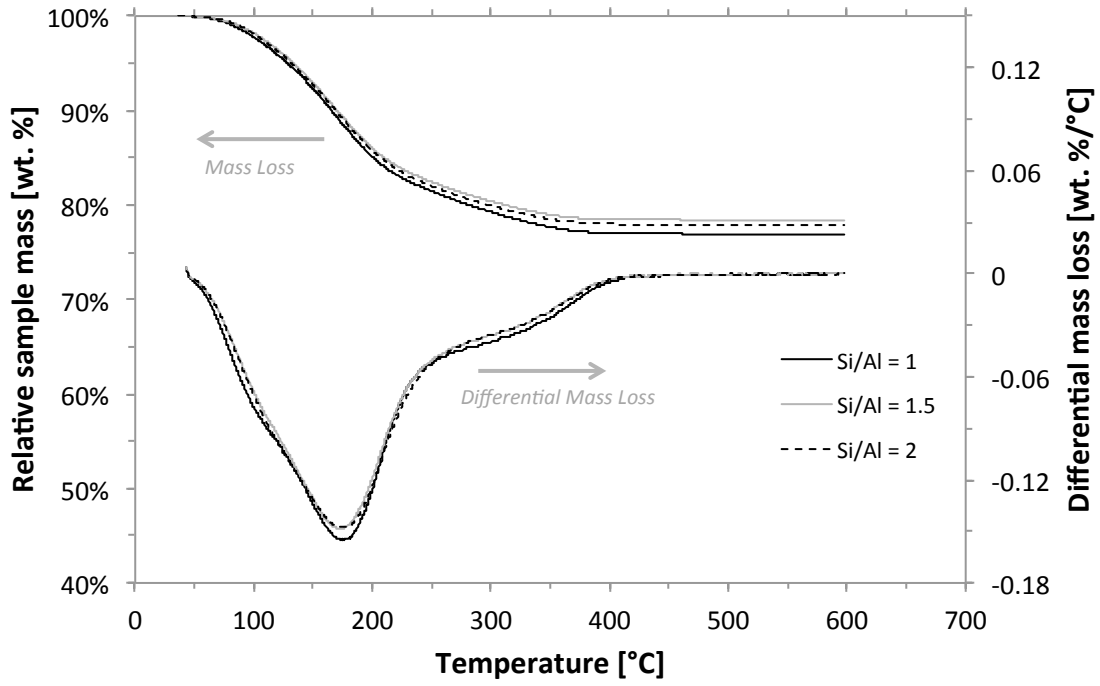

Figure 3.11: TGA data for N-A-S-H samples reacted at 50°C for 56 days with bulk Si/Al = 1, 1.5, and 2

Table 3.1 shows the compositions of the equilibrated solid N-A-S-H phases with bulk Si/Al molar ratios of 1, 1.5, and 2. The Al_2O_3 and SiO_2 stoichiometric coefficients shown in Table 3.1 were calculated by subtracting the equilibrium concentrations of Al^{3+} and Si^{4+} from the bulk concentrations. Each value represents the average concentration calculated from the same two or three independent samples whose supernatant concentrations are reported in Figure 3.10.

The molar fractions of Na_2O were assumed to be equal to the molar fraction of Al_2O_3 for each sample (i.e. $Na_2O/Al_2O_3 = 1$) based on the assumption that sodium is present as a charge balancing cation to alumina tetrahedra, which carry a -1 charge [1]. The molar water content was calculated from the measured TGA mass loss (Figure 3.11) for a single sample at each concentration, and the stoichiometric coefficients for water shown in Table 3.1 represent these measured values. Estimated absolute errors in Si/Al ratios are 0.01 based on the range of Si^{4+} and Al^{3+} supernatant concentrations measured (Figure 3.10). Estimated absolute errors in the H_2O/Al ratios are ± 0.2 units, consistent with the study by Myers et al. [18].

Table 3.1: Composition of N-A-S-H phases equilibrated with bulk Si/Al = 1 to 2 at 50°C

Bulk Si/Al ratio (molar)	N-A-S-H composition
1	$NaAlSi_{0.98}O_{3.96}\bullet(H_2O)_{1.77}$
1.5	$NaAlSi_{1.00}O_{3.99}\bullet(H_2O)_{1.50}$
2	$NaAlSi_{1.01}O_{4.03}\bullet(H_2O)_{1.31}$

To validate the solid composition measurements, a separate series of N-A-S-H samples was prepared in the same way as those described previously and analyzed by acid digestion followed by ICP analysis of the resulting solution. The Si/Al ratios determined by mass balance (the same way as the values presented in Table 3.1) varied from the Si/Al ratios determined by acid digestion by less that 1% for all three samples analyzed in this way. The assumed sodium concentrations could not be validated in the same way due to complications resulting from the complex matrix in the digested samples, which was composed of hydrofluoric acid as well as a buffer solution composed of triethanolamine and triethylenetetramine used to neutralize the acid prior to ICP analysis.

As shown in Table 3.1, there was only a slight increase in N-A-S-H Si/Al ratio as the bulk Si/Al ratio increased from 1 to 2, and the difference between all N-A-S-H Si/Al ratios was less than the estimated error. The Si/Al molar ratio in all solid N-A-S-H phases was close to 1, regardless of the bulk Si/Al ratio. Others have described three different framework units that make up inorganic polymers: 1) poly(sialate) (-Si-O-Al-O-), corresponding to N-A-S-H Si/Al = 1; poly(silate-siloxo) (Si-O-Al-O-Si-O), corresponding to N-A-S-H Si/Al = 2, and poly(sialate-disiloxo) (Si-O-Al-O-Si-O-Si-O) groups, corresponding to N-A-S-H Si/Al = 3 [58,59]. Although Al-O-Al bonds are not favored according to Loewenstein's principal [60], such bonds are possible if sufficient aluminum is present in the pore solution [23]. Here, since the N-A-S-H Si/Al ratio is close to one for all samples, it is presumed that poly(sialate) units dominate.

Based on the N-A-S-H composition presented here and the XRD diffractograms in Figures 3.5 and 3.6, a further discussion of characterization of the N-A-S-H is warranted. Figures 3.5 and 3.6 shows that the N-A-S-H reacted for 56 days with bulk Si/Al = 1 and 2 has a crystalline structure resembling that of faujasite. Faujasite is a zeolitic phase composed of sodalite cages connected by hexagonal prisms (see Figure 3.12) and can be split generally into two types based on its Si/Al ratio [61]. Faujasite with a molar Si/Al ratio less than 1.5 is referred to as zeolite-X, while faujasite with a molar Si/Al greater than 1.5 is referred to as zeolite-Y [62]. Since the Si/Al ratio in the present study was close to 1 for all bulk Si/Al compositions (Table 3.1), the faujasite is classified as zeolite-X.

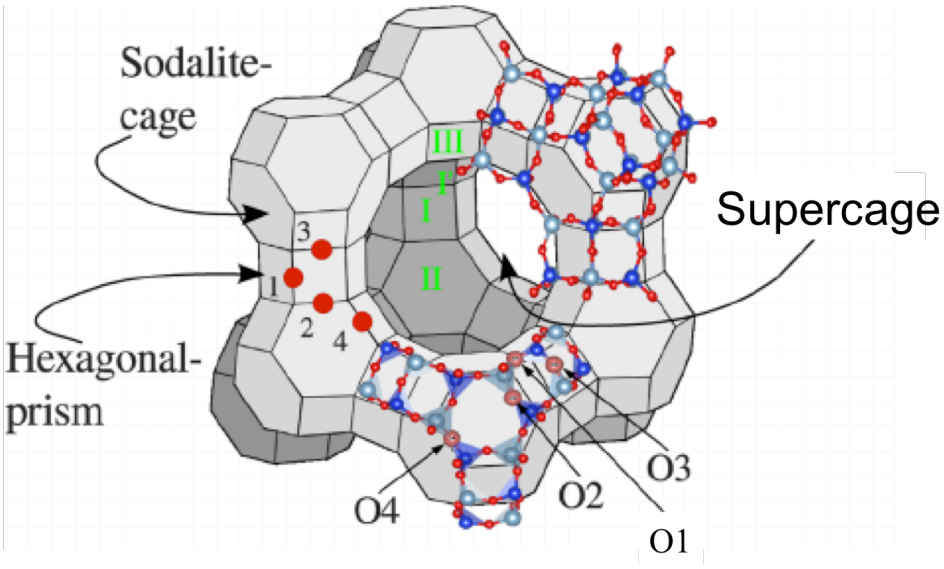

Figure 3.12: Atomic structure of faujasite-type zeolite. Dark blue spheres denote Si atoms, light blue spheres denote Al atoms, red spheres denote O atoms. Four types of oxygen atoms are shown with englared circles, and the green roman numerals indicate the locations of charge balancing Na atoms. Image modified from Bloński et al. [63]

Other researchers have successfully synthesized zeolite-X in the laboratory by combining solutions of sodium silicate and sodium aluminate. Buchwald et al. [64] found that zeolite-A, zeolite-X, and sodalite can form separately or coexist in different combinations depending on synthesis conditions, and the concentration of NaOH is the most important factor in determining which phases form. At 1 M NaOH, the Buchwald study found that zeolite-X with Si/Al = 1 was the preferred phase regardless of bulk Si/Al ratio, consistent with the findings of the study presented here.

Hajimohammadi et al. [65] previously observed the formation of Na-faujasite in synthetic inorganic polymers formed by mixing amorphous silica with sodium aluminate at 40 °C and Fletcher et al. [58] detected an unnamed crystalline zeolite in a metakaolin-based inorganic polymer with bulk Si/Al = 1.

It should be noted that fly ash Si/Al ratio is an important parameter with regards to IPB performance beyond its effect on N-A-S-H Si/Al ratio. Most notably, it has been shown to affect dissolution rates of fly ash [20], in turn impacting the transient concentrations of available silicon and aluminum to form the binding N-A-S-H phase. Bulk Si/Al ratios have also been shown to impact the microstructure of mature IPB in the case of metakaolin-based systems [4], so composition of the N-A-S-H is not the only factor impacting mechanical properties.

3.3.3 Effect of silicate activator Si/Na ratio on N-A-S-H composition

To test the impact of silicate solution Si/Na on N-A-S-H Si/Al ratio, a series of N-A-S-H solids were synthesized following the same procedure used for the experiments described previously, but with the silicate stock solution Si/Na molar ratio varying from 0.1 to 1.0 and bulk Si/Al varying from 0.89 to 9.58. The silicate stock solution Si/Na in the experiments described previously was held constant at 0.1. Here, the range of Si/Na values in the silicate activating solution was chosen to match the common range of silicate activators used in alkali-activated fly ash systems. The same sodium aluminate stock solution (0.1 M sodium aluminate) was used in this experiment as in the previous experiments. In these experiments, the samples were reacted at 50°C for 56 days.

Table 3.2 shows the Si/Al molar ratio of the solids increasing from 1.10 to 2.39 as the Si/Na molar ratio of the silicate stock solution increased from 0.10 to 1.05. While the highest bulk Si/Al ratio in this experiment (9.58) was much higher than in the first set of experiments, it is worth noting that, even with an increase of the silicate solution Si/Na molar ratio from 0.10 to 0.20, the N-A-S-H solid's Si/Al molar ratio increased from 1.10 to 1.30 despite the bulk Si/Al ratio only increasing from 0.89 to 1.86. This is noteworthy because in the previous experiments conducted with the Si/Na ratio held constant at 0.10,

increasing bulk Si/Al from 1 to 2 did not change the N-A-S-H Si/Al (constant at ca. 1.0, Table 3.1). Here, with a similar increase in bulk Si/Al ratio but with Si/Na also increasing from 0.10 to 0.20 rather than remaining constant, there was a significant increase in the solid N-A-S-H Si/Al ratio, indicating an increase in the frequency of Si-O-Si type bonds compared to the frequency of Si-O-Al type bonds.

Table 3.2: Si/Al molar ratios in N-A-S-H reacted at 50°C for 56 days with sodium silicate Si/Na molar ratios varying from 0.10 to 1.05 and bulk Si/Al ratios varying from 0.89 to 9.58

Si Solution Si/Na	Bulk Si/Al	N-A-S-H Si/Al
0.10	0.89	1.10
0.20	1.86	1.30
0.51	4.83	1.90
0.77	7.04	2.17
1.05	9.58	2.39

In alkali-activated systems, it is well known that the concentration of silicates in the sodium hydroxide/sodium silicate activating solution can greatly impact the microstructure and thus the engineering properties of the binder. The initial speciation of the silicates in sodium silicate activating solution is highly complex and greatly impacts network formation and structure. The properties of sodium silicate solutions, including viscosity and speciation of silicates, are highly dependent on the Si/Na ratio of the solution [24,25]. As Si/Na increases, the number of Q^0 and Q^1 Si sites (monomeric and dimeric silicates) in the solution decreases rapidly [25]. This can cause a large change in N-A-S-H microstructure [1], as aluminate anions react preferentially with silicate anions of lower connectivity [26]. Additionally, the formation of dissolved oligomers of silicates in the silicate activating solution leave fewer bonding sites on the silicate chains. Duxson et al. [1] state that silicate speciation in the activating solution is probably more important

than the absolute silicate concentration in determining N-A-S-H microstructure. The findings here support that claim, as changes in bulk Si/Al ratio had little effect on the N-A-S-H composition, while increasing silicate solution Si/Na ratio had a significant impact on the N-A-S-H composition.

3.3.4 Calculation of solubility products for N-A-S-H phases

Solubility products (K_{sp}) were calculated for each of the N-A-S-H solids with the bulk compositions shown Table 3.1. The dissolution reaction assumed to calculate solubility products is shown in Equation (3.1):

$$NaAlSi_xO_{(2x+2)} \cdot (H_2O)_{y(S)} + (2x - y - 2)H_2O_{(l)} + 4H^+_{(aq)} \leftrightarrow \mathrm{Na}^+_{(aq)} + Al^{3+*}_{(aq)} + xH_4SiO^o_{4(aq)} \quad (3.1)$$

where *x* is the Si/Al molar ratio of the solids and y is the stoichiometric coefficient of H_2O in the solids. This convention of calculating solubility products follows the convention presented by Sposito [66] for clays. Here, $\mathrm{Al}^{3+*}_{(aq)}$ refers to the specific species, where previously, $\mathrm{Al}^{3+}_{(aq)}$ referred to the total dissolved aluminum. Following the reaction in Equation (3.1), equilibrium solubility products were calculated with Equation (3.2):

$$K_{sp} = \left\{\mathrm{Na}^+_{(aq)}\right\} \cdot \left\{\mathrm{Al}^{3+*}_{aq}\right\} \cdot \left\{\mathrm{H_4SiO^o_{4(aq)}}\right\}^x \cdot \left\{\mathrm{H^+_{(aq)}}\right\}^{-4} \cdot \left\{\mathrm{H_2O_{(l)}}\right\}^{(y-2x+2)} \quad (3.2)$$

Equilibrium constants were also calculated based on the dissolution reaction shown in Equation (3.3):

$$NaAlSi_xO_{(2x+2)} \cdot (H_2O)_{y(S)} + (2 - y)H_2O_{(l)} + 2xOH^-_{(aq)} \leftrightarrow \mathrm{Na}^+_{(aq)} + Al(OH)^-_{4(aq)} + xH_2SiO^{2-}_{4(aq)} \quad (3.3)$$

Equation (3.3), in contrast to Equation (3.1), shows OH^- as a reactant to represent the alkaline conditions present in the study, and uses the dominant aluminum and silicon species. Following the reaction presented in Equation (3.3), equilibrium constants were calculated using Equation (3.4):

$$K_{sp} = \left\{Na^+_{(aq)}\right\} \cdot \left\{Al(OH)^-_{4(aq)}\right\} \cdot \left\{H_2SiO^{2-}_{4(aq)}\right\}^x \cdot \left\{OH^-_{(aq)}\right\}^{-2x} \cdot \left\{H_2O_{(l)}\right\}^{(y-2)} \quad (3.4)$$

Activities of $Na^+_{(aq)}$, $Al^{3+*}_{(aq)}$, $H_4SiO^o_{4(aq)}$, $H^+_{(aq)}$, and $H_2O_{(l)}$ were determined with PHREEQC using the measured supernatant concentrations of $Na^+_{(aq)}$, $Si^{4+}_{(aq)}$, $Al^{3+}_{(aq)}$ with the pH calculated from charge balance. The Truesdell-Jones version of the extended Debye-Hückel equation was used within PHREEQC with the LLNL database to determine activity coefficients of each species, shown in Equation (3.5):

$$log\gamma_i = \frac{-Az_i^2\sqrt{I}}{1+B\alpha_i\sqrt{I}} + bI \quad (3.5)$$

where γ_i is the activity coefficient of ion "*i*", *A* and *B* are Debye-Hückel parameters based on the dielectric constant of water and the temperature, z_i is the ion valance, α_i is a parameter accounting from the ionic radius, *b* is an empirical parameter, and *I* is the ionic strength of the solution. The concentrations of species for each sample, as well as the ionic strength and pH, can be found in Appendix A.

The calculated solubility constants for N-A-S-H solids equilibrated at 50°C with bulk Si/Al ratios varying from 1.0 to 2.0 are shown in Table 3.3. An absolute error of 0.2 log units was determined by varying all of the inputs in Equations (3.2) and (3.4) within their respective error ranges to determine the maximum and minimum value of K_{sp} and

K_{eq} that could be achieved with all of the inputs staying within their respective error bounds. Calculated K_{sp} and K_{eq} values do not vary significantly with bulk Si/Al ratio.

Table 3.3: Solubility products (K_{sp}) and equilibrium constants (K_{eq}) of N-A-S-H reacted at 50 °C with Si/Al = 1, 1.5, and 2 calculated using Equations (3.2) and (3.4), respectively

Bulk Si/Al	Log K_{sp}	Log K_{eq}
1	11.2 ± 0.2	-5.70 ± 0.2
1.5	11.1 ± 0.2	-5.74 ± 0.2
2	11.0 ± 0.2	-5.78 ± 0.2

Zeolite-X solubility was calculated previously by Šefčík et al. [67] from experimental data obtained from a separate study by Čizmek et al. [68]. In the Čizmek experiments, zeolite-X precipitated from a mixture of sodium hydroxide, sodium silicate, and aluminum trihydrate with Si/Al = 2 was rinsed and dissolved in 2 M sodium hydroxide at 80 °C (compared to the 50 °C reaction temperature in the present study). In Šefčík's calculations, the solubility product was defined according to Equation (3.4):

$$K_{sp} = \left[\mathrm{Na}^{+}_{(aq)}\right] \cdot \left[\mathrm{SiO}_{2(aq)}\right]^{b} \cdot \left[\mathrm{AlO}^{-}_{2(aq)}\right] \tag{3.4}$$

where the values inside brackets refer to concentrations rather than activities and *b* is the solid Si/Al ratio. Note that the concentration of neutrally charged SiO_2 species is used rather than the SiO_3^{2-} species used in the current study. The selection of silicon species to use in defining the solubility product is rather arbitrary, since simple acid-base reactions with well-defined acid ionization constants link the activities of silicon species. In the current study, SiO_3^{2-} activities were chosen to calculate solubility products since this the dominant species at pH 14 [69].

For comparison purposes, a K_{sp} value was calculated with experimental data from the present study using Equation (3.4). For these calculations, Na^+, SiO_2, and AlO_2^- concentrations were determined using PHREEQC. The $\log_{10}(K_{sp})$ values calculated from the present study using Equation (3.4) are shown in Table 3.4 and range from -8.86 to -9.05. The $\log_{10}(K_{sp})$ calculated by Šefčík et al. for zeolite-X with Si/Al = 1.2 was reported as -9.18, which is in close agreement with the values calculated in the present study.

Table 3.4: Solubility products of N-A-S-H synthesized at 50 °C with Si/Al = 1, 1.5, and 2 calculated using Equation (3.4)

Bulk Si/Al	Log K_{sp}
1	-8.86
1.5	-8.98
2	-9.05

In addition to the solubility products and equilibrium constants presented for the equilibrated crystalline phases presented in Table 3.3, equilibrium constants were determined for the amorphous N-A-S-H phases using the 7-day Si^{4+} and Al^{3+} concentrations presented in Figures 3.2, 3.3, and 3.4. Equilibrium constants were calculated using Equation (3.4), corresponding to the reaction presented in Equation (3.2), which uses the dominant species of Si^{4+} and Al^{3+} rather than the Spositio convention. Using the dominant species of Si^{4+} and Al^{3+} to determine equilibrium constants allows for a stronger correlation with total Si^{4+} and Al^{3+} concentrations to better understand the relationship between the amorphous and crystalline N-A-S-H solids. It should be noted that supernatant Na^+ concentrations and water content were not measured for the amorphous phases, as the original intent of this study was to understand equilibrium conditions. As such, to calculate amorphous phases solubility products 1000 mmol/kg was assumed for the Na^+ supernatant concentrations, and the water contents were set equal to the same water contents measured in the analogous crystalline phases.

While these assumptions may not be completely accurate, deviations in these values have relatively little impact on the amorphous phase equilibrium constants. The equilibrium constants for N-A-S-H reacted with Si/Al = 1, 1.5, and 2 for 7 and 56 days are presented in Table 3.5.

The amorphous N-A-S-H equilibrium constants are approximately two orders of magnitude higher than the crystalline N-A-S-H equilibrium constants, indicating that the amorphous N-A-S-H is more soluble than the crystalline N-A-S-H under the conditions studied here. There is no significant change in amorphous N-A-S-H solubility with bulk Si/Al, suggesting that a single amorphous phase precipitates at 50 °C when bulk Si/Al varies between 1 and 2.

Table 3.5: Equilibrium constants of crystalline N-A-S-H reacted for 56 days and amorphous N-A-S-H reacted for 7 days.

	Log K_{eq}	
Bulk Si/Al	Crystalline N-A-S-H	Amorphous N-A-S-H
1	-5.71	-3.10
1.5	-5.74	-3.15
2	-5.78	-3.13

3.4 CONCLUSIONS

This study has analyzed the relationship between the aqueous chemistry and the composition and structure of solids for N-A-S-H phases synthesized at a constant temperature. It was shown that early N-A-S-H products are x-ray amorphous, but a rapid transition to a crystalline structure, faujasite, occurs after several weeks to several months, depending on the equilibration temperature. The bulk Si/Al ratio was shown to have little impact on N-A-S-H solid Si/Al ratio when synthesized using sodium silicate solutions with Si/Na ratios low enough that all silicate species are monomeric. Only

slight changes in sodium silicate Si/Na ratio were shown to have a significant impact on the N-A-S-H Si/Al ratio, an important finding that has implications for the understanding and optimization of activator solution chemistries. Additionally, solubility products of N-A-S-H were calculated for a range of compositions, and these values will allow for thermodynamic modeling of N-A-S-H systems, which can have a substantial impact on our ability to predict engineering properties for these low-CO_2 binders. Finally, amorphous phase equilibrium constants were determined, and it was found that amorphous N-A-S-H is more soluble than its crystalline counterpart.

Chapter 4: The Effect of Temperature on N-A-S-H Composition, Solubility, and Structure

4.1 INTRODUCTION

Inorganic polymer binders (IPBs) are a promising low-CO_2 alternative to ordinary portland cement (OPC) made by activating an aluminosilicate powder with a highly alkaline aqueous solution, most often sodium hydroxide [1,44,45,49,60]. The resulting binder is composed primarily of a sodium aluminosilicate hydrate (N-A-S-H) phase with the general formula $n[Na_2O{\cdot}xSiO_2{\cdot}Al_2O_3{\cdot}yH_2O]$, where n is the degree of polymerization, x is the ratio SiO_2/Al_2O_3, and y is the number of water molecules. As with OPC, temperature plays an important role in the development of mechanical properties of inorganic polymer binders (IPBs), and heat curing is used frequently to improve compressive strength [70–72]. Temperatures experienced in service can also vary with local climate and ambient temperature fluctuations. The equilibrium phase balances and, perhaps more importantly, the ratio of solid phases to voids, are affected by temperature and directly determine the mechanical and durability properties of IPBs [73].

A variety of crystalline and amorphous phases, generally zeolitic in nature, can exist in equilibrated N-A-S-H, either separately or in combination with each other, and temperature can significantly impact what phases are present [73]. The optimum curing temperature for IPBs varies depending on the composition and structure of the solid and liquid precursors as well as on the relative proportions of those precursors. Determining the optimum curing temperature for a given IPB mixture is not straightforward, but understanding the effect of temperature on solubility can help, facilitating mixture design. Furthermore, our ability to understand the chemistry and predict the phase composition of these materials is an important step towards understanding their durability. While the consensus in the literature is that IPBs are generally superior to OPC with regards to

durability, there has been relatively little research on IPB durability and further work is needed to fully predict how these materials will withstand various environmental conditions [6,7,13,74].

L'Hopital et al. [31] studied calcium aluminosilicate hydrate (C-A-S-H) solubility at constant temperature, and Myers et al. [18] expanded on that work, investigating the effect of temperature on C-A-S-H solubility. C-A-S-H is present in the binding phases of portland cement systems that have high levels of supplementary cementitious materials [16,18,75] as well as in high-calcium inorganic polymers [35,76,77]. The work of L'Hopital et al. [14] and Myers et al. [15] was built on previous studies of calcium silicate hydrate (C-S-H) solubility that have allowed for the successful prediction of phase balances and engineering properties through the use of thermodynamic modeling [15]. There is little information, however, regarding the solubility of N-A-S-H, and such data are needed in order to develop thermodynamic models for these systems.

The research presented here examines the effect of temperature on the composition, structure, and solubility of N-A-S-H synthesized at bulk Si/Al molar ratios of 1 to 2 and pH 14. N-A-S-H composition was determined by mass balance and thermogravimetric analysis (TGA). X-ray diffraction (XRD) was used to study the crystalline structure of N-A-S-H as a function of solution composition. Additionally, temperature-dependent solubility products (K_{sp}) of N-A-S-H were determined by monitoring the ionic concentration of the supernatant solution at equilibrium using inductively coupled plasma optical emission spectroscopy (ICP-OES). The resulting understanding of the effect of temperature on N-A-S-H properties is in an important step towards the development of thermodynamic models for IPBs across the range of temperatures they are subjected to. Additionally, quantifying the relationship between N-

A-S-H solubility and temperature allows for the quantification of dissolution enthalpies, another important thermodynamic property.

4.2 MATERIALS AND METHODS

4.2.1 N-A-S-H synthesis

N-A-S-H samples were prepared by mixing appropriate proportions of de-aired (by boiling for 10 minutes) Milli-Q water (Merk Millipore) with sodium silicate and sodium aluminate solutions in an N_2-filled glove box to achieve bulk molar Si/Al ratios of 1 to 2. Various studies in the literature have aimed at optimizing inorganic polymer composition have reported optimum molar Si/Al ratios in this range [2,23,39,40]. In the present study, N-A-S-H phases with Si/Al ratios of 1, 1.5, and 2 were synthesized and tested at 4, 25, 50, and 70 °C, and N-A-S-H phases with intermediate compositions were studied at some temperatures for validation of the observed trends.

The sodium silicate activating solution had a Si/Na molar ratio of 0.1. This ratio was intentionally selected to be low enough so that the dissolved silicate species in this solution would be monomeric [25]. The synthesis methods were based loosely on those employed by Myers et al. [18] and L'Hôpital et al. [31] in the synthesis of calcium aluminosilicates. Sodium silicate solution was prepared by dissolving silicic acid (20 μm, Sigma-Aldrich) in 5 M sodium hydroxide (Dilut-It, J.T. Baker) and diluting with de-aired Milli-Q water to final concentrations of 2 M sodium hydroxide and 0.2 M Si^{4+}. Sodium aluminate solution was prepared at a concentration of 0.1 M Al^{3+} by dissolving sodium aluminate (Sigma-Aldrich) in de-aired Milli-Q water.

The samples were reacted at 4, 25, 50, and 70 °C in 40mL polyethylene tubes, rotated continuously at 8 rpm until they reached equilibrium. Equilibration times were determined by monitoring the change in supernatant Si^{4+} and Al^{3+} concentrations over

time; samples were said to have equilibrated when there was a relatively small change (<10%) in Si^{4+} and Al^{3+} concentrations between subsequent measurements. Equilibrium times were 28 days for 70 °C samples, 56 days for 50 °C samples, 182 days for 25 °C samples, and 407 days for 4°C samples. For each concentration and temperature, multiple samples were prepared so that a fresh sample (with no aliquot removed previously) could be analyzed at the equilibrium time.

4.2.2 Aqueous and solid-state characterization

Aliquots from supernatants of equilibrated samples were filtered using a 0.2 μm polyvinylidene fluoride syringe filter and diluted with 3% (v/v) nitric acid. Supernatant Na^{+}, Si^{4+}, and Al^{3+} concentrations were determined using a Varian 10-ES ICP-OES with a SPS 3 autosampler and *ICP Expert II* software (v 1.1). All ICP measurements were taken in triplicate, and each concentration value reported represents the average of three measurements. The solution concentrations along with solid compositions (calculated by mass balance using solution concentrations combined with thermogravimetric data) were used to calculate temperature-dependent solubility products using PHREEQC software (version OS X).

Solids were vacuum-filtered using nylon filter membranes with a pore size of 0.45 μm and a diameter of 47 mm. The vacuum-filtered solids were triple-washed and then stored under N_2 at 4 °C until undergoing TGA analysis. Thermogravimetric data were collected using a Mettler Thermogravimetric Analyzer, Model TGA/DSC 1 with a sensitivity of 2 μg. The vacuum-filtered samples were equilibrated at 40 °C for one hour and then heated from 40 °C to 600 °C under N_2 at a flow rate of 20 ml/minute with a heating rate of 20 °C/minute in pure aluminum oxide crucibles. The 40 °C equilibration

period was to allow for the evaporation of excess water so that the water content contained in the solid phases could be accurately quantified.

4.3 RESULTS AND DISCUSSION

4.3.1 Aqueous chemistry evolution

Changes in solution Si^{4+} and Al^{3+} concentrations were measured over time in order to establish the time required for N-A-S-H solids to reach equilibrium. Changes in Si^{4+} and Al^{3+} were chosen over changes in Na^{+} concentrations because the relatively high concentrations of Na^{+} (>1M) in all systems meant that the relative change in Na^{+} was small compared to the total Na^{+}. As a result, the absolute error would have been higher compared to the measured values.

Figures 4.1 to 4.8 shows changes in Si^{4+} and Al^{3+} concentrations with time for N-A-S-H with bulk molar Si/Al of about 1 and 2, and reacted at 4, 25, 50, and 70 °C for 407, 183, 56, and 28 days, respectively. The changes in Si^{4+} and Al^{3+} shown in Figure 4.1 to 4.8 are representative of those measured in other samples, and the primary motive for measuring changes over time was to determine reaction times necessary for the N-A-S-H to reach equilibrium so that the thermodynamic properties at equilibrium could be quantified.

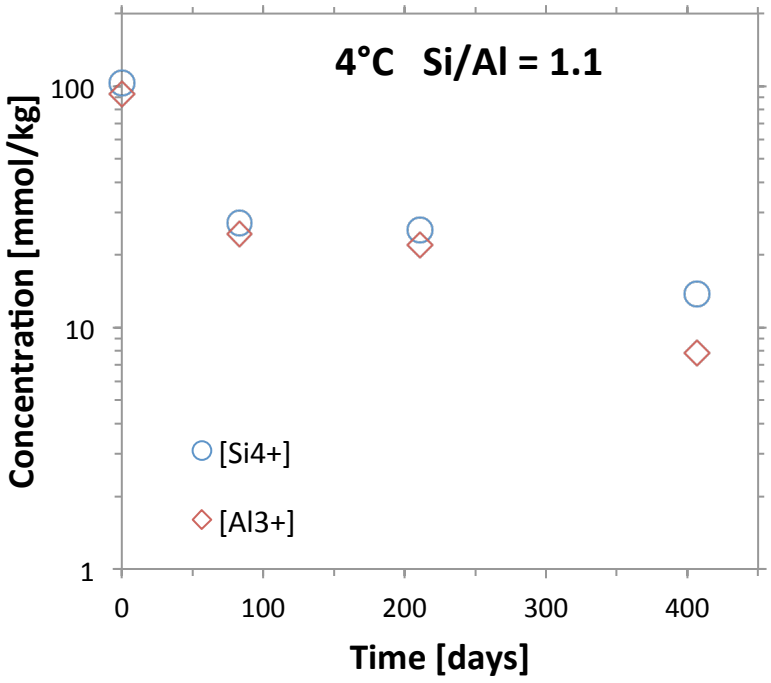

Figure 4.1: Changes in supernatant Si^{4+} and Al^{3+} concentrations over time for N-A-S-H equilibrated at 4 °C with bulk molar Si/Al ratio equal to 1.1

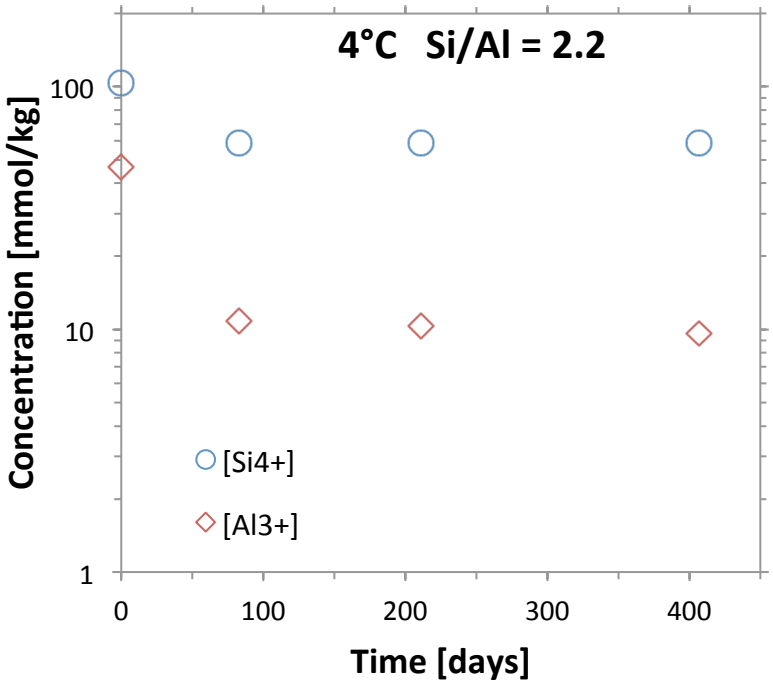

Figure 4.2: Changes in supernatant Si^{4+} and Al^{3+} concentrations over time for N-A-S-H equilibrated at 4 °C with bulk molar Si/Al ratio equal to 2.2

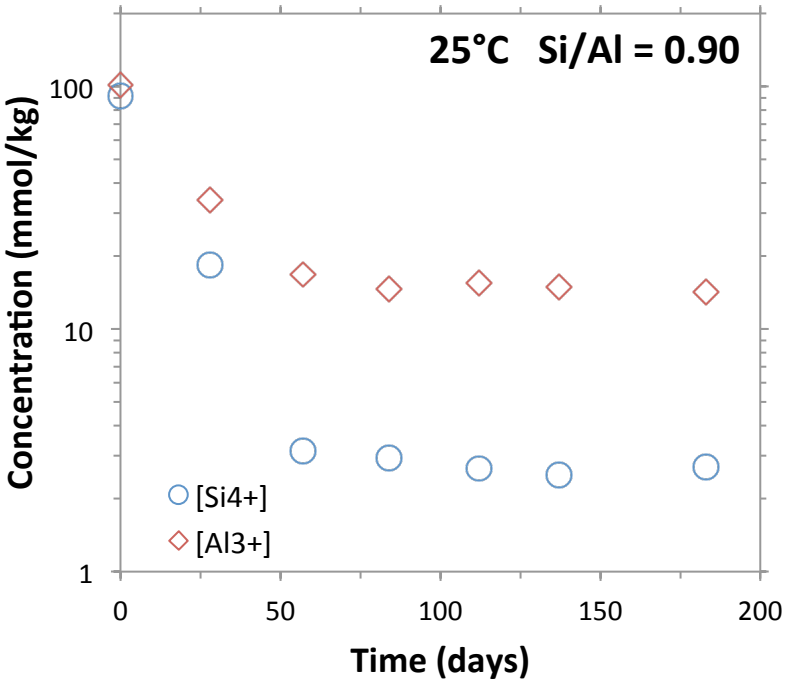

Figure 4.3: Changes in supernatant Si^{4+} and Al^{3+} concentrations over time for N-A-S-H equilibrated at 25 °C with bulk molar Si/Al ratio equal to 0.90

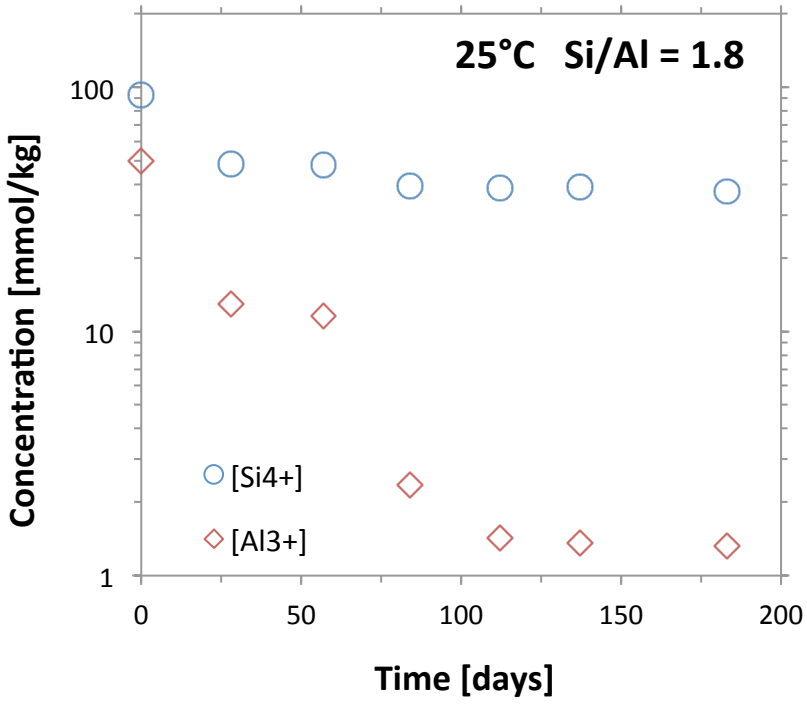

Figure 4.4: Changes in supernatant Si^{4+} and Al^{3+} concentrations over time for N-A-S-H equilibrated at 25 °C with bulk molar Si/Al ratio equal to 1.8

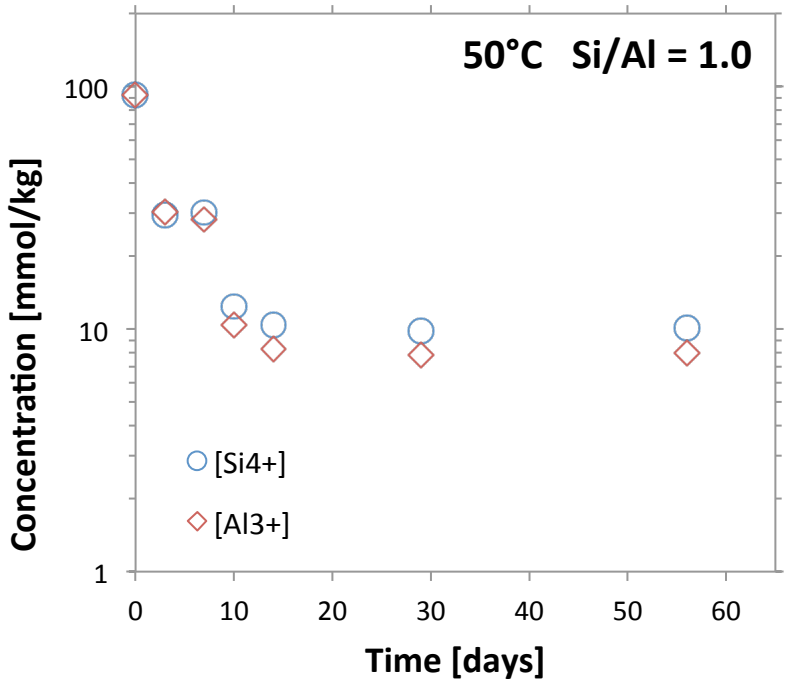

Figure 4.5: Changes in supernatant Si^{4+} and Al^{3+} concentrations over time for N-A-S-H equilibrated at 50 °C with bulk molar Si/Al ratio equal to 1.0

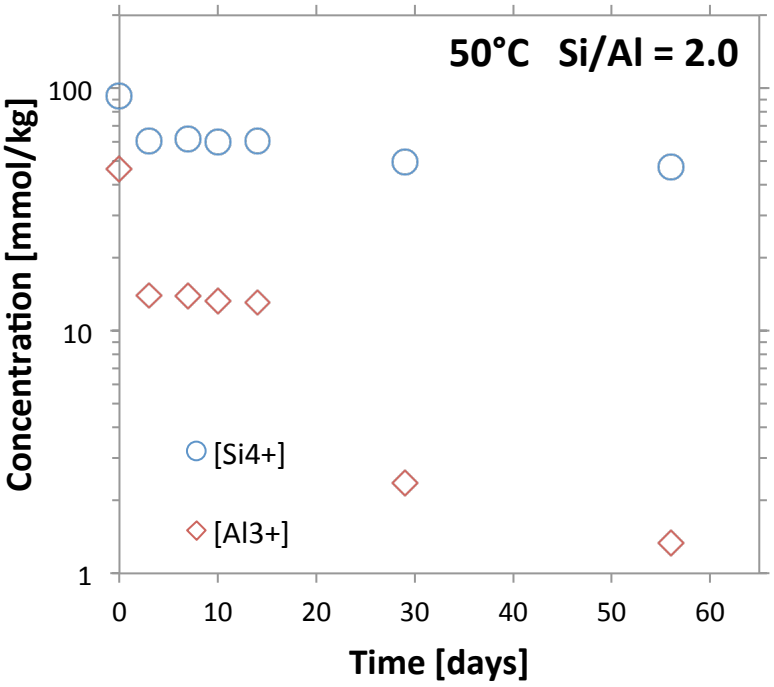

Figure 4.6: Changes in supernatant Si^{4+} and Al^{3+} concentrations over time for N-A-S-H equilibrated at 50 °C with bulk molar Si/Al ratio equal to 2.0

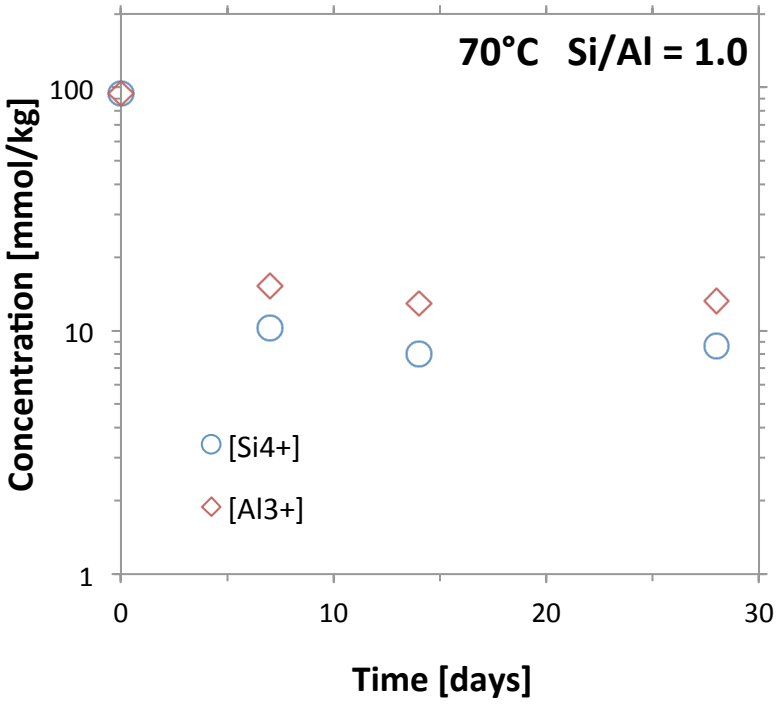

Figure 4.7: Changes in supernatant Si^{4+} and Al^{3+} concentrations over time for N-A-S-H equilibrated at 70 °C with bulk molar Si/Al ratio equal to 1.0

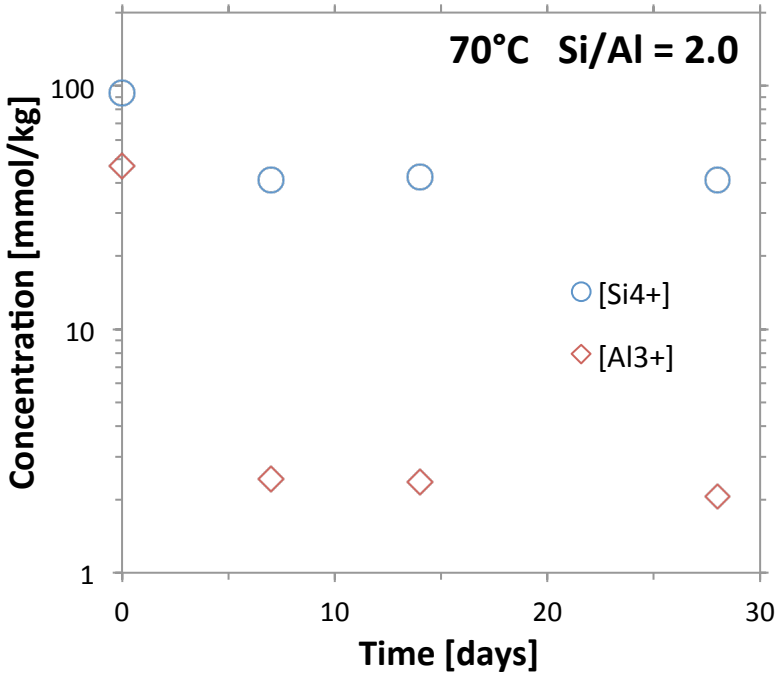

Figure 4.8: Changes in supernatant Si^{4+} and Al^{3+} concentrations over time for N-A-S-H equilibrated at 70 °C with bulk molar Si/Al ratio equal to 2.0

In all samples, both Si^{4+} and Al^{3+} concentrations decreased rapidly at all compositions, corresponding to the rapid early formation of N-A-S-H solids. Indeed, precipitated solids were observed visually in all experiments within seconds of mixing the sodium aluminate and sodium silicate stock solutions. After the initial rapid decrease in Si^{4+} and Al^{3+} concentrations, the concentrations generally continued to decrease over time, and eventually leveled off, at which points the equilibrated N-A-S-H solids and supernatant solutions were analyzed to determine the compositions of both.

Interestingly, the presence of an early plateau in Si^{4+} and Al^{3+} concentrations can be observed in several of the samples, where concentrations leveled off as if approaching equilibrium, but then rapidly decreased again. This is very visible in the sample reacted at 50 °C with bulk molar Si/Al = 2.0 (Figure 4.6), and was discussed in Chapter 3. Between

3 and 14 days, Si^{4+} and Al^{3+} concentrations leveled off, but dropped significantly again between 14 and 29 days. A similar plateau can be observed in the sample reacted at 25 °C with bulk molar Si/Al = 1.8 between 28 and 57 days (Figure 4.4). The plateau, followed by the rapid drop in Si^{4+} and Al^{3+} concentrations, is attributed to a transition from an x-ray amorphous N-A-S-H phase to the zeolitic phase Na-faujasite (discussed in detail in Chapter 3).

Comparing the plateaus observed in the two samples reacted at 50 °C (Figures 4.5 and 4.6), it is apparent that the plateau is significantly longer in the N-A-S-H reacted with bulk Si/Al = 2, lasting from 3 days to 14 days, compared to the N-A-S-H with bulk Si/Al = 1, where the plateau is only observed between 3 and 7 days. This trend was observed across all samples, where the higher the bulk Si/Al ratio, the longer the plateau lasted. For some N-A-S-H, such as the N-A-S-H with bulk molar Si/Al = 1 reacted at 25 °C (Figure 4.3), no plateau was observed at all. It is presumed that this is simply a result of measurements at insufficient time points to observe the plateau, rather than an absence of a plateau altogether. In the two N-A-S-H samples reacted at 70 °C (Figures 4.7 and 4.8), for example, the plateau presumably occurred before the 7 day samples were prepared for testing. Again, the primary intent with measuring supernatant concentrations over time was to determine the time required to reach equilibrium, rather than to resolve a detailed temporal path to equilibrium.

Notably, when the reaction temperature changed, the equilibrium concentrations and the path to equilibrium appear relatively consistent, aside from the expected increase in reaction rate as temperature increases. Generally, at equilibrium, Si^{4+} and Al^{3+} concentrations both reached roughly 10 mmol/kg for bulk Si/Al = 1 and reached roughly 40 and 2 mmol/kg, respectively, for bulk Si/Al = 2. There are two noteworthy exceptions: the N-A-S-H with Si/Al = 0.9 reacted at 25 °C (Figure 4.3) and the N-A-S-H with bulk

Si/Al = 2.2 reacted at 4 °C (Figure 4.2). In the former, the Si^{4+} concentration was notably lower at equilibrium, presumably because this is the only sample shown with Si/Al below 1, so Si^{4+} was the limiting reagent. In the latter, [Si^{4+}] and [Al^{3+}] remained higher than in other samples, at 58.5 mmol/kg and 9.60 mmol/kg, respectively. These concentrations are very similar to those observed at other temperatures with bulk Si/Al = 2 during the plateau, rather than at equilibrium. As mentioned previously, N-A-S-H with bulk Si/Al = 2 generally showed a longer plateau with respect to Si^{4+} and Al^{3+} concentrations, and the samples reacted at 4 °C were the slowest to equilibrate. As such, it is presumed that this N-A-S-H had not reached equilibrium even after 407 days, and the Si^{4+} and Al^{3+} concentrations are still in the plateau phase. Therefore, this particular N-A-S-H is not included in the calculation of thermodynamic quantities that follows.

4.3.2 Equilibrium aqueous chemistry and solid composition

Equilibrium supernatant concentrations for samples reacted at 4, 25, 50, and 70 °C with bulk Si/Al (molar) ranging from 0.9 to 2.2 are shown in Figure 4.9. For samples reacted at all temperatures, as bulk molar Si/Al increased from 0.9 to 2.2, supernatant Si^{4+} concentrations increased linearly from 2.5 to 59 mmol/kg and Al^{3+} concentrations decreased from 14.9 to 1.15 mmol/kg. It should be noted that bulk Si/Al ratios were manipulated by adjusting the bulk Al^{3+} in each sample, so at lower Si/Al ratios, Al^{3+} concentrations were highest. Na^{+} concentrations were measured as well in order to calculate thermodynamic properties. Relative changes in Na^{+} concentrations were small compared to the original concentrations (~1000 mmol/kg for all samples), and all measured values were within a few percent of the original values. While the actual measured values were used to calculate thermodynamic properties, there were no interesting trends in the values themselves, so they are not presented on their own.

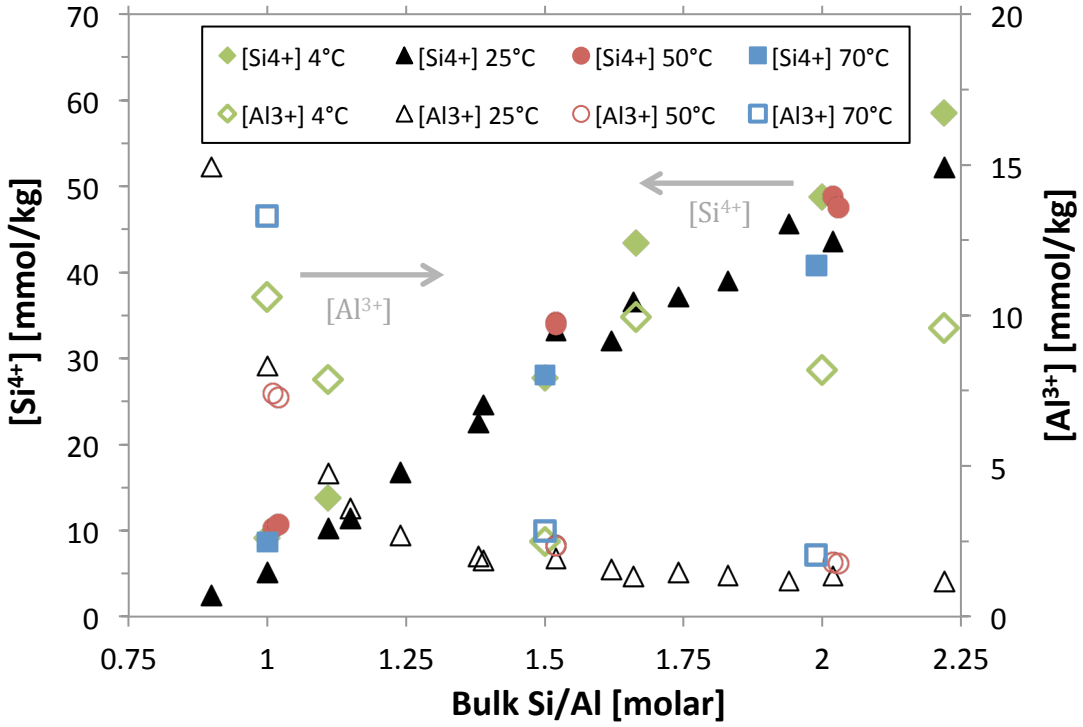

Figure 4.9: Si^{4+} and Al^{3+} concentrations versus bulk Si/Al molar ratio of N-A-S-H reacted at 4, 25, 50, and 70 °C for 365, 182, 56, and 28 days, respectively

Figure 4.10 to 4.12 show that temperature seems to have little effect on equilibrium supernatant concentrations. For a given bulk Si/Al ratio, Si^{4+} and Al^{3+} supernatant concentrations remained relatively constant across all temperatures. The obvious outlier, again, is the N-A-S-H samples reacted at 4°C with bulk Si/Al = 2, which did not reach equilibrium after the 407 day reaction time.

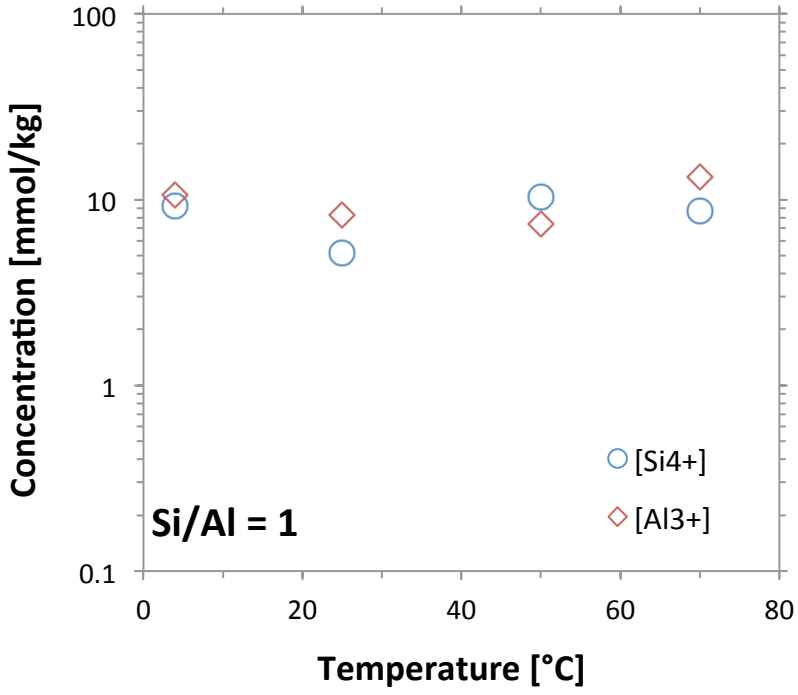

Figure 4.10: Changes in supernatant Si^{4+} and Al^{3+} concentrations with temperature for N-A-S-H with bulk Si/Al = 1 reacted at 4, 25, 50, and 70 °C for 407, 182, 56, and 28 days, respectively

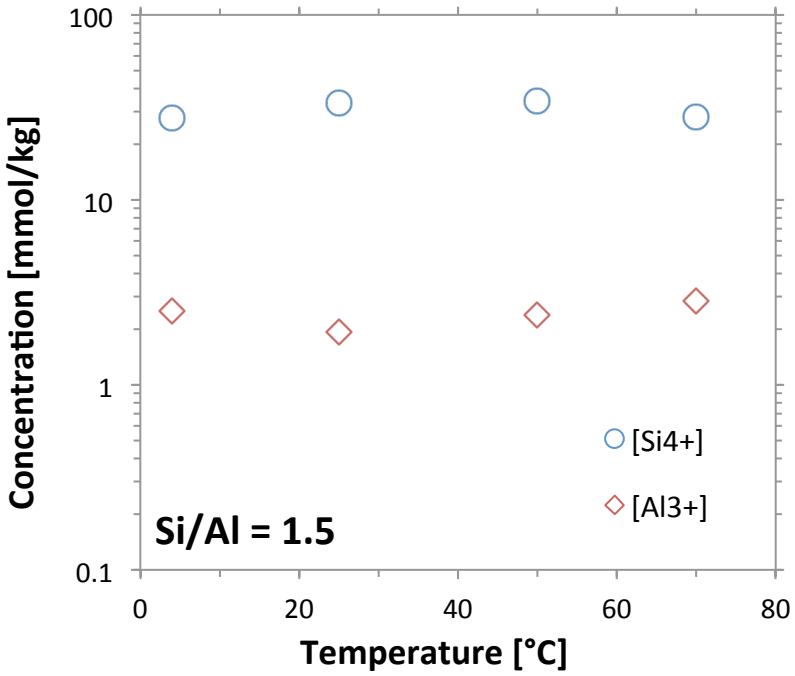

Figure 4.11: Changes in supernatant Si^{4+} and Al^{3+} concentrations with temperature for N-A-S-H with bulk Si/Al = 1.5 reacted at 4, 25, 50, and 70 °C for 407, 182, 56, and 28 days, respectively

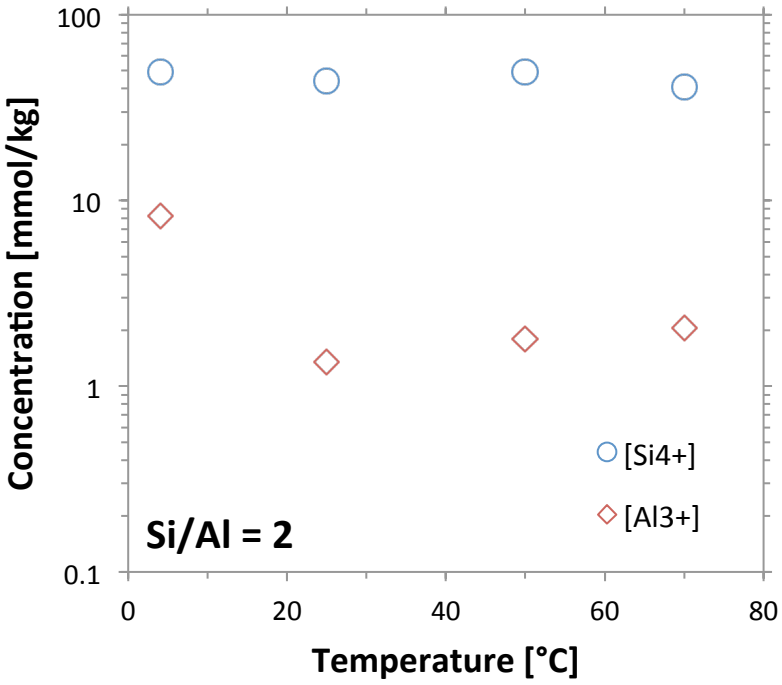

Figure 4.12: Changes in supernatant Si^{4+} and Al^{3+} concentrations with temperature for N-A-S-H with bulk Si/Al = 2 reacted at 4, 25, 50, and 70 °C for 407, 182, 56, and 28 days, respectively

Thermogravimetric data for N-A-S-H solids synthesized with bulk Si/Al = 1 to 2 at temperatures of 4, 25, 50, and 70 °C are shown in Figures 4.13 to 4.16. All of the samples showed continuous mass loss with peaks centered at 150 °C – 200 °C with the exception of the N-A-S-H with Si/Al = 2 equilibrated at 4 °C that did not reach equilibrium, which showed a peak centered at approximately 100°C. Three of the equilibrated N-A-S-H phases (4 °C, Si/Al = 1; 70 °C, Si/Al = 1.5; 70 °C, Si/Al = 2) showed a small additional peak at 100 °C – 150 °C. The mass losses correspond to a loss in evaporable and non-evaporable water, and total mass loss increased with increasing equilibration temperature for all samples. There was no systematic variation in the temperature at which peak mass loss occurred (i.e. the temperature at which the

derivative of mass loss was the most negative) across bulk compositions, and there was no substantial difference in total water loss across bulk compositions. All of the mass losses for all samples occurred between 40°C and approximately 400°C. Peak mass loss is generally observed between 175°C and 400°C for faujasite, and thermogravimetric data often show small additional peaks between 100 °C and 150°C [56], so the TGA data presented in Figures 4.13 to 4.16 are consistent with the x-ray diffractograms presented in Chapter 3.

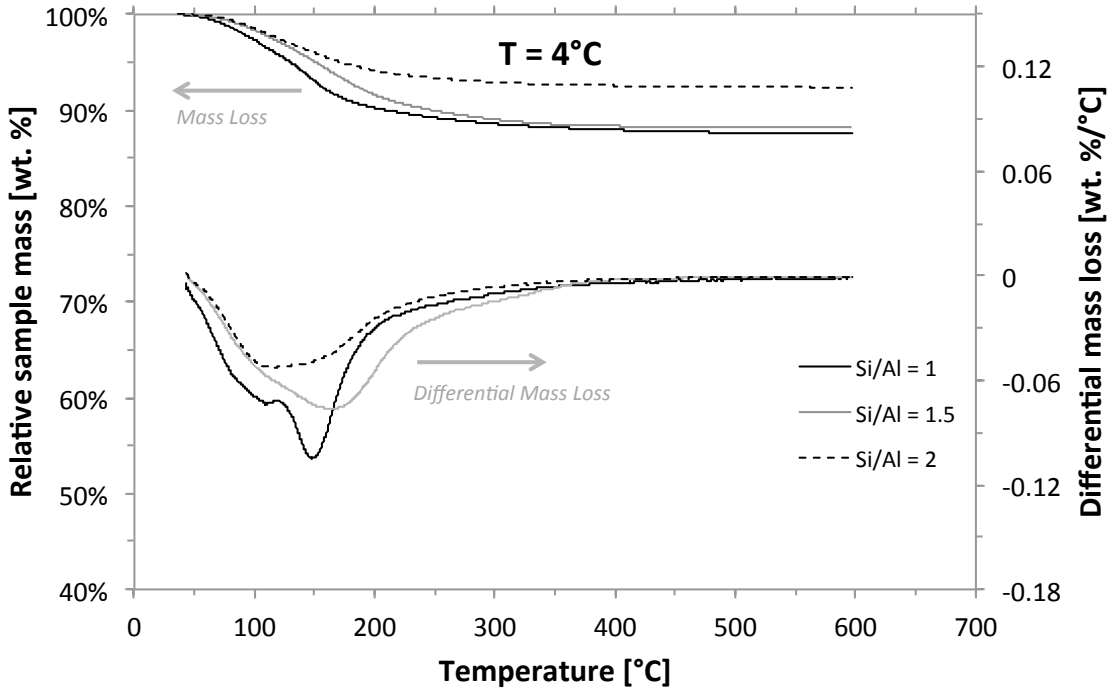

Figure 4.13: TGA data for N-A-S-H samples reacted at 4 °C for 364 days with bulk Si/Al = 1 to 2

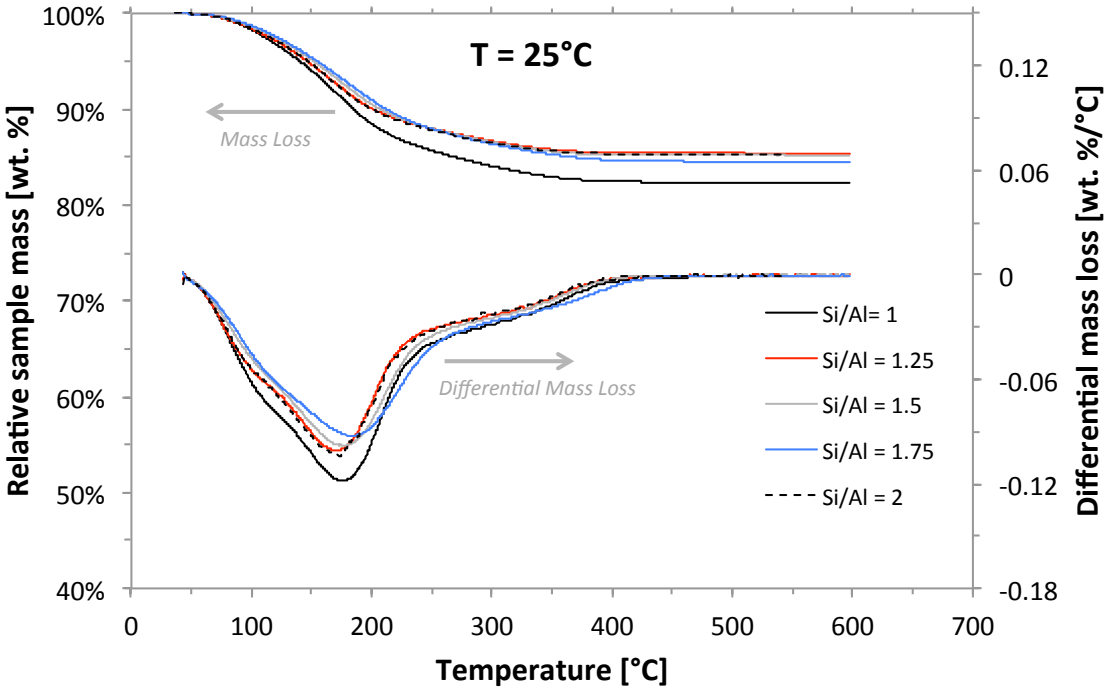

Figure 4.14: TGA data for N-A-S-H samples reacted at 25 °C for 182 days with bulk Si/Al = 1 to 2

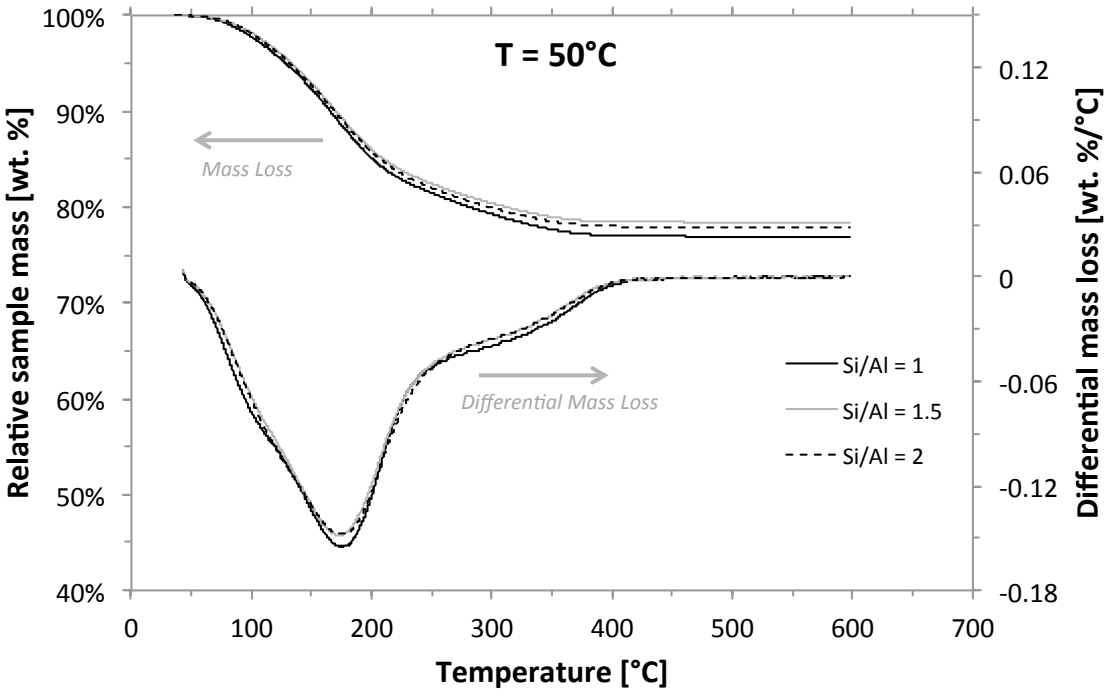

Figure 4.15: TGA data for N-A-S-H samples reacted at 50 °C for 56 days with bulk Si/Al = 1 to 2

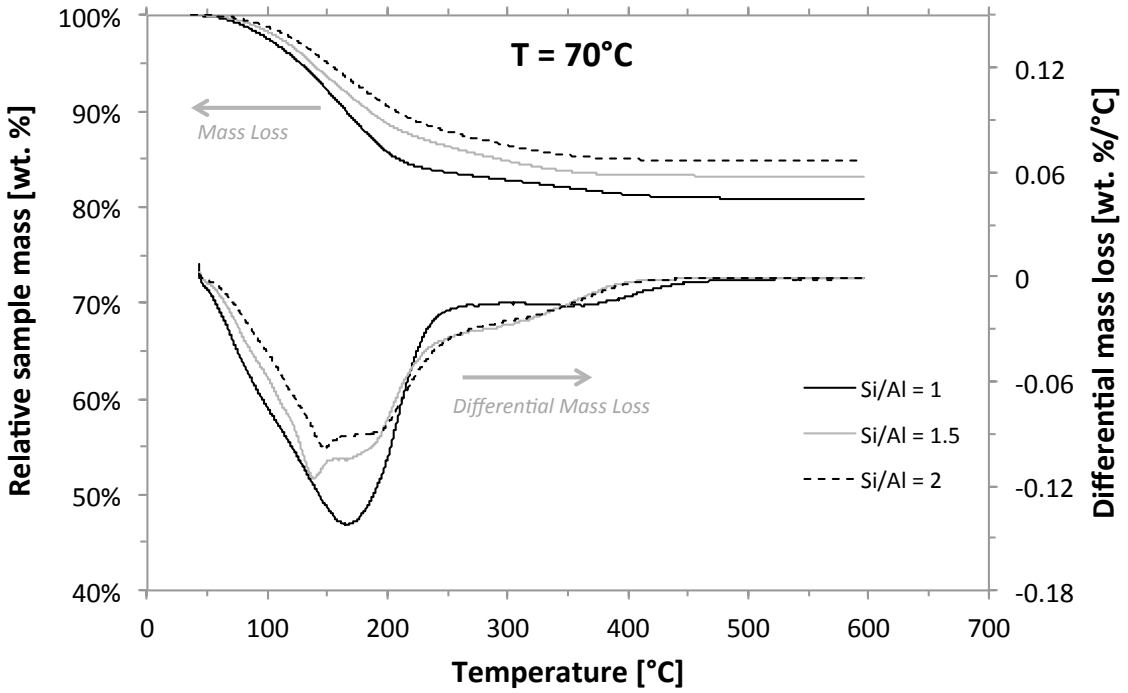

Figure 4.16: TGA data for N-A-S-H samples reacted at 70 °C for 28 days with bulk Si/Al = 1 to 2

Table 4.1 shows the compositions of the equilibrated solid N-A-S-H phases for bulk Si/Al molar ratios of 1, 1.5, and 2 for N-A-S-H equilibrated at 50 °C, 25 °C, and 4 °C. Compositions of additional N-A-S-H phases for bulk Si/Al molar ratios of 1.25 and 1.75 are shown for samples equilibrated at 25°C. Al_2O_3 and SiO_2 stoichiometric coefficients were calculated from changes in the aqueous phase concentrations. The molar fraction of Na_2O was assumed to be equal to the molar fraction of Al_2O_3 for each sample (i.e. $Na_2O/Al_2O_3 = 1$) based on the assumption that sodium is present as a charge balancing cation to alumina tetrahedra, which carry a -1 charge [1,78]. The mass losses from the TGA data presented in Figures 4.13 to 4.16 were used to calculate the water content of the equilibrated N-A-S-H phases.

Table 4.1: Composition of N-A-S-H with bulk Si/Al = 1 to 2 reacted at 4, 25, 50, and 70 °C for 407, 182, 56, and 28 days, respectively

Bulk Si/Al ratio (molar)	N-A-S-H composition
Temp = 70°C	
1	$NaAlSi_{1.06}O_{4.12}\bullet(H_2O)_{1.92}$
1.5	$NaAlSi_{1.10}O_{4.21}\bullet(H_2O)_{1.66}$
2	$NaAlSi_{1.17}O_{4.34}\bullet(H_2O)_{1.51}$
Temp = 50°C	
1	$NaAlSi_{0.98}O_{3.96}\bullet(H_2O)_{1.77}$
1.5	$NaAlSi_{1.00}O_{3.99}\bullet(H_2O)_{1.50}$
2	$NaAlSi_{1.01}O_{4.03}\bullet(H_2O)_{1.31}$
Temp = 25°C	
1	$NaAlSi_{1.04}O_{4.09}\bullet(H_2O)_{1.73}$
1.25	$NaAlSi_{1.06}O_{4.13}\bullet(H_2O)_{1.39}$
1.5	$NaAlSi_{1.08}O_{4.17}\bullet(H_2O)_{1.42}$
1.75	$NaAlSi_{1.10}O_{4.20}\bullet(H_2O)_{1.51}$
2	$NaAlSi_{1.10}O_{4.20}\bullet(H_2O)_{1.62}$
Temp = 4°C	
1	$NaAlSi_{1.02}O_{4.13}\bullet(H_2O)_{1.14}$
1.5	$NaAlSi_{1.09}O_{4.21}\bullet(H_2O)_{1.10}$
2	$NaAlSi_{1.15}O_{4.34}\bullet(H_2O)_{0.69}$

Figure 4.17 shows a weak, increasing trend in N-A-S-H Si/Al molar ratio with increasing bulk Si/Al ratio for all reaction temperatures. The Si/Al molar ratio of N-A-S-H was relatively close to 1 for all bulk compositions and temperatures studied, ranging from 0.98 to 1.17. Previous studies [4,79–81] have shown that inorganic polymer activating solution chemistry and, more specifically, the degree of silicate polymerization, greatly affect the structure and composition of product phases. In the

present study, the silicate stock solution contained 2 M NaOH and 0.2 M Si^{4+}, yielding a Si/Na ratio of 0.1. At this pH and Si/Na ratio, all silicates are expected to be monomeric with $H_2SiO_4^{2-}$ being the dominant species [25,82] .

As discussed in Chapter 3, the x-ray diffraction of the N-A-S-H precipitated from solution indicated that the N-A-S-H has the structure of faujasite. Faujasite is in the zeolite family, and is classified more specifically as zeolite-X or zeolite-Y depending on its Si/Al ratio. Faujasite with Si/Al molar ratio less than 1.5 is classified as zeolite-X, while faujasite with Si/Al ratio greater than 1.5 is classified as zeolite-Y [62]. Here, all Si/Al ratios are less than 1.5, so the N-A-S-H is classified as zeolite-Z. As discussed in Chapter 3, zeolite-X has been synthesized in previous studies under similar conditions [58,64,65].

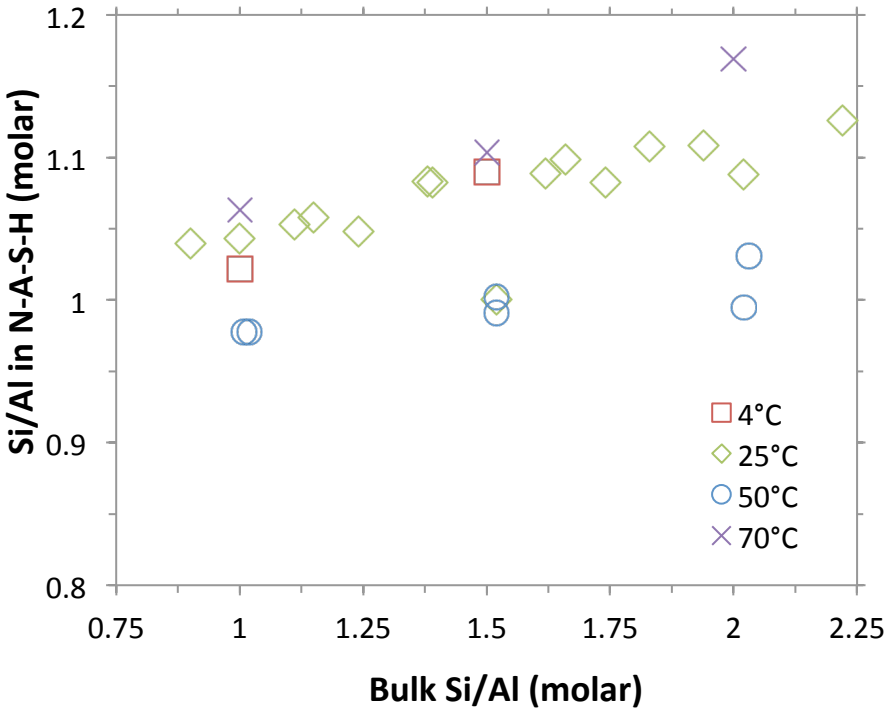

Figure 4.17: N-A-S-H Si/Al molar ratio as a function of bulk Si/Al molar ratio. N-A-S-H Si/Al molar ratios were calculated from mass balance by subtracting supernatant Si^{4+} and Al^{3+} compositions from bulk Si^{4+} and Al^{3+} concentrations

Solubility products (K_{sp}) were calculated for each of the N-A-S-H solids with the bulk compositions shown Table 4.1. The dissolution reaction assumed to calculate solubility products is shown in Equation (4.1):

$$NaAlSi_xO_{(2x+2)} \cdot (H_2O)_{y(S)} + (2x - y - 2)H_2O_{(l)} + 4H^+_{(aq)} \leftrightarrow \mathrm{Na}^+_{(aq)} + Al^{3+*}_{(aq)} + xH_4SiO^o_{4(aq)} \quad (4.1)$$

where x is the Si/Al molar ratio of the solids and y is the stoichiometric coefficient of H_2O in the solids. Here, $Al^{3+*}_{(aq)}$ refers to the specific species, where previously, $Al^{3+}_{(aq)}$

referred to the total dissolved aluminum. Following the reaction in Equation (4.1), equilibrium solubility products were calculated with Equation (4.2):

$$K_{sp} = \left\{Na^{+}_{(aq)}\right\} \cdot \left\{Al^{3+*}_{aq}\right\} \cdot \left\{H_4SiO^{o}_{4(aq)}\right\}^{x} \cdot \left\{H^{+}_{(aq)}\right\}^{-4} \cdot \left\{H_2O_{(l)}\right\}^{(y-2x+2)} \quad (4.2)$$

Activities of $Na^{+}_{(aq)}$, $Al^{3+*}_{(aq)}$, $H_4SiO^{o}_{4(aq)}$, $H^{+}_{(aq)}$, and $H_2O_{(l)}$ were determined with PHREEQC using the measured supernatant concentrations of $Na^{+}_{(aq)}$, $Si^{4+}_{(aq)}$, $Al^{3+}_{(aq)}$ with the pH calculated from charge balance. It should be noted that in Equations (4.1) and (4.2), $Al^{3+}_{(aq)}$ refers to the specific species, where previously it referred to the total dissolved aluminum. The Truesdell-Jones version of the extended Debye-Hückel equation was used within PHREEQC with the LLNL database to determine activity coefficients of each species, shown in Equation (4.3):

$$log\gamma_i = \frac{-Az_i^2\sqrt{I}}{1+B\alpha_i\sqrt{I}} + bI \quad (4.3)$$

Figure 4.18 shows a decreasing trend in solubility product with increasing temperature with $\log_{10}(K_{sp})$ ranging from 13.7 to 8.8. A weak increasing trend in solubility product with increasing bulk Si/Al ratio exists, but changes with Si/Al ratio remain within the 0.5 log unit error. A solubility product was not calculated for Si/Al = 2, 4 °C because equilibrium conditions were not achieved for this N-A-S-H.

While there is a large difference in solubility products for N-A-S-H reacted at 4 °C and 70 °C, it should be noted once again that aqueous concentrations of Si^{4+}, Al^{3+}, and Na^{+} changed very little with temperature (Figures 4.10 to 4.12). The differences in solubility products of these systems stem from the changing pH of these systems with

temperature, which affects the H^+ reactant term that is raised to the -4 power and thus has a major impact on the solubility products.

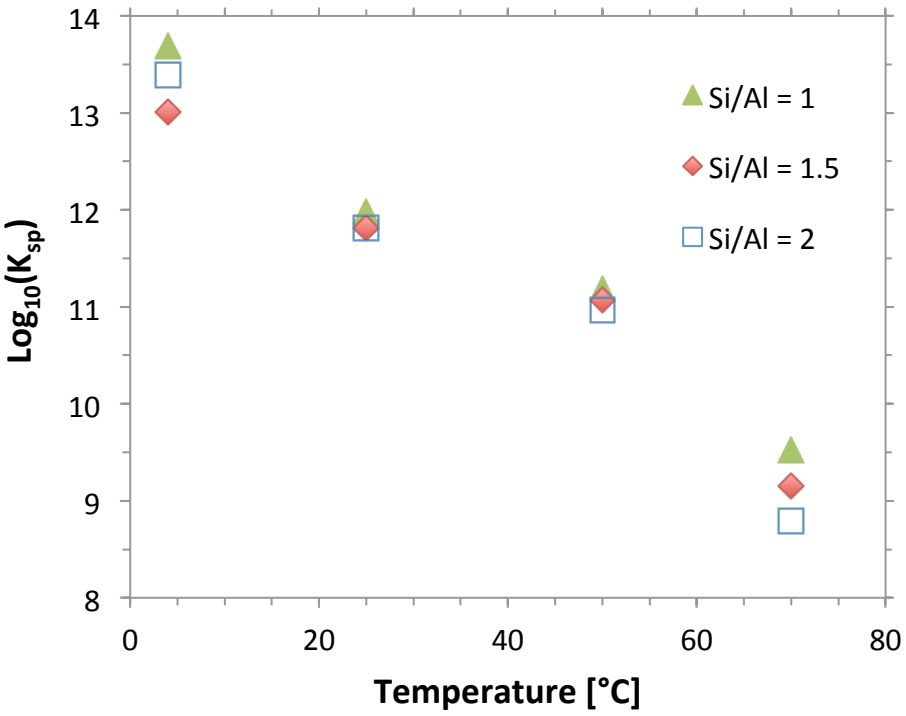

Figure 4.18: Solubility products of N-A-S-H reacted at 4, 25, 50, and 70 °C for 365, 182, 56, and 28 days, respectively

Since both temperature and Si/Al ratio both have relatively small impacts on N-A-S-H solubility, but both of these factors have been shown previously to impact the phase balances and engineering properties of IPBs, the primary effects of these two parameters most likely arise from non-thermodynamic considerations.

As in Chapter 3, equilibrium constants of both amorphous and crystalline N-A-S-H phases were determined using a reaction that represents the dominant species rather than the convention presented by Sposito [66]. The reaction used to determine these equilibrium constants is shown again in Equation (4.4):

$$NaAlSi_xO_{(2x+2)} \cdot (H_2O)_{y(S)} + (2-y)H_2O_{(l)} + 2xOH^-_{(aq)} \leftrightarrow \mathrm{Na}^+_{(aq)} + Al(OH)^-_{4(aq)} + xH_2SiO^{2-}_{4(aq)} \quad (4.4)$$

Following the reaction shown in Equation (4.4), equilibrium constants were calculated as using Equation (4.5):

$$K_{sp} = \left\{\mathrm{Na}^+_{(aq)}\right\} \cdot \left\{\mathrm{Al(OH)}^-_{4(aq)}\right\} \cdot \left\{\mathrm{H_2SiO}^{2-}_{4(aq)}\right\}^x \cdot \left\{\mathrm{OH}^-_{(aq)}\right\}^{-2x} \cdot \left\{\mathrm{H_2O}_{(l)}\right\}^{(y-2)} \quad (4.5)$$

Equilibrium constants were calculated using Equation (4.5) for both crystalline and amorphous N-A-S-H samples, and are shown in Figure 4.19. The amorphous samples were reacted for 211, 28, and 7 days for 4, 25, and 50 °C reaction temperatures, respectively. These times correlated well with the temporal plateaus in Si^{4+} and Al^{3+} concentrations shown in Figures 4.1 to 4.8. No solubility data are available for amorphous phases reacted at 70 °C since the samples N-A-S-H was crystalline prior to the first supernatant concentration measurements. It should be noted that supernatant Na^+ concentrations and water content were not measured for the amorphous phases, as the original intent of this study was to understand equilibrium conditions. As such, to calculate amorphous phase solubility products 1000 mmol/kg was assumed for the Na^+ supernatant concentrations, and the water contents were set equal to the same water contents measured in the analogous crystalline phases. While these assumptions may not be completely accurate, deviations in these values have relatively little impact on the amorphous phase equilibrium constants.

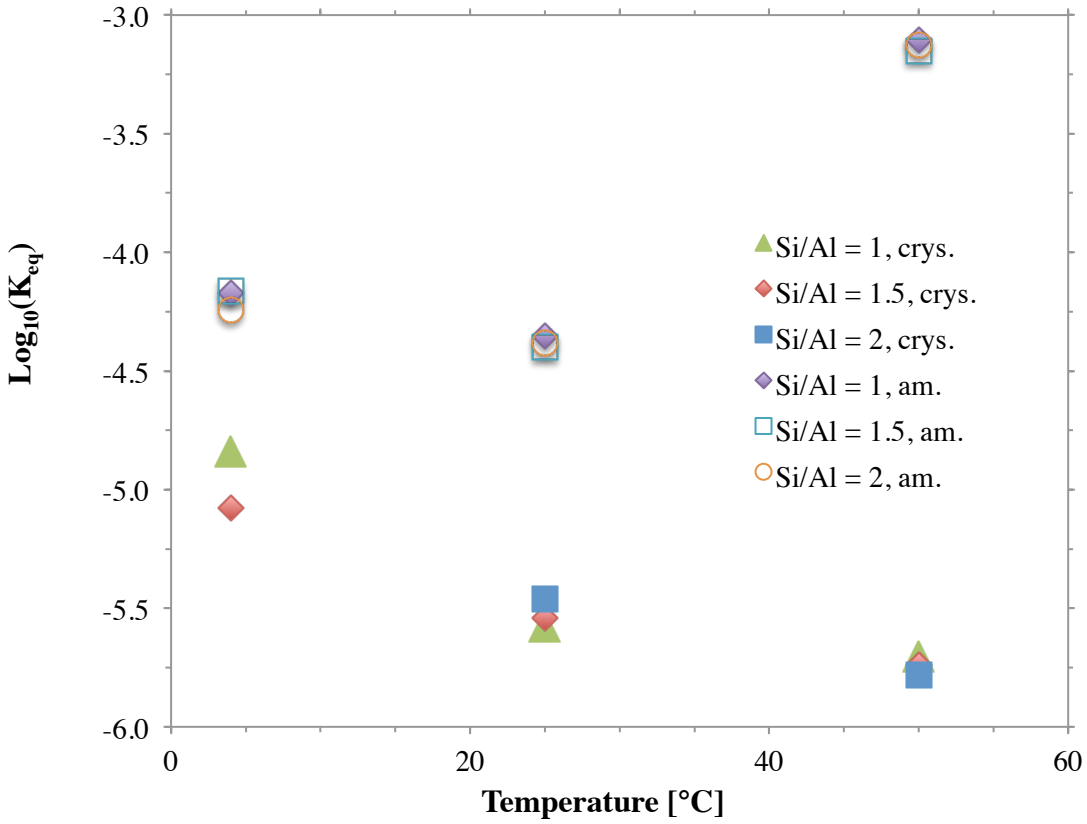

Figure 4.19: Equilibrium constants of crystalline and amorphous N-A-S-H samples reacted at 4, 25, and 50 °C with bulk Si/Al = 1, 1.5, and 2 calculated using Equation (4.5)

At all temperatures, the equilibrium constants for amorphous phases were significantly higher than the equilibrium constants for the crystalline analogues. The equilibrium constants of the amorphous phases were lowest at 25 °C and highest at 50 °C, although care should be taken in making a direct comparison since the amorphous N-A-S-H phases are believed to be in a pseudo-equilibrium state, and the time points studied, while based on the plateaus shown in Figures 4.1 to 4.8, were somewhat arbitrary. There were no significant differences between equilibrium constants across

bulk Si/Al ratios for the amorphous phases at a given temperature, suggesting that the same phase was formed regardless of Si/Al ratio.

The enthalpy of dissolution for a given phase can be determined by looking at the relationship between solubility product and temperature. Doing so, however, requires that the solubility product of one specific phase is determined at various temperatures. The solubility products shown in Figure 4.18 represent the solubilities of N-A-S-H phases with slightly different compositions (Table 4.1). To determine enthalpy of dissolution, the same solid phase must be analyzed across temperatures. As such, for N-A-S-H synthesized at bulk compositions of Si/Al =1, 1.5, and 2, average compositions across the four temperatures were taken to represent that phase across all temperatures. These solubility products were then used to determine the enthalpy of dissolution using the Van't Hoff relationship. The N-A-S-H compositions used for bulk Si/Al ratios of Si/Al = 1, 1.5, and 2 were determined by averaging the stoichiometric coefficients shown in Table 4.1 across all temperatures for a given bulk Si/Al ratio. These compositions are shown in Table 4.2. Again, the N-A-S-H synthesized at 4 °C with bulk Si/Al = 2 was excluded when determining the average composition and from all enthalpy calculations, since it was not believed to have reached equilibrium.

Table 4.2: Average compositions of N-A-S-H synthesized at 4, 25, 50, and 70 °C for bulk Si/Al molar ratios of 1, 1.5, and 2 used to determine enthalphies of dissolution.

Bulk Si/Al ratio (molar)	N-A-S-H composition
1	$NaAlSi_{1.03}O_{4.07}\bullet(H_2O)_{1.64}$
1.5	$NaAlSi_{1.07}O_{4.14}\bullet(H_2O)_{1.42}$
2	$NaAlSi_{1.09}O_{4.19}\bullet(H_2O)_{1.48}$

The temperature dependence of the solubility product is expressed in the Van't Hoff relationship, shown in Equation (4.4):

$$\ln\left(\frac{K_2}{K_1}\right) = -\frac{\Delta H^\circ}{R}\left(\frac{1}{T_2} - \frac{1}{T_1}\right) \tag{4}$$

where K_2 and K_1 are the solubility products at temperatures T_2 and T_1, ΔH° is the enthalpy of the dissolution reaction, and R is the universal gas constant, 8.314 J/K-mol. It follows that plotting $\log_{10}(K_{sp})$ versus the reciprocal of temperature yields a line, referred to as the Van't Hoff plot, whose slope is $-\Delta H^\circ/2.3R$.

Van't Hoff plots for N-A-S-H with bulk Si/Al = 1, 1.5, and 2 are shown in Figures 4.20, 4.21, and 4.22, respectively.

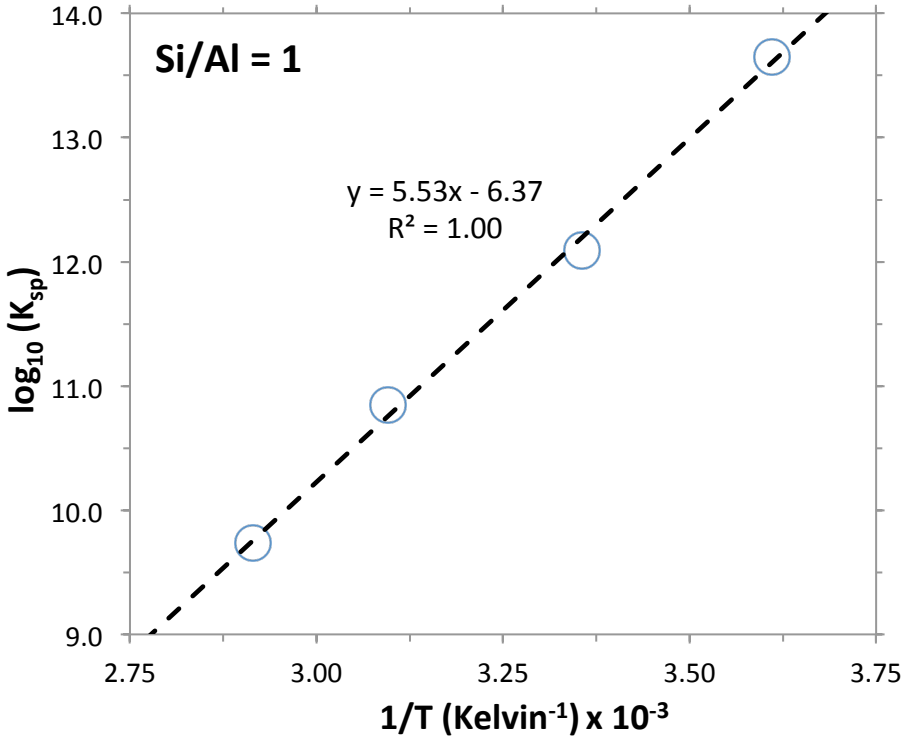

Figure 4.20: Solubility products versus the reciprocal of temperature for N-A-S-H with bulk Si/Al = 1 reacted at 4, 25, 50, and 70 °C for 407, 182, 56, and 28 days, respectively

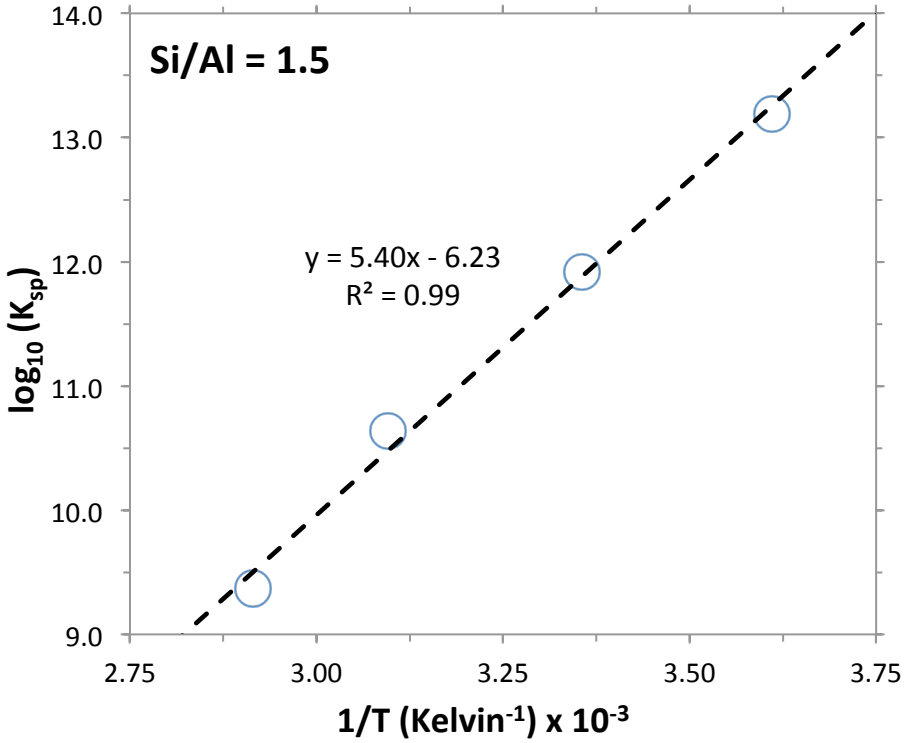

Figure 4.21: Solubility products versus the reciprocal of temperature for N-A-S-H with bulk Si/Al = 1.5 reacted at 4, 25, 50, and 70 °C for 407, 182, 56, and 28 days, respectively

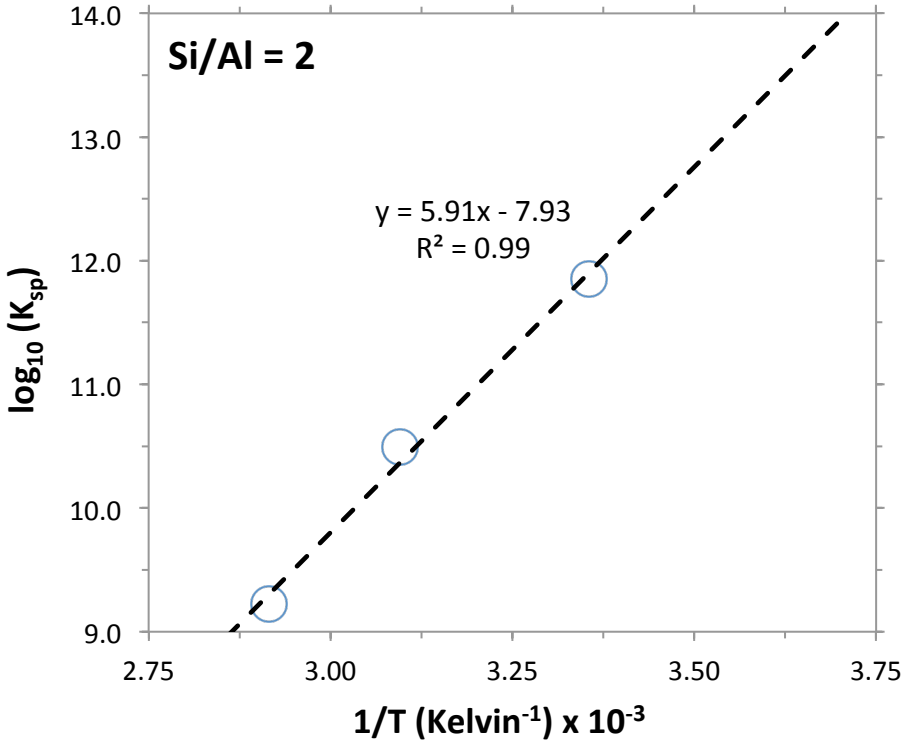

Figure 4.22: Solubility products versus the reciprocal of temperature for N-A-S-H with bulk Si/Al = 2 reacted at 25, 50, and 70 °C for 182, 56, and 28 days, respectively

Enthalpies of reaction, $\Delta H°$, were calculated for the N-A-S-H dissolution reaction shown in Equation (4.1) and are shown in Table 4.3. The absolute errors were determined from the line fit using the LINEST function in Microsoft Excel. Enthalpies of reaction ranged from -103 to -113 kJ/mol with no observable trend between enthalpy and bulk composition. The negative values of $\Delta H°$ indicate that the dissolution of N-A-S-H is exothermic.

Table 4.3: Enthalpies of reaction of N-A-S-H synthesized with bulk Si/Al = 1, 1.5, and 2 calculated from slopes of lines the Van't Hoff plots shown in Figures 4.19 to 4.21.

Bulk Si/Al	$\Delta H°$ (kJ/mol)
1	-105 ± 3
1.5	-103 ± 6
2	-113 ± 9

4.4 CONCLUSIONS

This chapter has examined the effect of temperature on the composition, structure, and solubility of sodium aluminosilicate hydrate, the primary binding phase in IPBs. Temperature had little effect on the composition of N-A-S-H across the range of bulk compositions studied, and while solubility decreased with increasing temperature, that trend was attributed to the changing speciation of silicates with the temperature-dependent pH. Additionally, solubility products of N-A-S-H were calculated for a range of compositions across various temperatures, and these values will allow for thermodynamic modeling of N-A-S-H systems, which can have a substantial impact on our ability to predict engineering properties for these low-CO_2 binders. Equilibrium constants were determined for the dissolution reaction of amorphous N-A-S-H, and were found to vary little based on bulk Si/Al ratio. Additionally, the solubility of amorphous phases was found to be significantly higher than that of the crystalline analogues. Enthalpies of dissolution, another important thermodynamic parameter, were also determined for N-A-S-H reacted with bulk Si/Al molar ratios from 1 to 2.

Chapter 5: Conclusions and Future Work

IPBs provide an exciting new opportunity to reduce CO_2 emissions and energy expenditure from the construction industry. While their performance is promising, the wide variation in source material properties presents a challenge that has prevented their widespread use. A better understanding of the fundamental chemistry of these binders can help facilitate property prediction, especially through the use of thermodynamic models.

The work presented here is an important step in that direction. A rigorous method was developed, refined, and presented in detail for measuring the solubility of N-A-S-H, the primary binding phase in IPBs. Then, solubility data and the relationship between bulk composition and N-A-S-H composition was presented. It was found that activator Si/Na ratios play a much bigger role in predicting N-A-S-H Si/Al ratios than bulk Si/Al ratios do. This is a significant finding, as it points to the fact that there is a need for future research to look very carefully at the effects of activator chemistry. Finally, the effect of temperature on N-A-S-H composition and solubility was studied. It was found that solubility changes slightly with temperature, though dissolved supernatant concentrations vary little with temperature.

The method for measuring the composition and solubility of N-A-S-H presented in Chapter 2 will facilitate future studies that expand on the work presented in this dissertation. While the methods presented are familiar to many environmental engineers and geochemists, the version presented here is the most detailed to date with regards to cementitious materials. After a discussion regarding the importance and significance of thermodynamic modeling of IPBs, a detailed literature review of previous studies on the solubility and thermodynamic model development of cementitious materials was

presented. Then, specific considerations for synthesizing and analyzing lab-grade N-A-S-H, such as the importance of working in a CO_2-free environment, were discussed. Finally, a rigorous method for synthesizing and analyzing N-A-S-H with controlled compositions and at various temperatures was presented.

In Chapter 3, the temporal evolution of N-A-S-H composition and structure, as well as supernatant chemistry, were discussed. It was found that supernatant Si^{4+} and Al^{3+} concentrations drop quickly from their original concentrations as an initial solid precipitates from solution. The concentrations then plateau, corresponding to pseudo-equilibrium with the early formation of an amorphous N-A-S-H phase, and then later drop again as a crystalline N-A-S-H phase forms. The crystalline phase was identified as zeolite-X using XRD, and NMR showed that the local structural environment continues to change even after the transition to an XRD-crystalline structure.

Once supernatant Si^{4+} and Al^{3+} concentrations stabilized, the equilibrium solid and solution conditions were analyzed. The composition of solids was presented, and it was found that the Si/Na ratio of sodium silicate solution has a much greater impact on N-A-S-H composition than does bulk Si/Al ratio. Solubility of the crystalline phase, zeolite-X, was quantified using three distinct approaches and agreed closely with existing literature. The solubility of the amorphous phase was presented as well, and will be important in the development in stepwise thermodynamic models of these systems. The solubility of the amorphous phases changed very little across bulk Si/Al compositions, suggesting that a single amorphous phase was formed independent of bulk Si/Al.

Chapter 4 presented the effects of temperature on the composition and solubility of N-A-S-H phases. It was found that temperature has little effect on N-A-S-H composition, and while solubility products varied slightly with temperature, these changes were attributed to the speciation of silicon and aluminum species resulting from

pH changes with temperature. The solubility of amorphous phases varied across temperatures, with the lowest solubility occurring at 25 °C, although it is not clear how much these differences arise from the fact that time points that were somewhat arbitrary were choses for amorphous phase analysis. Finally, enthalpies of solution were determined using the Van't Hoff relation. The enthalpy of solution varied little between bulk Si/Al compositions, reinforcing the notion that a single N-A-S-H phase is formed regardless of bulk Si/Al ratio.

There are several important opportunities to expand on the work presented here. Perhaps first and foremost is the development and validation of thermodynamic models for synthetic N-A-S-H, predicting the phase assemblages based on precursor properties and processing conditions. The next obvious step from there is to expand those models to real IPB systems, incorporating impurities that exist in fly ash and other aluminosilicate precursors. If the balance of phases in the binders can be predicted, it is not unreasonable to think that one could extrapolate from there to predict engineering properties as well as volume changes. Similar models for OPC have enabled the prediction of phase development in OPC systems based on the minimization of free energy. For IPBs, these models could serve as a tool to screen for promising IPB solid precursor sources and predict the properties of IPBs. Additionally, the models could be used to evaluate and optimize IPB formulations and processing conditions.

Once a preliminary thermodynamic model for IPB formation is developed, it should be iteratively validated and refined. This could be accomplished by comparing model predictions with experimental results for the evolution of heat release (by calorimetry), pore solution composition, and volume changes. To validate such models, glasses with controlled compositions could be used to eliminate the complicating effects of impurities and regulate the rate of dissolution of the solid precursors. Ultimately, the

aim is to model "real-life" IPBs, enabling the rapid prediction of engineering properties for a given set of precursors and processing conditions. Additionally, continued work in this area will advance the general understanding of IPB chemistry, and may lead to discoveries that allow for the reduction in activator pH and improve the safety of these materials.

Another opportunity to expand on this work would be to widen the range of compositions studied. Here, bulk Si/Al ratios from 1 to 2 were studied based on previous literature stating that this is the optimum range. It is possible, though, that even if precursor or bulk compositions remain in the range of Si/Al = 1 to 2, there may be time when the pore solution composition falls outside of that range. Understanding the implications of that occurrence may prove useful. Furthering our understanding of the effect of precursor Si/Na ratio will also be an important step in enabling the widespread use of IPBs.

In addition to varying the compositions within N-A-S-H systems, adding impurities to these systems will take them a step closer to "real-life" IPBs. Calcium is the obvious starting point, as calcium plays an important role in IPBs, especially when high-calcium solid precursors are selected. The solubility and composition relations of C-A-S-H have been studied extensively by Myers et al. [18] and L'Hopital et al. [31]. Additionally, C-A-S-H with the addition of alkalis has been studied by Myers et al. [16,19]. Eventually, understanding a continuum of compositions from N-A-S-H to C-A-S-H with varying level of calcium would facilitate the understanding of using precursors with varying levels of calcium. Introducing controlled amounts of CO_2 is another important step toward a more realistic system.

Finally, while the method for measuring N-A-S-H solubility presented in Chapter 2 is a step in the right direction, there is certainly room for improvement in refining this

method. The hope is that this work will inspire new research by setting the stage for the importance of measuring N-A-S-H solubility and of developing thermodynamic models. Ultimately, IPBs can serve as a low-CO_2 alternative to portland cement concrete, and the contributions of this work are an important step in that direction.

Appendix A

Ionic strength, pH, and aqueous species compositions of the amorphous and crystalline N-A-S-H phases are presented in Table A.1 and Table A.2, respectively.

Table A.1: Ionic strength, pH, and aqueous species compositions for the amorphous N-A-S-H systems

Temp. (°C)	Bulk Si/Al Ratio (molar)	Replicate (No.)	Ionic Strength (mol/kg soln.)	pH	$\{H^+\}$ (mol/kg soln.)	$\{OH^-\}$ (mol/kg soln.)	$\{H_4SiO_4^o\}$ (mol/kg soln.)	$\{H_3SiO_4^-\}$ (mol/kg soln.)	$\{H_2SiO_4^{-2}\}$ (mol/kg soln.)	$\{AlO_2^-\}$ (mol/kg soln.)	$\{Al^{3+}\}$ (mol/kg soln.)	$\{Na^+\}$ (mol/kg soln.)
4	1	1	9.55E-01	14.54	2.84E-15	5.54E-01	8.72E-13	5.17E-05	3.45E-03	1.38E-02	2.06E-35	6.20E-01
	1.5	1	9.75E-01	14.52	2.94E-15	5.35E-01	5.62E-09	9.83E-05	6.33E-03	8.29E-03	1.43E-35	6.20E-01
	2	1	9.86E-01	14.51	3.01E-15	5.23E-01	7.35E-09	1.26E-04	7.91E-03	6.47E-03	1.22E-35	6.20E-01
25	1	1	9.41E-01	13.79	1.60E-14	5.56E-01	5.05E-08	3.41E-04	1.93E-03	1.79E-02	1.06E-34	6.14E-01
	1.25	1	9.43E-01	13.79	1.60E-14	5.54E-01	6.79E-08	4.57E-04	2.59E-03	1.22E-02	7.26E-35	6.12E-01
	1.5	1	9.46E-01	13.78	1.62E-14	5.48E-01	9.05E-08	6.02E-04	3.37E-03	9.66E-03	6.05E-35	6.10E-01
	1.75	1	9.47E-01	13.78	1.64E-14	5.43E-01	1.06E-07	7.01E-04	3.88E-03	8.78E-03	5.71E-35	6.09E-01
	2	1	9.49E-01	13.77	1.65E-14	5.37E-01	1.22E-07	8.00E-04	4.39E-03	8.04E-03	5.43E-35	6.07E-01
50	1	1	9.21E-01	13.05	8.66E-14	5.50E-01	4.61E-07	1.27E-03	2.38E-02	1.66E-02	3.07E-34	5.96E-01
	1	2	9.21E-01	13.05	8.65E-14	5.51E-01	4.56E-07	1.26E-03	2.36E-02	1.63E-02	3.00E-34	5.96E-01
	1.5	1	9.12E-01	13.05	8.74E-14	5.45E-01	7.48E-07	2.05E-03	3.78E-02	1.01E-02	1.94E-34	5.89E-01
	1.5	2	9.12E-01	13.05	8.73E-14	5.46E-01	7.41E-07	2.03E-03	3.75E-02	9.89E-03	1.89E-34	5.89E-01
	2	1	9.06E-01	13.04	8.82E-14	5.40E-01	9.47E-07	2.57E-03	4.71E-02	8.14E-03	1.63E-34	5.84E-01
	2	2	9.05E-01	13.04	8.83E-14	5.39E-01	9.61E-07	2.60E-03	4.77E-02	8.04E-03	1.61E-34	5.83E-01

Table A.2: Ionic strength, pH, and aqueous species compositions for the crystalline N-A-S-H (zeolite-X) systems

Temp. (°C)	Bulk Si/Al Ratio (molar)	Replicate (No.)	Ionic Strength (mol/kg soln.)	pH	$\{H^+\}$ (mol/kg soln.)	$\{OH^-\}$ (mol/kg soln.)	$\{H_4SiO_4^o\}$ (mol/kg soln.)	$\{H_3SiO_4^-\}$ (mol/kg soln.)	$\{H_2SiO_4^{-2}\}$ (mol/kg soln.)	$\{AlO_2^-\}$ (mol/kg soln.)	$\{Al^{3+}\}$ (mol/kg soln.)	$\{Na^+\}$ (mol/kg soln.)
4	1	1	9.38E-01	14.56	2.72E-15	5.79E-01	9.62E-10	1.82E-05	1.27E-03	6.66E-03	8.41E-36	6.18E-01
	1.5	1	9.43E-01	14.54	2.85E-15	5.54E-01	3.16E-09	5.72E-05	3.81E-03	1.57E-03	2.36E-36	6.10E-01
	2	1	9.58E-01	14.51	3.01E-15	5.24E-01	6.13E-09	1.05E-04	6.62E-03	5.14E-03	9.67E-36	6.08E-01
25	1	1	9.51E-01	13.82	1.49E-14	5.95E-01	9.08E-09	6.56E-05	3.98E-04	4.98E-03	2.24E-35	6.27E-01
	1.25	1	9.37E-01	13.80	1.54E-14	5.77E-01	3.17E-08	2.22E-04	1.31E-03	1.56E-03	7.92E-36	6.14E-01
	1.5	1	9.40E-01	13.80	1.57E-14	5.67E-01	5.69E-08	3.92E-04	2.27E-03	9.78E-04	5.34E-36	6.11E-01
	1.75	1	9.39E-01	13.79	1.59E-14	5.58E-01	7.60E-08	5.15E-04	2.93E-03	8.05E-04	4.69E-36	6.08E-01
	2	1	9.36E-01	13.78	1.62E-14	5.49E-01	9.38E-08	6.25E-04	3.50E-03	7.46E-04	4.65E-36	6.03E-01
50	1	1	9.35E-01	13.07	8.27E-14	5.77E-01	1.53E-07	4.42E-04	2.18E-04	4.27E-03	6.57E-35	6.07E-01
	1	2	9.52E-01	13.08	8.12E-14	5.87E-01	1.39E-07	4.10E-04	2.06E-04	4.70E-03	6.74E-35	6.18E-01
	1	3	9.32E-01	13.07	8.30E-14	5.75E-01	1.47E-07	4.25E-04	2.09E-04	4.35E-03	6.78E-35	6.05E-01
	1.5	1	9.17E-01	13.06	8.50E-14	5.61E-01	5.09E-07	1.43E-03	6.88E-04	1.38E-03	2.37E-35	5.93E-01
	1.5	2	9.20E-01	13.06	8.48E-14	5.63E-01	5.10E-07	1.44E-03	6.93E-04	1.40E-03	2.38E-35	5.95E-01
	2	1	8.78E-01	13.04	8.96E-14	5.34E-01	7.83E-07	2.10E-03	9.58E-04	1.05E-03	2.22E-35	5.68E-01
	2	2	9.16E-01	13.06	8.57E-14	5.57E-01	7.19E-07	2.01E-03	9.57E-04	7.85E-04	1.39E-35	5.91E-01
	2	3	9.12E-01	13.05	8.61E-14	5.54E-01	7.47E-07	2.07E-03	9.84E-04	1.05E-03	1.91E-35	5.89E-01
70	1	1	8.97E-01	12.57	2.64E-13	5.43E-01	3.50E-07	5.46E-04	4.92E-05	7.52E-03	2.46E-34	5.74E-01
	1.5	1	8.87E-01	12.57	2.66E-13	5.40E-01	1.15E-06	1.78E-03	1.60E-04	1.61E-03	5.40E-35	5.67E-01
	2	1	9.41E-01	12.59	2.50E-13	5.70E-01	1.50E-06	2.45E-03	2.33E-04	1.16E-03	3.07E-35	6.01E-01

References

[1] P. Duxson, A. Fernández-Jiménez, J.L. Provis, G.C. Lukey, A. Palomo, J.S.J. Deventer, Geopolymer technology: the current state of the art, J. Mater. Sci. 42 (2006) 2917–2933.

[2] K.L. Aughenbaugh, T. Williamson, M.C.G. Juenger, Critical evaluation of strength prediction methods for alkali-activated fly ash, Mater. Struct. 48 (2014) 607–620.

[3] H. Xu, J.S.J. Van Deventer, The geopolymerisation of alumino-silicate minerals, Int. J. Miner. Process. 59 (2000) 247–266.

[4] P. Duxson, J.L. Provis, G.C. Lukey, S.W. Mallicoat, W.M. Kriven, J.S.J. van Deventer, Understanding the relationship between geopolymer composition, microstructure and mechanical properties, Colloids Surfaces A Physicochem. Eng. Asp. 269 (2005) 47–58.

[5] A. Fernández-Jiménez, A. Palomo, López-H, C. Ombrados, Engineering Properties of Alkali-Activated Fly Ash Concrete, ACI Mater. J. (2006) 106–112.

[6] S.A. Bernal, J.L. Provis, Durability of alkali-activated materials: Progress and perspectives, J. Am. Ceram. Soc. 97 (2014) 997–1008.

[7] A. Fernández-Jiménez, I. García-Lodeiro, A. Palomo, Durability of alkali-activated fly ash cementitious materials, J. Mater. Sci. 42 (2006) 3055–3065.

[8] I. García-Lodeiro, A. Palomo, A. Fernández-Jiménez, Alkali–aggregate reaction in activated fly ash systems, Cem. Concr. Res. 37 (2007) 175–183.

[9] W.D. Callister, Materials Science and Engineering, Seventh Ed, John Wiley and Sons, 2007.

[10] D.A. Kulik, M. Kersten, Aqueous solubility diagrams for cementitious waste stabilization systems. 4. A carbonation model for Zn-Doped calcium silicate hydrate by Gibbs energy minimization, Environ. Sci. Technol. 36 (2002) 2926–2931.

[11] R.S. Barneyback, S. Diamond, Expression and analysis of pore fluids from hardened cement pastes and mortars, Cem. Concr. Res. 11 (1981) 279–285.

[12] L.. Struble, The Influence of Cement Pore Solution on Alkali Silica Reaction, 1987.

[13] T. Williamson, M.C.G. Juenger, The role of activating solution concentration on alkali–silica reaction in alkali-activated fly ash concrete, Cem. Concr. Res. 83 (2016) 124–130.

[14] F. Rajabipour, E. Giannini, C. Dunant, J.H. Ideker, M.D. a. Thomas, Alkali–silica reaction: Current understanding of the reaction mechanisms and the knowledge gaps, Cem. Concr. Res. 76 (2015) 130–146.

[15] B. Lothenbach, T. Matschei, G. Möschner, F.P. Glasser, Thermodynamic modelling of the effect of temperature on the hydration and porosity of Portland cement, Cem. Concr. Res. 38 (2008) 1–18.

[16] R.J. Myers, E. L'Hopital, J.L. Provis, B. Lothenbach, Composition-solubility-structure relationships in calcium (alkali) aluminosilicate hydrate (C-(N,K-)A-S-H), Dalt. Trans. (2015) 13530–13544.
[17] R.J. Myers, Thermodynamic Modelling of CaO-Al2O3-SiO2-H2O-Based Cements, The University of Sheffield, 2015.
[18] R.J. Myers, E. L'Hôpital, J.L. Provis, B. Lothenbach, Effect of temperature and aluminium on calcium (alumino)silicate hydrate chemistry under equilibrium conditions, Cem. Concr. Res. 68 (2015) 83–93.
[19] R.J. Myers, S. a. Bernal, J.L. Provis, A thermodynamic model for C-(N-)A-S-H gel: CNASH_ss. Derivation and validation, Cem. Concr. Res. 66 (2014) 27–47.
[20] P. Duxson, J.L. Provis, Designing Precursors for Geopolymer Cements, J. Am. Ceram. Soc. 91 (2008) 3864–3869.
[21] W.K.W. Lee, J.S.J. Van Deventer, Structural reorganisation of class F fly ash in alkaline silicate solutions, Colloids Surfaces A Physicochem. Eng. Asp. 211 (2002) 49–66.
[22] T.W. Swaddle, J. Salerno, P.A. Tregloan, Aqueous Alulminates, Silicates, and Aluminosilicates, Chem. Soc. Rev. 23 (1994) 319–325.
[23] P. Duxson, G.C. Lukey, F. Separovic, J.S.J. van Deventer, Effect of Alkali Cations on Aluminum Incorporation in Geopolymeric Gels, Ind. Eng. Chem. Res. 44 (2005) 832–839.
[24] R.K. Iler, The Chemistry of Silica, John Wiley and Sons, New York, 1979.
[25] J.L. Provis, P. Duxson, G.C. Lukey, F. Separovic, W.M. Kriven, J.S.J. Van Deventer, Modeling Speciation in Highly Concentrated Alkaline Silicate Solutions, Ind. Eng. Chem. Res. 44 (2005) 8899–8908.
[26] A.V. McCormick, A.T. Bell, C.J. Radke, Multinuclear NMR Investigation of the Formation of Aluminosilicate Anions, J. Phys. Chem. 93 (1989) 1741–1744.
[27] B. Lothenbach, A. Nonat, Calcium silicate hydrates: Solid and liquid phase composition, Cem. Concr. Res. 78 (2015) 57–70.
[28] S.A. Greenberg, T.N. Chang, Investigation of the Colloidal Hydrated Calcium Silicates. II. Solubility Relationships in the Calcium Oxide-Silica-Water System at 25°, J. Phys. Chem. B. 69 (1965) 182–188.
[29] D.E. Macphee, K. Luke, F.P. Glasser, E.E. Lachowski, Solubility and Aging of Calcium Silicate Hydrates in Alkaline Solutions at 25°C, J. Am. Ceram. Soc. 72 (1989) 646–654.
[30] A. Atkinson, J.A. Hearne, C.F. Knights, Aqueous chemistry and thermodynamic modelling of CaO-SiO2-H2O gels, J. Chem. Soc. Dalt. Trans. 0 (1989) 2371–2379.
[31] E. L'Hôpital, B. Lothenbach, G. Le Saout, D. Kulik, K. Scrivener, Incorporation of aluminium in calcium-silicate-hydrates, Cem. Concr. Res. 75 (2015) 91–103.
[32] D. Sugiyama, T. Fujita, A thermodynamic model of dissolution and precipitation of calcium silicate hydrates, Cem. Concr. Res. 36 (2006) 227–237.
[33] U.R. Berner, Evolution of pore water chemistry during degredation of cement in a radioactive waste repository environment, Waste Manag. 12 (1992) 201–219.

[34] A.R. Ramachandran, M.W. Grutzeck, Effect of pH on the hydration of Tricalcium Silicate, J. Am. Ceram. Soc. 76 (1993) 72–80.
[35] I. Garcia-Lodeiro, A. Palomo, A. Fernández-Jiménez, D.E. Macphee, Compatibility studies between N-A-S-H and C-A-S-H gels. Study in the ternary diagram Na2O–CaO–Al2O3–SiO2–H2O, Cem. Concr. Res. 41 (2011) 923–931.
[36] I. García-Lodeiro, A. Fernández-Jiménez, A. Palomo, D.E. Macphee, Effect of Calcium Additions on N-A-S-H Cementitious Gels, J. Am. Ceram. Soc. 1940 (2010) 1934–1940.
[37] B.R.W. Pinsent, L. Pearson, F.J.W. Roughton, The kinetics of combination of carbon dioxide with hydroxide ions, Trans. Farady Soc. 52 (1956) 1512–1520.
[38] P.M. Dove, The dissolution kinetics of quartz in aqueous mixed cation solutions, Geochim. Cosmochim. Acta. 63 (1999) 3715–3727.
[39] M. Rowles, B. O'Connor, Chemical optimisation of the compressive strength of aluminosilicate geopolymers synthesised by sodium silicate activation of metakaolinite, J. Mater. Chem. 13 (2003) 1161–1165.
[40] V.F.F. Barbosa, K.J.D. MacKenzie, C. Thaumaturgo, Synthesis and characterisation of materials based on inorganic polymers of alumina and silica: sodium polysialate polymers, Int. J. Inorg. Mater. 2 (2000) 309–317.
[41] H. Xiandeng, R.S. Amais, B.T. Jones, G.L. Donati, Inductively Coupled Plasma Optical Emission Spectrometry, in: Encycl. Anal. Chem., John Wiley and Sons, 2000: pp. 1–25.
[42] R.A. Robinson, R.H. Stokes, Electrolyte Solutions, 2nd Editio, London, 1959.
[43] K.S. Pitzer, The Treatment of Ionic Solutions over the Entire Miscibility Range, Reports Bunsen Soc. Phys. Chem. 85 (1981) 952–959.
[44] A. Fernández-Jiménez, A. Palomo, M. Criado, Microstructure development of alkali-activated fly ash cement: a descriptive model, Cem. Concr. Res. 35 (2005) 1204–1209.
[45] J. Davidovits, High-Alkali Cements for 21st Century Concretes, in: Concr. Technol., n.d.: pp. 383–397.
[46] A.S. de Vargas, D.C.C. Dal Molin, A.C.F. Vilela, F.J. Da Silva, B. Pavão, H. Veit, The effects of Na2O/SiO2molar ratio, curing temperature and age on compressive strength, morphology and microstructure of alkali-activated fly ash-based geopolymers, Cem. Concr. Compos. 33 (2011) 653–660.
[47] Y. Zhang, W. Sun, Z. Li, Infrared Spectroscopy Study of Structural Nature of Geopolymeric Products, J. Wuhan Univ. Technol. Sci. Ed. 23 (2008) 522–527.
[48] J.M. Miranda, A. Fernández-Jiménez, J.A. González, A. Palomo, Corrosion resistance in activated fly ash mortars, Cem. Concr. Res. 35 (2005) 1210–1217.
[49] J.L. Provis, A. Palomo, C. Shi, Advances in understanding alkali-activated materials, Cem. Concr. Res. (2015).
[50] A. Fernández-Jiménez, A. Palomo, I. Sobrados, J. Sanz, The role played by the reactive alumina content in the alkaline activation of fly ashes, Microporous Mesoporous Mater. 91 (2006) 111–119.
[51] P. Duxson, S.W. Mallicoat, G.C. Lukey, W.M. Kriven, J.S.J. van Deventer, The

effect of alkali and Si/Al ratio on the development of mechanical properties of metakaolin-based geopolymers, Colloids Surfaces A Physicochem. Eng. Asp. 292 (2007) 8–20.
[52] E.H. Oelkers, J. Schott, J.-L. Devidal, The effect of aluminum, pH, and chemical affinity on the rates of aluminosilicate dissolution reactions, Geochim. Cosmochim. Acta. 58 (1994) 2011–2024.
[53] J.G. Thompson, 29Si and 27Al Nuclear Magnetic Resonance Spectroscopy of 2:1 Clay Minerals, Clay Miner. 19 (1984) 229–236.
[54] G. Engelhardt, U. Lohse, High resolution 29 Si n.m.r. of dealuminated and ultrastable Y-zeolites, Zeolites. 2 (1982) 59–62.
[55] G.J. Ray, B.L. Meyers, C.L. Marshall, 29Si and 27Al n.m.r study of steamed faujasites — evidence for non-framework tetrahedrally bound aluminium, Zeolites1. 7 (987) 307–310.
[56] M. Földvári, Handbook of the thermogravimetric system of minerals and its use in geological practice, 2011.
[57] N.M. Musyoka, L.F. Petrik, E. Hums, A. Kuhnt, W. Schwieger, Thermal stability studies of zeolites A and X synthesized from South African coal fly ash, Res. Chem. Intermed. 41 (2015) 575–582.
[58] R.A. Fletcher, K.J.D. MacKenzie, C.L. Nicholson, S. Shimada, The composition range of aluminosilicate geopolymers, J. Eur. Ceram. Soc. 25 (2005) 1471–1477.
[59] J. Davidovits, Geopolymers: Inorganic polymeric new materials, J. Therm. Anal. 37 (1991) 1633–1656.
[60] J.L. Provis, Geopolymers and other alkali activated materials: why, how, and what?, Mater. Struct. 47 (2013) 11–25.
[61] O.D. Ozdemir, S. Pişkin, Zeolite X Synthesis with Different Sources, Int. J. Chem. Environ. Biol. Sci. 1 (2013) 229–232.
[62] W. Lutz, Zeolite Y: Synthesis, modification, and properties - A case revisited, Adv. Mater. Sci. Eng. (2014) 1–20.
[63] P. Błoński, A. Birczyński, Z.T. Lalowicz, J. Datka, Z. Łodziana, Structure of the Hydroxyl Groups and Adsorbed D2O Sites in the DX Zeloite: DFT and Experimental NRM Data, J. Phys. Chem. C. 119 (2015) 19548–19557.
[64] A. Buchwald, H.D. Zellmann, C. Kaps, Condensation of aluminosilicate gels-model system for geopolymer binders, J. Non. Cryst. Solids. 357 (2011) 1376–1382.
[65] A. Hajimohammadi, J.L. Provis, J.S.J. van Deventer, Time-resolved and spatially-resolved infrared spectroscopic observation of seeded nucleation controlling geopolymer gel formation, J. Colloid Interface Sci. 357 (2011) 384–392.
[66] G. Spositio, The Chemistry of Soils, Oxford University Press, New York, 1989.
[67] J. Šefčík, A.V. McCormick, Prediction of cystallization diagrams for synthesis of zeolites, Chem. Eng. Sci. 54 (1999) 3513–3519.
[68] A. Čizmek, L. Komunjer, B. Subotić, Kinetics of zeolite dissolution. Part 2. Dissolution of zeolite X in hot sodium hydroxide solutions, Zeolites. 11 (1991) 810–815.

[69] S. Sjöberg, Silica in aqueous environments, J. Non. Cryst. Solids. 196 (1996) 51–57.
[70] J. Xie, O. Kayali, Effect of initial water content and curing moisture conditions on the development of fly ash-based geopolymers in heat and ambient temperature, Constr. Build. Mater. (2013) 1–9.
[71] M.C.G. Juenger, F. Winnefeld, J.L. Provis, J.H. Ideker, Advances in alternative cementitious binders, Cem. Concr. Res. 41 (2011) 1232–1243.
[72] J.R. Yost, A. Radlińska, S. Ernst, M. Salera, Structural behavior of alkali activated fly ash concrete. Part 1: mixture design, material properties and sample fabrication, Mater. Struct. 46 (2012) 435–447.
[73] M.S. Muñiz-Villarreal, a. Manzano-Ramírez, S. Sampieri-Bulbarela, J.R. Gasca-Tirado, J.L. Reyes-Araiza, J.C. Rubio-Ávalos, et al., The effect of temperature on the geopolymerization process of a metakaolin-based geopolymer, Mater. Lett. 65 (2011) 995–998.
[74] A.A. Adam, Strength and Durability Properties of Alkali Activated Slag and Fly Ash-Based Geopolymer Concrete, (2009).
[75] C. Patapy, G. Sant, N. Myers, L. Steger, K. Scrivener, The Influence of Slag Characteristics on Reaction and Strength Evolutions in OPC-Slag Blends, Cem. Concr. Res. (n.d.).
[76] C.K. Yip, J.S.J. Van Deventer, Microanalysis of calcium silicate hydrate gel formed within a geopolymeric binder, 38 (2003) 3851–3860.
[77] J. Temuujin, A. van Riessen, R. Williams, Influence of calcium compounds on the mechanical properties of fly ash geopolymer pastes., J. Hazard. Mater. 167 (2009) 82–88.
[78] X. Guo, H. Shi, W.A. Dick, Compressive strength and microstructural characteristics of class C fly ash geopolymer, Cem. Concr. Compos. 32 (2010) 142–147.
[79] M.M.A. Abdullah, H. Kamarudin, M. Bnhussain, I. Khairul Nizar, A.R. Rafiza, Y. Zarina, The relationship of NaOH Molarity, Na2SiO3/NaOH Ratio, Fly Ash/Alkaline Activator Ratio, and Curing Temperature to the Strength of Fly Ash-Based Geopolymer, Adv. Mater. Res. 328–330 (2011) 1475–1482.
[80] A.M. Mustafa Al Bakri, H. Kamarudin, M. Bnhussain, A.R. Rafiza, Y. Zarina, Effect of Na2SiO3/NaOH Ratios and NaOH Molarities on Compressive Strength of Fly-Ash-Based Geopolymer, ACI Mater. J. 109 (2012) 503–508.
[81] A. Hajimohammadi, J.L. Provis, J.S.J. Van Deventer, The effect of silica availability on the mechanism of geopolymerisation, Cem. Concr. Res. 41 (2011) 210–216.
[82] H.A. Gasteiger, W.J. Frederick, R.C. Streisel, Solubility of aluminosilicates in alkaline solutions and a thermodynamic equilibrium model, Ind. Eng. Chem. Res. 31 (1992) 1183–1190.